

Giving an Enzyme Scissors: Serotonin Derivatives as Potent Organocatalytic Switches for DNA Repair Enzyme OGG1

Marek Varga,* Florian Ortis, Alicia Del Prado, Alice Eddershaw, Emma Scaletti Hutchinson, Emily C. Hank, Kaixin Zhou, Natálie Rudolfová, Alessia Dodaro, Elisée Wiita, Ingrid Almlöf, Stella Karsten, Kirill Mamonov, Sara H. Ahmed, Kirsty Bentley, Olov Wallner, Evert J. Homan, Martin Scobie, Thomas Helleday, Mario Prejanò, Pål Stenmark, Miguel de Vega, Allan J. B. Watson,* and Maurice Michel*



Cite This: https://doi.org/10.1021/acs.jmedchem.5c01454



ACCESS |

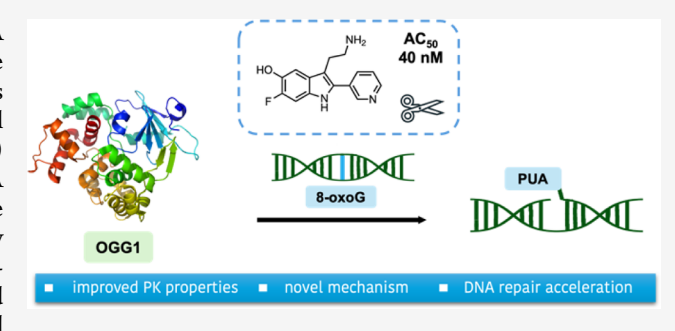
pubs.acs.org/jmc

Metrics & More

Article Recommendations

Supporting Information

ABSTRACT: The base excision repair enzyme 8-oxoguanine DNA glycosylase 1 (OGG1) plays a central role in maintaining genome integrity and mediating cellular responses to oxidative stress. As such, it represents an attractive target for pharmaceutical modulation. Small-molecule organocatalytic switches (ORCAs) greatly enhance the rate of OGG1-catalyzed cleavage of DNA abasic sites, thereby accelerating DNA repair. Here, we present the discovery and hit-to-lead optimization of a novel class of highly potent serotonin-derived ORCAs with greatly improved pharmacokinetic properties. Biochemical assays, X-ray crystallography, and molecular dynamics simulations point toward a water-mediated



mechanism of activation, distinct from previously proposed Brønsted base-assisted models. These findings establish serotonin-based ORCAs as promising chemical probes and potential leads for therapeutic modulation of OGG1 in oxidative stress-driven diseases.

INTRODUCTION

Enzymes represent an attractive target across many fields of science. From the medicinal chemistry perspective, 29% of all small-molecule drugs approved by the FDA in 2023 target enzymes, exclusively through enzyme inhibition. This success stems from the fact that aberrant or overactive enzymatic function is often associated with disease. However, there are many cases where enzymatic activity is beneficial, and smallmolecule modulators which add or enhance an enzyme function are desirable. Reflecting this, recent years have seen a growing number of reports of "small-molecule activators".^{2,3} The first of these are also appearing in the market, although only two, Mitapivat^{4,5} and Vericiguat,⁶ have been approved by the FDA in the past decade. 1,4,6-13

The disparity between the number of enzyme inhibitors and activators likely reflects the inherent challenges in identifying activators. While both inhibitors and activators can bind allosterically, orthosteric activators must bind to the active site without blocking substrate binding or catalysis. Nevertheless, several classes of small-molecule activators have been successfully identified, including kinase, 14-17 deacetylase, 18,19 protease, 20-22 and dehydrogenase 23 activators, among others, with some advancing into clinical trials. 24-26

8-Oxoguanine DNA glycosylase 1 (OGG1) is a prime example of an enzyme for which activation offers substantial

therapeutic potential. OGG1 initiates the repair of 8oxoguanine (8-oxoG),²⁷ a common oxidative DNA lesion that accumulates under conditions of oxidative stress and has been linked to cancer, neurodegeneration, inflammation, aging, as well as other human conditions. 28-31 The prevalence of 8oxoG arises from the low redox potential of guanine compared to the other nucleobases.³² By excising 8-oxoG, OGG1 plays a critical role in preventing its accumulation, 33,34 and has demonstrated protective effects in cancer,^{35–37} neurodegeneration,³⁸ cardiovascular disease,^{39,40} as well as diabetes and aging.41-44 Furthermore, recent studies continue to uncover roles for OGG1 in regulating transcription within several signaling pathways, including those involved in inflammation, 45-52 cancer, 53-56 and pulmonary fibrosis. 44,57-60

OGG1 acts as a monofunctional glycosylase, catalyzing the excision of 8-oxoG and forming a Schiff-base between Lys249 and the resulting apurinic/apyrimidinic (AP) site. 61 Release of this covalent intermediate is rate-limiting and requires the

Received: May 28, 2025 Revised: September 26, 2025 Accepted: October 6, 2025



action of apurinic/apyrimidinic endonuclease 1 (APE1) to cleave the DNA (Figure 1a). 62,63 It has been proposed that 8-

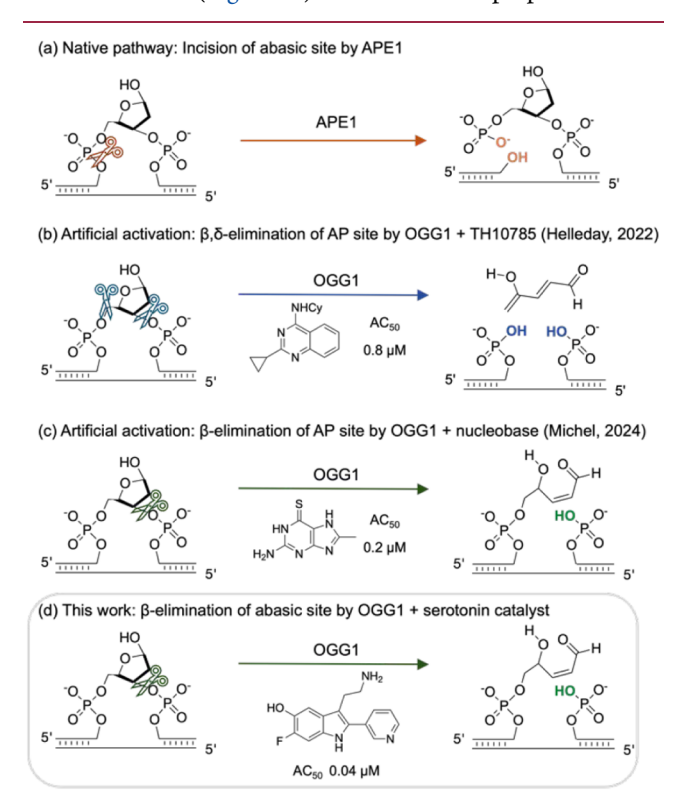


Figure 1. (a) Native incision pathway for AP sites generated by OGG1. (b) β , δ -elimination of AP sites by OGG1 in the presence of TH10785. (c) β -elimination of AP sites by OGG1 in the presence of nucleobase catalysts. (d) This work: β -elimination of AP sites by OGG1 in the presence of serotonin catalysts.

oxoG and its synthetic analogues 8-amino and 8-bromoguanine can promote proton abstraction at the C2'-position of the Schiff-base, triggering β -elimination and product release. ^{61,64} However, in later studies free 8-oxoG acted as an inhibitor of both glycosylase and AP lyase activities of OGG1, ⁶⁵ and this mechanism appears to have a negligible effect in cells. ^{66,67} Coenzyme-Q₁₀ has been shown to increase OGG1 glycosylase activity while inhibiting the AP-lyase activity. ⁶⁸ In contrast, we and others have disclosed small-molecule *organocatalytic switches* (ORCAs) that increase OGG1 turnover by 10- to 20-fold, dramatically accelerating DNA repair. ^{55,67,69–71} We postulated that ORCAs bind within the OGG1 active site, enabling either β , δ -elimination (Figure 1b), or β -elimination (Figure 1c) through Brønsted-base catalysis. ^{67,70} Allosteric activators have also been suggested. ⁷²

The therapeutic potential of OGG1 ORCAs has been demonstrated *in vitro*. For example, ORCAs protect DNA against KBrO₃-induced damage at telomeres, ⁶⁷ and against paraquat-induced damage to mitochondrial DNA, metabolism, and membrane stability. ^{69,72} Certain ORCAs can even restore activity to the OGG1 Ser326Cys variant, commonly found in Alzheimer's disease and cancer patients. ⁶⁹ Given their mechanism, ORCAs hold the greatest promise in diseases characterized by elevated oxidative damage.

Notably, ORCAs have been shown to reduce fibrosis in a patient-derived 3D model of metabolic dysfunction-associated steatohepatitis (MASH),^{71,73} a leading cause of chronic liver-disease with limited therapeutic options.^{74,75}

In this work, we sought to expand beyond established nucleobase and quinazoline-derived ORCAs to develop a new series of ORCAs with improved potency and pharmacological properties. Through the identification of a novel ORCA scaffold (Figure 1d), we also aimed to gain a deeper insight into the molecular mechanism of OGG1 activation.

RESULTS AND DISCUSSION

Hit Identification. To identify novel ORCAs, an in-house small molecule library and a filtered selection of the National Cancer Institute (NCI) and National Institutes of Health (NIH) compound libraries were computationally screened. Of these, 40 were selected by docking score, structural appeal, and availability for screening (Table S1). A previously disclosed fluorescence assay featuring an 8-oxoA-containing oligonucleotide with one strand ligated to a quencher and the other to a fluorophore was used to measure the rate of incision (Figure 2). 8-oxoA was used in place of 8-oxoG due to increased

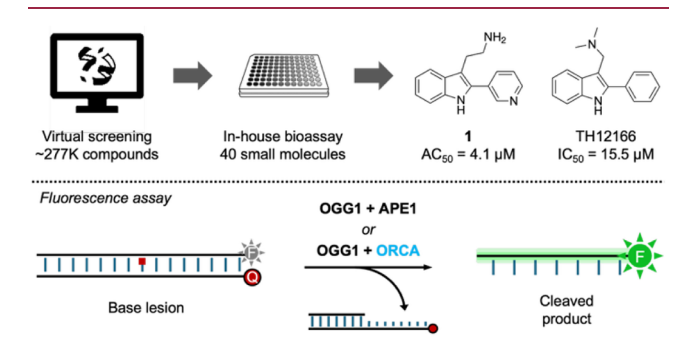


Figure 2. Identification of OGG1 ORCA **1** and inhibitor TH12166 (top). Illustration of fluorescence assay (bottom). F = 6-carboxyfluoresceine, Q = dabcyl.

stability while remaining a good substrate for OGG1. Compound potency was measured by the AC₅₀, defined as the concentration of compound at which OGG1 achieved 50% of the incision rate observed with OGG1 in the presence of APE1. In this way, the 2-pyridyltryptamine derivative, 1, was identified as an ORCA with an AC₅₀ of 4.1 μ M, while the *N,N*-dimethyl 2-phenyltryptamine derivative, TH12166, was identified as an inhibitor with an IC₅₀ of 15.5 μ M.

Synthesis and SAR of 2-Aryltryptamines. For initial structure—activity relationship (SAR) exploration, 2-pyridyltryptamines were synthesized via a Pd-catalyzed C2-arylation (Scheme 1A). The RuPhos ligand was essential for reactivity; however, conversions were generally poor. An initial library of 2-pyridyltryptamine derivatives was prepared (Table 1, 1-6). Substitution on the indole scaffold was not tolerated (2-5), and conversion of the tryptamine amine chain to a tryptophan amino acid (6) abolished activity as well. Further SAR development was hindered by the requirement of prefunctionalized tryptamines and the low reliability of the C2-arylation methodology.

In parallel, 2-phenyltryptamines, were evaluated for OGG1 activation (Table 1, 7–9). These were accessible via a previously reported method for the C2-arylation of tryptophans (Scheme 1B), which was, however, incompatible with pyridine substrates. To our surprise, although 2-phenyltryptamine was inactive, the 5-hydroxy derivative, 8, showed potency despite lacking the pyridyl motif. This observation suggested that the primary role of the pyridyl group may be to

Scheme 1. (A) Pd-Catalyzed Coupling of Tryptamines with 3-Bromopyridine. (B) Pd-Catalyzed Coupling of Tryptamines with Iodobenzene

Table 1. Initial In Vitro Evaluation of 2-Pyridyl and 2-Phenyltryptamines with Previously Disclosed ORCAs as Positive Controls

Compound #	Structure	AC ₅₀ (Cl95%) [μΜ]	Compound #	Structure	AC ₅₀ (Cl95%) [μΜ]
8-BrG	HN N Br	21 (5.8–76)	4	CI NH2	inactive
8-Me-6-TG	H ₂ N N Me	0.32 (0.27–0.39) ⁷⁰	5	NH ₂	inactive
TH10785	NHCy N	0.87 (0.70–1.1)	6	HO ₂ C-N	inactive
1	NH ₂	4.1 (3.0–5.6)	7	NH ₂	inactive
2	Me NH2	inactive	8	HO NH ₂	4.0 (1.1–14)
3	MeO N	inactive	9	F N N N N N N N N N N N N N N N N N N N	inactive

Table 2. In Vitro Evaluation of 2-Arylindoles

Compound #	Structure	AC ₅₀ (Cl95%) [μΜ]	Compound #	Structure	AC ₅₀ (Cl95%) [μΜ]
10		1.7 (0.9–3.2)	20	OH OH	2.8 (2.3–3.4)
11	Me N N N	5.7 (3.8–8.6)	21	N OH	inactive
12	F	1.9 (1.4–2.4)	22	NH CI	inactive
13	Br N	1.0 (0.9–1.0)	23	$\begin{array}{c} \\ \\ \\ \\ \\ \\ \\ \\ \\ \\ \\ \\ \\ \\ \\ \\ \\ \\ \\$	14 (5.8–36)
14	MeO N	13 (4.7–38)	24		inactive
15	HO N N	6.0 (1.8–21)	25		inactive
16	C N N N N N N N N N N N N N N N N N N N	1.4 (1.0–2.0)	26	NH NH	1.4 (0.7–2.6)
17	N F	inactive	27		inactive
18	NH ₂	>100	28		4.1 (3.8–4.4)
19	NH ₂	9.3 (3.4–25)			

promote active site binding, rather than direct participation in Brønsted base catalysis of β -elimination.

Synthesis and SAR Analysis of 2-Pyridylindoles. To further explore the SAR of ORCAs, we turned our attention to the more synthetically accessible 3-unsubstituted 2-pyridylindoles (Table 2). These compounds were primarily prepared using either the Fischer indole synthesis, or the Suzuki-Miyaura cross-coupling of *N*-Boc-indole-2-boronic acid (see Experimental).

Interestingly, removal of the ethylamine chain, present in the tryptamine series, led to an increase in potency, with the 2-pyrid-3-ylindole, ${\bf 10}$, having an AC₅₀ of 1.7 μ M. However, despite extensive SAR efforts, further improvements in potency proved challenging. Substitutions at the 5-position of the indole ring had limited effects (11–15), whereas substitution on the pyridine was generally detrimental (16–23). Replacement of the pyridin-3-yl motif with other heterocycles, pyridin-4-yl (24), pyrimidin-5-yl (25), or quinoline (27) was not

Journal of Medicinal Chemistry

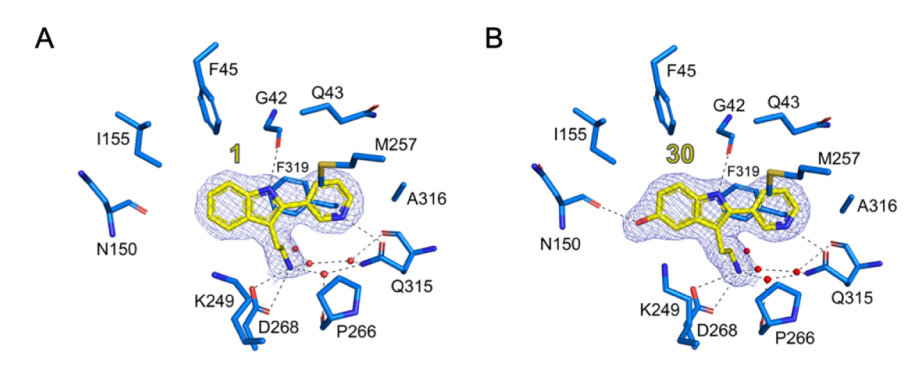
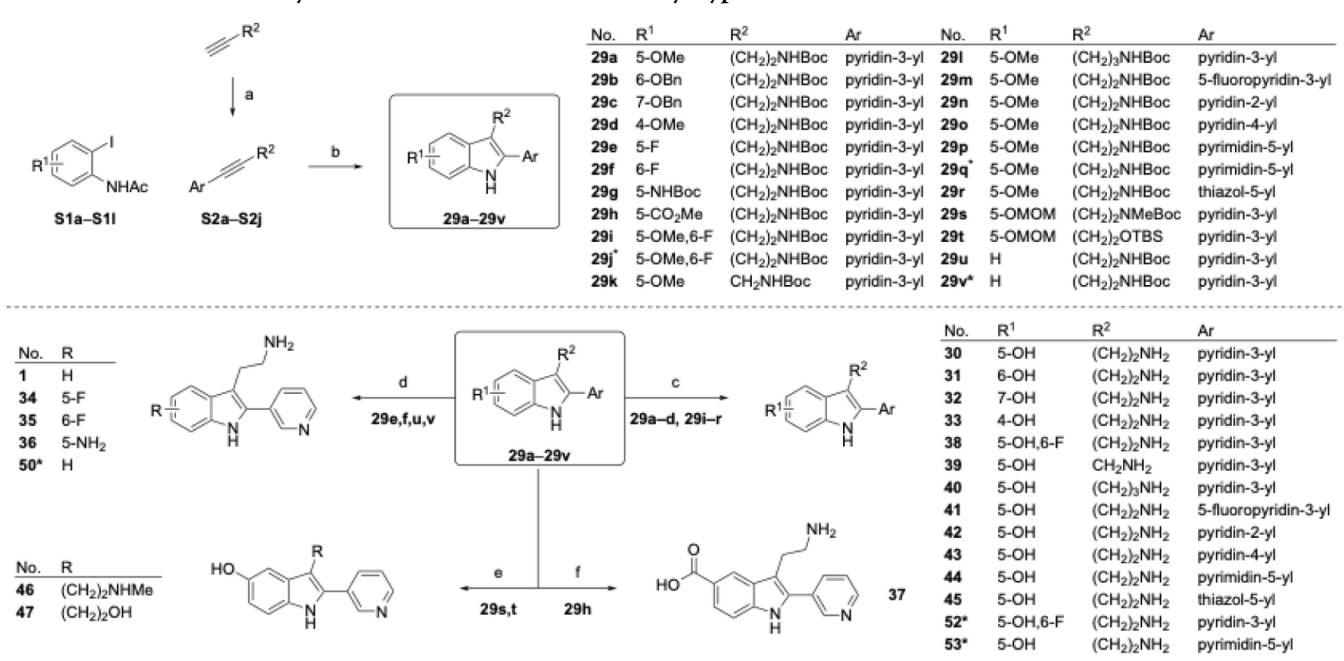


Figure 3. (A) Recognition of 1 by mOGG1 (PDB ID: 9FNV). (B) Recognition of 30 by mOGG1 (PDB ID: 9FNU). Amino acids contributing to ligand binding are depicted as sticks: C atoms are colored blue, O atoms red, and N atoms dark blue. Ligands are depicted as stick models: C atoms colored yellow, N atoms dark blue, and O atoms red. Hydrogen bond interactions are shown as dashed lines. Water molecules are shown as red spheres. The 2Fo-Fc electron density maps around the ligands are contoured at 1.0 σ (blue) and the Fo-Fc electron density maps are contoured at +3.5 s (green) and -3.5 s (red). Figure produced using PyMOL (v.2.3.3, Schrödinger).

Scheme 2. Larock Indole Synthesis Route to Substituted 2-Aryltryptamines.^a



"(a) $PdCl_2(PPh_3)_2$ (3 mol %), CuI (9 mol %), ArX (1.5 equiv), RT for X = I, 90 °C for X = Br, NEt₃, 3 h; (b) 1. $Pd(^tBu_3)_2$ (5 mol %), S1a-S11 (1.3 equiv), Cy_2NMe (2 equiv), DMF, 80 °C, 24 h 2. LiOH (5 equiv), Cy_2NHe (2 equiv), Cy_2NHe (3 equiv), Cy_2NHe (6 equiv), Cy_2NHe (2 equiv), Cy_2NHe (3 equiv), Cy_2NHe (3 equiv), Cy_2NHe (6 equiv), Cy_2NHe (7 equiv), Cy_2NHe (8 equiv), Cy_2NHe (9 mol %), Cy_2NHe (1.5 equiv), Cy_2NHe (

tolerated, with the exception of the azaindole (26). Similarly, substitution of the indole core for a benzofuran scaffold (28) did not improve potency.

Cocrystal of OGG1 and 1. To rationalize the observed SAR and guide further efforts, we solved the cocrystal structure of mouse OGG1 (mOGG1) in complex with 1 (Figure 3A and Table S2). mOGG1 was utilized for structural studies as it has an identical active site structure to human OGG1 but is significantly more amenable to crystallization. The crystal structure was obtained in the absence of a DNA substrate, which may not fully represent the active catalytic conformation. However, we have previously observed correlations between binary OGG1-ORCA complex structures and catalytic potency. Furthermore, we noted significant overlap between the active site structure of the NaBH₄-trapped Schiff-base ternary complex with 8-oxoG (PDB ID: 1HU0)

and the binary complexes of nucleobase ORCAs (PDB IDs: 8BQ7, 9F8U, 9F8 V, 9F8Z), 70 supporting the use of these structures as reasonable approximations of the catalytic conformation. The crystal structure unambiguously placed 1 within the OGG1 active site, engaging in a binding mode consistent with previously reported ORCAs. 67,70,71 Key interactions included H-bonds to Gly42, Gln315, a salt bridge to Asp268, π -stacking with Phe319, and a water-mediated H-bonding network. Analogous to previous ligands where the Gly42 H-bond was mediated via an aniline or a secondary amine, the indole NH formed this crucial interaction.

As hypothesized, the pyridyl moiety was involved in bonding interactions and was found deep in the OGG1 catalytic pocket, forming a H-bond to Gln315. Importantly, the H5 of 1 was found to reside within 3.2 Å of Asn150 (Figure S2), providing a possible explanation for the potency of 8 via a tentative H-

Table 3. Second Round In Vitro Evaluation of 2-Pyridyltryptamines

Compound #	Structure	AC₅₀ (Cl95%) [μΜ]	Compound #	Structure	AC₅₀ (Cl95%) [μM]
30	HO NH2	0.58 (0.37–0.92)	34	F NH ₂	6.4 (1.8–23)
31	HO H	inactive	35	F NH2	5.3 (3.1–9.0)
32	NH ₂	inactive	36	H ₂ N NH ₂	inactive
33	OH NH ₂	inactive	37	HO NH ₂	inactive

Table 4. Third Round In Vitro Evaluation of 2-Pyridyltryptamines

Compound #	Structure	AC ₅₀ (CI95%) [μΜ]	Compound #	Structure	AC ₅₀ (Cl95%) [μΜ]
38	HO NH ₂	0.040 (0.014– 0.11)	46	NHMe HO NHME	0.29 (0.13–0.65)
39	HO NH ₂	inactive	47	HO	8.7 (7.0–11)
40	HO NH2	inactive	48	HO NH ₂	inactive
41	HO NH ₂ F	0.74 (0.59–0.93)	49	HO NH2	inactive
42	HO NH2	inactive	50	N N NH ₂	28 (6.8–113)
43	HO NH2	inactive	51	HO NH2	inactive
44	HO NH ₂	0.25 (0.14–0.45)	52	HO NH2	8.5 (7.5–9.6)
45	HO NH ₂	0.40 (0.20–0.81)	53	HO NH ₂	12 (4.8–29)

bonding interaction between its 5-OH substituent and Asn150. This insight provided the rationale to develop an alternative synthetic strategy that would enable the incorporation of the 5-OH onto 1, as well as further SAR exploration of the tryptamine scaffold.

Larock Indole Synthesis of 2-Pyridyltryptamines. The new synthetic route centered around the Pd-catalyzed Larock indole synthesis, which allowed for far greater modularity (Scheme 2).^{77,78} This approach allowed for broad variation of starting materials: 2-iodoacetanilides (S1a–l) could often be prepared from commercially available 2-iodoanilines or 2-iodonitrobenzenes, while Boc-protected aminoalkynes (S2a–j) were prepared through Sonogashira coupling reactions. Following Larock cyclization, intermediates bearing methyl or benzyl ethers were treated with BBr₃ to afford the corresponding phenols (30–33, 38–45, 52–53). Other derivatives were deprotected under a variety of acidic conditions to afford the desired tryptamines (1, 34–37, 46–47, 50).

Second Round of 2-Pyridyltryptamine Optimization.

This new synthetic route enabled the preparation of a second library of 2-pyridyltryptamines (Table 3). Notably, we found that introduction of a 5-OH substituent in 30 improved potency 10-fold over 1, consistent with the activity of the 2phenyl analogue, 8. Evaluation of other hydroxy-substitution patterns revealed that the 5-OH position was essential for activity as the 4-OH, 6-OH, and 7-OH derivatives (31-33) were universally inactive. 5-F (34), and 6-F (35) derivatives were tolerated but neither improved on the potency of 1. Replacement of the 5-OH with other H-bond donors, such as aniline (36) or carboxylic acid (37) analogues, was not tolerated. To elaborate on the enhanced potency of 30, a cocrystal structure with mOGG1 was obtained (Figure 3B). As expected, the 5-OH formed a new H-bond to Asn150 while maintaining all key interactions observed for 1. In contrast, the 4-, 6-, and 7-OH derivatives were likely positioned too far to Asn150 to enable this interaction.

Computational Analysis. A computational docking screen of the tryptamines synthesized was performed to

guide further SAR exploration (Table S3). This was conducted using the mOGG1-30 cocrystal structure. Interestingly, the highest-scoring ligand was the 6-F tryptamine 35, despite its moderate activity in the fluorescence assay. A hydrophobic interaction with Ile155 was identified as the possible origin of this affinity (Figure S3A). Another novel interaction was observed for 32 where the 7-OH moiety formed a H-bond to Gly42 (Figure S3B). These insights prompted the synthesis of 5-OH-6-F, and 5,7-diOH hybrid compounds. The synthesis of the latter was unsuccessful, likely due to product instability. In addition, a series of further serotonin-derived analogues was prepared (Table 4).

Third Round of 2-Pyridyltryptamine Optimization. Importantly, the 5-OH-6-F hybrid, 38, exhibited the highest potency identified in this series with an AC₅₀ of 0.040 μ M, consistent with novel hydrophobic interactions or increased H-bond donating ability of the phenol. Shortening (39) or lengthening (40) of the ethylamine chain of 30 was not tolerated.

Substitution on the pyridin-3-yl group was also explored. Fluorination did not significantly affect potency (41), whereas the position of the pyridine N was essential as the pyridin-2-yl (42) and pyridin-4-yl (43) derivatives lost activity. However, the pyridine could be substituted with either pyrimidine (44) or thiazole (45) heterocycles to achieve a slight increase in activity. Amine monomethylation produced a similar increase in potency (46), unlike N1-methylation of the indole (48), which attenuated activity, presumably by interrupting H-bonding to Gly42. These results were consistent with previous work where interaction with Gly42 was essential for activation. The ethanol derivative 47 decreased activity \sim 10-fold, demonstrating the importance of the ionic interactions of the amino group. An isomer placing the ethylamine on the pyridine ring rather than the indole (49) was inactive.

Finally, regioisomeric side products of the Larock cyclization, in which the positions of the ethylamine chain and the aryl group were reversed, were isolated and evaluated (50–53). Despite some residual activity for 52 and 53, these isomers were generally less potent or inactive compared to their tryptamine analogues.

Selectivity and Toxicity. To ascertain the selectivity of the tryptamine ORCAs, **30** was screened against a panel of DNA glycosylases and nucleotide-binding NUDIX hydrolases. **30** had no effect on NUDIX hydrolases or APE1, and a >150-fold selectivity for OGG1 activation over inhibition of other glycosylases (Table S4). This represents a slight improvement over the already high (>120-fold) selectivity of the established ORCA, TH10785. Compound **30** also improves on the toxicity of TH10785 which shows some toxicity in the immortalized BJ-TERT and oncogene-driven BJ-RAS, ^{79,80} and inhibits proliferation in activated peripheral blood mononuclear cells (PBMCs, Figure S4). In contrast, **30** showed no detectable toxicity when incubated with the BJ-derived cells at 100 μ M over several days (Figure S5).

Pharmacokinetic Analysis. The primary goal of this series was to improve on the physicochemical properties of known ORCAs. For example, TH10785 has a relatively high clogP of 4.54, a low aqueous solubility of 6 μ M and a suboptimal efflux ratio of 3.3 (Table 5). In addition to improved toxicity, **30** also exhibits a 58-fold higher aqueous solubility, and a 5-fold lower clogP compared to TH10785. The efflux ratio (4.1) remains at an acceptable level but should

Table 5. Comparison of 30 and TH10785

	30	TH10785
$AC_{50} [\mu M]$	0.58	0.78 ⁶⁷
incision mode	β	β , δ
selectivity ^a	>150-fold	>120-fold ⁷⁰
toxicity $[\mu M]^b$	>100	>18 (20)
$c \log P^c$	0.84	4.54
$AcLE^d$	0.456	0.419
AcLLE ^e	5.49	1.57
aq. solubility $(\mu M)^f$	345	6
$Cl_{int} (\mu L/min/mg)^g$	8	18 (347)
$t_{1/2} \; (\min)^g$	213	-
$k_{\rm el}~({ m min}^{-1})^{ m g}$	0.003	-
$P_{\rm app}$ (AB) $(nm/s)^h$	5.3 (10.7)	15.0
$P_{\rm app}$ (BA) $(nm/s)^h$	21.5 (18.7)	49.0
Efflux ratio ⁱ	4.1 (1.7)	3.3

 $^a\text{Calculated}$ as lowest IC $_{50}$ measured against a panel of DNA glycosylases and NUDIX nucleotide binding proteins/OGG1 AC $_{50}$. Incubation in BJ-RAS and BJ-TERT cell lines. Value in parentheses obtained using PBMCs. $^c\text{Calculated}$ using InstantJChem version 23.16. $^d\text{AcLE} = (1.37/\#\text{heavy atoms}) \times \text{pAC}_{50}$. $^e\text{AcLLE} = \text{pAC}_{50} - c\log\text{P}$. $^f\text{Kinetic}$ solubility in PBS buffer (pH 7.4). $^g\text{Metabolic}$ stability evaluated in human (mouse) liver microsomes. $^h\text{Using}$ Caco-2 cell line. Value in parentheses obtained in the presence of P-gp inhibitor (verapamil). $^i\text{Calculated}$ by dividing P_{app} (B to A) by P_{app} (A to B).

be addressed for further clinical development. The substantial decrease in efflux (1.7 vs. 4.1) in the presence of a P-glycoproptein (P-gp) efflux protein inhibitor, verapamil, suggests that 30 is a P-gp substrate and subject to active efflux.

Surprisingly, **30** was remarkably stable when exposed to liver microsomes, despite the presence of phenol⁸¹ and amine⁸² functionalities, both typically liable to rapid metabolism, with serotonin itself being a natural substrate of monoamine oxidase.⁸³ Here, **30** showed less than half the clearance rate of TH10785 with a microsomal half-life exceeding 3.5 h.

Finally, to evaluate the drug-likeness of ORCAs we propose the metrics "AcLE" and "AcLLE", modified forms of the ligand efficiency (LE) ligand-lipophilicity efficiency (LLE) metrics, where pIC_{50} is substituted by the pAC_{50} in the standard calculations of these measures. ⁸⁴ Using these metrics, **30** showed a slightly better AcLE than TH10785 and a markedly higher AcLLE, attributable to its significantly lower lipophilicity.

Activity of OGG1 in the Presence of 2-Pyridyltryptamines. Different ORCAs have been shown to have distinct effects on the OGG1-catalyzed incision of apurinic/apyrimidinic (AP) sites. Nucleobase-derived ORCAs facilitate β -elimination of the Schiff-base intermediate, generating 3'-phosphate unsaturated aldehyde (3'-PUA) products that are further processed by APE1. Other ORCAs, such as TH10785, enable β , δ -elimination, which produces 3'-phosphate (3'-P) termini that cannot be processed by APE1, thereby redirecting the repair pathway toward polynucleotide kinase phosphatase (PNKP1).

To investigate the molecular mechanism of OGG1 activation by 2-pyridyltryptamines, a PAGE assay was performed. A [32P]-labeled double-stranded DNA substrate containing 8-oxoG (Figure 4A) was incubated in the presence (+) or absence (-) of hOGG1 and either ORCAs 30, 38, or TH10785, or the OGG1 inhibitor TH5487. The resulting products were analyzed by urea-PAGE (Figure 4B). Stimulation of OGG1 AP lyase activity was observed for

Journal of Medicinal Chemistry

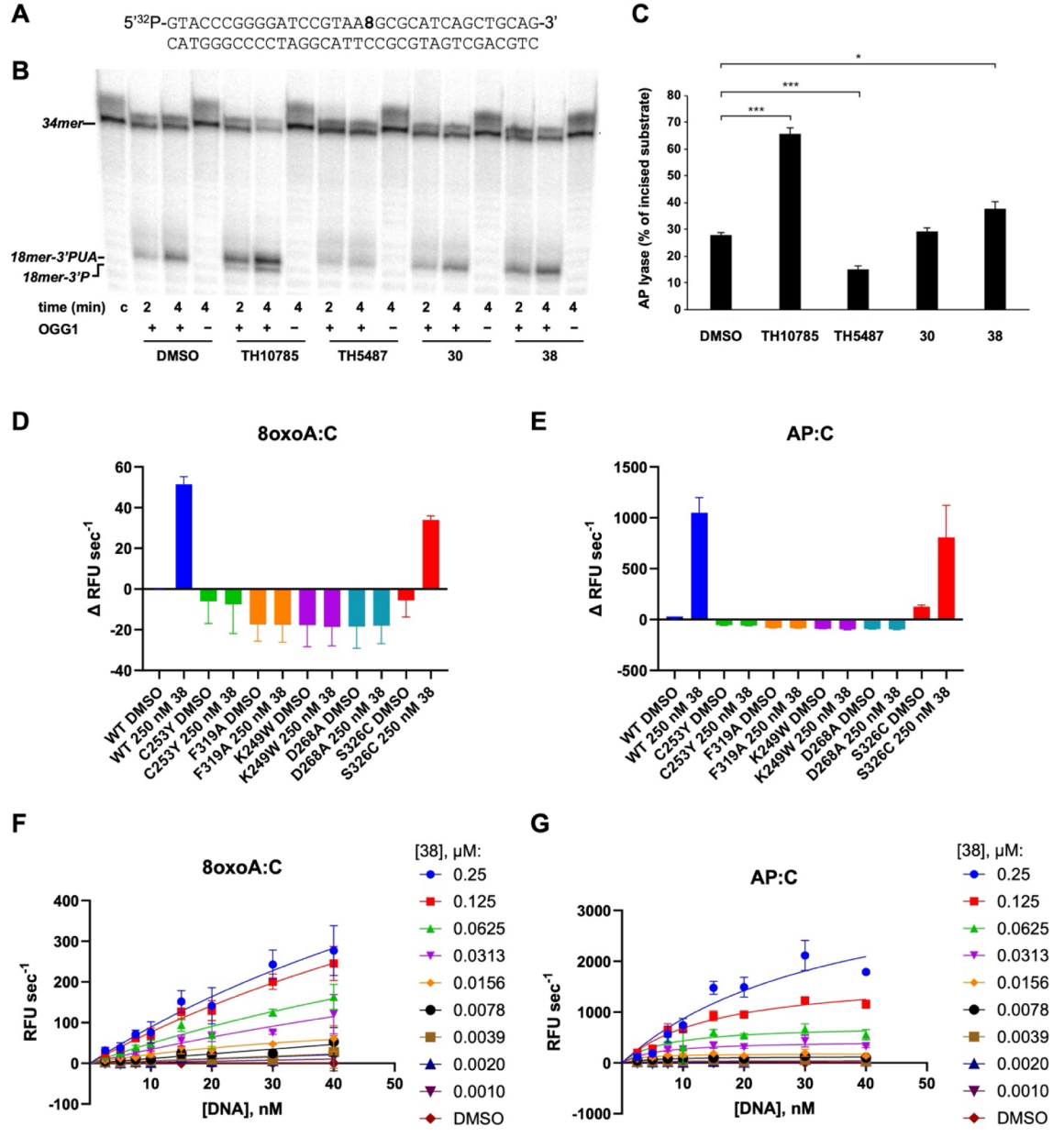


Figure 4. Effect of tryptamine ORCAs on the catalytic activity of OGG1. (A) $[^{32}P]$ 5′-labeled 8-oxoG-containing DNA substrate used during the reaction (8 stands for 8-oxoG). (B) 2 nM of the 8-oxoG-containing DNA substrate was incubated with either 10% DMSO, 6.25 μM TH10785, 50 μM TH5487, 6.25 μM **30**, or 10 μM **38**, as indicated, and in the presence (+) or absence (-) of 10 nM hOGG1. After incubation for the indicated times at 37 °C, reactions were stopped, the products were resolved by 7 M urea-20% PAGE and visualized by autoradiography. Position of products is indicated. (C) Bar chart shows the percentage of incised substrate obtained by hOGG1 after 4 min of reaction in the presence of the indicated compound (n = 3 each; means \pm SEM). Significance of results was determined with a two-tailed paired t-test. *p < 0.05; **p < 0.01; ***p < 0.001. (D) and (E) Assessment of wt and mutant OGG1 activation by **38**. Initial rates measured in the standard fluorophore-quencher assay using 10 nM 8-oxoA:C (D) or AP:C (E) substrate, 10 nM of wt, C253Y, F319A, K249W or D268A hOGG1, or 50 nM S326C hOGG1 and 0.25 μM of **38**; Δ RFU s⁻¹ = change of relative fluorescence units per second relative to wt hOGG1 DMSO. (F) and (G) Initial slope measured in the standard fluorophore-quencher assay using either the 8oxoA:C (F) or AP:C (G) DNA substrate at indicated concentrations in the presence of 10 nM hOGG1 and either DMSO or **38** at indicated concentrations. AP-sites were generated from U:C substrate using UDG.

TH10785 and **38**, whereas the effect of **30** was not significant (Figure 4C). This lack of effect may be attributed to differences in assay conditions relative to the fluorescence assay, which contains 2 mM MgCl₂, a known inhibitor of OGG1 AP lyase activity. ⁶⁵ As previously reported, ⁶⁷ TH10785 generated both β and β , δ -elimination products (3'-PUA and 3'-P, respectively), whereas **30** and **38** primarily induced β -elimination.

Because the assay in Figure 4B reflects the combined outcome of OGG1 glycosylase and AP-lyase activity, we next assessed the effect of serotonin ORCAs on each reaction individually. No significant effect on OGG1 glycosylase activity was detected (Figure S6), whereas cleavage of an AP-substrate was accelerated (Figure S7). The requirement for OGG1-ORCA cocatalysis was demonstrated by the lack of reaction in the absence of hOGG1.

Journal of Medicinal Chemistry

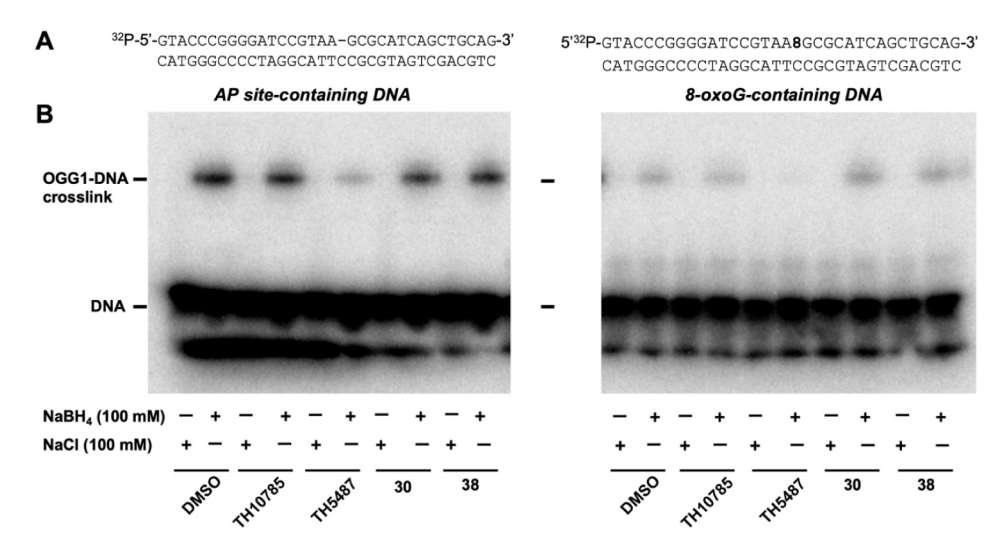


Figure 5. (A) The $[^{32}P]S'$ -labeled DNA substrates used. The AP-containing DNA substrate was prepared by treating an uracil-containing substrate with *E. coli* UDG. (B) Schiff-base trapping assay. 78 pM hOGG1 was incubated with either 1 nM of the $[^{32}P]S'$ -labeled AP-site-containing substrate (*left panel*), or 2 nM of the $[^{32}P]S'$ -labeled 80xoG-containing substrate (*right panel*), and 100 mM of either NaBH₄ or NaCl (as indicated), in the presence of 6.25 μM TH10785, 50 μM TH5487, 6.25 μM compound 30 or 10 μM compound 38. Products were resolved by SDS–PAGE and visualized by autoradiography.

Compound 38 was further evaluated against a panel of OGG1 mutants including mutations within and outside the active site, using the established fluorescence assay with either an 8-oxoA or AP substrate (Figure 4D,E). Promisingly, 38 accelerated the AP-lyase activity of the disease-associated mutant Ser326Cys. In contrast, 38 did not restore activity in active site mutants, consistent with the active site binding mode observed in the mOGG1-38 crystal structure.

Kinetic Analysis. Saturation kinetic studies where the rate of DNA cleavage was measured at increasing concentrations of DNA substrate revealed a faster resolution of AP-sites (Figure 4G) than 8-oxo sites (Figure 4F). This preference is consistent with previous observations for TH10785, 7 nucleobase, 10 and pyridine ORCAs. The increased rate likely stems from a lack of competition for active-site binding between the ORCA and the 8-oxo substrate, and the hydrolysis of the glycosidic bond being the rate-determining step in the presence of ORCAs. Another consequence of this acceleration was that a plateau was not achieved at 40 nM of the AP:C substrate, the highest concentration achievable within the assay.

Mechanistic Discussion. Various mechanisms have been postulated for the acceleration of OGG1 AP-lyase activity by small-molecules. 61,67,70,72 It has been suggested that the excised 8-oxoG may remain in the active site and catalyze β-elimination, although with negligible activity. 61,64,65,67 Structurally similar, but significantly more potent nucleobase ORCAs seem to follow the same mechanism, binding in a similar manner to 8-oxoG. 61,70 This hypothesis is further supported by the pH-dependence of nucleobase and pyridine ORCA activity, with compounds performing best at pH levels close to the p K_a of their basic nitrogen. 70,71 Similarly, the quinazoline ORCA TH10785 has been shown to bind in the active site and seems to rely on the basicity of its nitrogen (p K_a \approx 6.55) for activity.

Base-Assisted Catalysis. Our initial screening results were consistent with a base-assisted catalysis mechanism of activation. While the 2-pyridyltryptamine ORCA 1 enhanced activity, the 2-phenyltryptamine derivative TH12166 bound to OGG1, but inhibited activity. This was further supported by

the complete loss of activity in the phenyl analogue of 1, compound 7. Therefore, we hypothesized that a basic nitrogen able to participate in proton exchange was required for activation. However, the activity of the 2-phenyltryptamine 8 was not consistent with base-mediated activation. Although the activity of 8 is lower compared to its pyridyl analogue, the acceleration of AP-lyase activity was significant and implied the pyridine moiety in binding interactions rather than directly in activation.

Allosteric Activation. These results prompted us to investigate other possible modes of activation, including allosteric modulation. An allosteric mode of action has previously been proposed for the 8-oxoG analogue 8-bromoguanine as well as other undisclosed ORCAs. This was based on the argument that active site binding would result in competition between the 8-oxoG substrate and the ORCA. In contrast, initial rate analysis suggested that 8-bromoguanine binds with a similar affinity to the free enzyme and to the enzyme—substrate complex, consistent with a noncompetitive binding model. However, this could alternatively reflect the low affinity of the enzyme to 8-oxoG following base excision, as previously reported, 64,85 which would enable a rapid displacement of 8-oxoG by an ORCA following base excision.

In principle, an ideal ORCA would selectively bind to the Schiff-base DNA-enzyme complex without interfering with substrate binding. Nonetheless, partial inhibition of substrate binding can still result in net rate acceleration, since OGG1-catalyzed base excision is orders of magnitude faster than AP-lyase cleavage in the absence of an ORCA.⁶⁴ This balancing act between activation and inhibition is often visible in the form of a bell-shaped dose—response curve for TH10785 as well as ORCAs identified here and previously.^{67,70,71} In these cases, rate acceleration peaks at a certain concentration, and then declines at higher loadings, consistent with active-site inhibition. These observations, along with several OGG1-ORCA crystal structures presenting clear active-site binding and extensive SAR relationships with regards to active-site interactions, further supported by active-site mutant studies,

argue against an allosteric mechanism. Nevertheless, allostery remains a possible mechanism of activation for other ORCAs, and putative allosteric binding sites have been identified computationally. ^{72,86}

Schiff-Base Surrogate. DNA glycosylases can be broadly classified as monofunctional or bifunctional, depending on whether they possess AP-lyase activity in addition to base excision. Structurally, bifunctional glycosylases are distinguished by the presence of an N-terminal valine or proline α -NH₂ or a catalytic lysine residue in the active site — Lys249 in OGG1 — which traps the S_N1 oxocarbenium intermediate generated during base excision (Figure S1).87,88 This results in the formation of a Schiff-base intermediate. In contrast, monofunctional glycosylases rely on a nucleophilic water molecule within the active site to trap the oxocarbenium species.⁸⁹ Given the lysine-like ethylamine tail present in the tryptamine ORCAs, we considered whether this moiety might act as a surrogate for Lys249. For this purpose, we expressed the Lys249Ala and Lys249Trp mutants of OGG1, which lack glycosylase and AP-lyase activity. However, both 30 and 41 failed to restore AP-lyase activity of the Lys249Ala mutant in a PAGE assay (Figure S8), while 38 failed to restore activity of the Lys249Trp mutant in the standard fluorescence assay, suggesting 2-pyridyltryptamines cannot replace Lys249 in the active site.

Additionally, we confirmed that ORCAs do not exhibit their effect through accelerating the rate of Schiff-base formation, a key step for AP-lyase activity of bifunctional glycosylases. To test this, we trapped the Schiff base intermediate using NaBH₄ to generate an OGG1-DNA cross-link. As shown in Figure 5B, ORCAs TH10785, 30 and 38 had no discernible effect on the level of cross-linked product formed with either AP or 8-oxoG DNA substrates. These findings are consistent with rapid Schiff-base formation during/immediately after base excision, followed by ORCA binding to facilitate its cleavage.

Changes in Active Site Structure. The precise mechanism by which bifunctional glycosylases catalyze β -elimination is not completely understood. Nevertheless, it is agreed that deprotonation at the C2' of the Schiff-base intermediate is a key step. In addition to Lys249, another key catalytic residue shared by bifunctional glycosylases is an aspartic acid — Asp268 in OGG1. This residue likely stabilizes the developing negative charge on 8-oxoG during base excision, but may play a role in the ensuing elimination. ⁸⁷

Comparison of the cocrystal structures of mOGG1 with 30, TH10785 (Figure S9A,B), the inhibitor TH5487 (Figure S9C,D), and 1 (Figure S10) revealed little overall change in the active site structure with most amino acids occupying the same position. However, the absence of the DNA substrate presumed to influence active-site structure prevents more concrete conclusions.

Conserved Water Molecule. A conserved water molecule held in place by Asp45, has been proposed as the base responsible for C2' deprotonation in a related glycosylase, endonuclease III (Nth). Notably, Nth performs β -elimination orders of magnitude faster than OGG1, and does not retain the excised nucleobase in the active site. These mechanistic features raise the possibility of a similar catalytic strategy in tryptamine ORCA-mediated β -elimination by OGG1 facilitated by a network of water molecules stabilized by the ORCA as observed in the mOGG1-30 crystal structure (Figure 3B).

Consistent with this hypothesis, the water network lies in close proximity to the catalytic residues Lys249 and Asp268. Further support includes the loss of activity observed when the ethylamine chain was removed (15), shortened (39), extended (40) or replaced by an alcohol (47). In contrast, amine monomethylation (46) increased potency. Together, these results suggest that both the charged nature, and precise positioning of the ammonium moiety are critical for activation, potentially by maintaining the position of the catalytic water molecule within the active site.

Molecular Dynamics. OGG1-ORCA cocrystal structures were instrumental in guiding virtual docking studies during hit identification and lead optimization. However, their relevance with regards to the catalytic mechanism is limited by the absence of DNA, which may alter the catalytic pocket and ligand binding interactions. To obtain a more representative model of the OGG1-ORCA-DNA complex, we computationally replaced 8-oxoG with ligands **30** or **38** in the NaBH₄-trapped Schiff-base OGG1-DNA-8-oxoG complex (PDB: 1HU0). We then performed molecular dynamics (MD) simulations, over 200 ns in duplicate using AMBER20.

The clustered pose of the OGG1-DNA-30 complex following MD simulations revealed a "flipped" ligand orientation (Figure 6A) compared to the OGG1-30 crystal

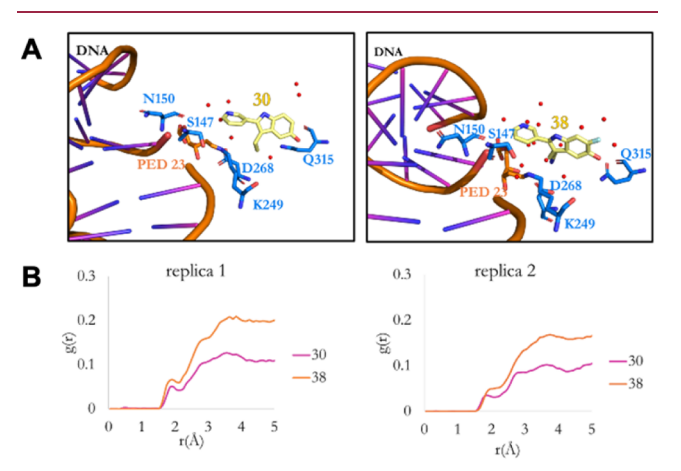


Figure 6. (A) Binding modes of ligands 30 and 38 obtained from clustering analysis of MD trajectories of OGG1:DNA:30 and OGG1:DNA:38 systems. Water molecules are colored in red. (B) Calculated RDF profiles calculated for ligand- O_{water} pairs.

structure (Figure 3B). The hydroxy group was directed away from Asn150, while the amine—Asp268 salt bridge persisted (Figure 3B). This challenges the SAR rationale that led to compounds 30 and 38.

Root mean square deviation (RMSD) values for DNA and protein backbones remained within 2.5 Å (Figure S11), and no secondary-structure changes were apparent by clustered geometry inspection. Root mean square fluctuation (RMSF) analysis showed most active-site residues were flexible except the ligand-binding residues Ser147, Asn150, Lys249, Asp268, and Gln315, which were more rigid (Figure S12). Both ligands retained conformations close to their docked poses (Figure S13), and RMSF profiles were similar, indicating that residue flexibility differences are unlikely to explain catalytic variation.

As in the cocrystal structures, multiple water molecules occupied the active site. Radial distribution function (RDF) analysis revealed greater hydration for 38 than for 30, with peaks at ~ 2 Å and ~ 3 Å corresponding to the first and second

Ī

hydration shells (Figure 6B). Waters within 5 Å of the ligand averaged up to 17 for 38 versus 12 for 30 (Table S5), enabling more extensive water-mediated hydrogen-bond networks with Ser147, Asn150, Lys249, Asp268, and Gln315 (Figure 6A). This enhanced hydration correlates with 38's superior β -elimination potency and supports a water-mediated catalytic mechanism.

CONCLUSION

We identified a novel class of serotonin-based small-molecule organocatalytic switches of OGG1-catalyzed cleavage of AP sites with improved potency, pharmacokinetic properties, and a distinct mechanism compared to previously reported ORCAs. Computational screening revealed 2-pyrid-3-yltryptamine (1) as a hit compound (AC₅₀ = 4.1 μ M). Guided by X-ray crystallography, molecular modeling, and enabled by Pdcatalyzed Larock chemistry, hit-to-lead optimization yielded the 5-OH derivative 30 (AC₅₀ = 0.58 μ M) and 5-OH-6-F derivative 38 (AC₅₀ = 0.040 μ M) over three rounds of optimization. 3-Unsubstituted 2-pyridylindoles also showed ORCA activity but remained less potent than optimized serotonin derivatives. Notably, compound 30 displayed improved pharmacokinetic properties over the benchmark ORCA TH10785, including enhanced solubility (>300 μ M), metabolic stability (>3.5 h in human microsomes), and superior lipophilic efficiency, although active efflux remains a limitation for future optimization.

Mechanistically, serotonin ORCAs promote β -elimination of AP-sites by OGG1. Yet, experimental data suggest a distinct activation mode from the previously proposed base-assisted catalysis mechanism. Lack of activity rescue in Lys249 mutants and lack of influence on native Schiff-base formation argue against tryptamine/AP-site Schiff-base formation. Competitive binding as well as crystallographic, SAR studies and MD simulations likewise disfavor an allosteric mechanism. Instead, the data support active-site binding of ORCAs in the 8-oxoG pocket. Once bound, ORCAs stabilize a network of water molecules to trigger β -elimination in an analogous manner to the bifunctional glycosylase Nth.

While this study advances understanding of OGG1 activation by serotonin-derived ORCAs, further mechanistic investigations will be required to fully elucidate their mode of action. Nevertheless, given the growing evidence for the therapeutic potential of ORCAs in reducing oxidative DNA damage, ^{67,72} and attenuating fibrosis in MASH, ⁷¹ the compounds reported herein provide valuable chemical tools for further investigations of OGG1 activation in a range of oxidative stress-driven diseases.

■ EXPERIMENTAL SECTION

Chemistry General Methods. Reagents and solvents were obtained from commercial suppliers and were not purified further unless specified. Dry solvents (THF, CH₂Cl₂, Et₂O, DMF) were provided by a PureSolv SPS-400-5 solvent purification system. Reactions were carried out in standard borosilicate glassware, 2 mL microwave vials with septum caps, or Pyrex culture tubes sealed with a phenolic cap with a PTFE liner. Room temperature was approximately 18–20 °C. Reactions at high temperature were heated using either a DrySyn metal heating bath, a sand bath, or a silicone oil bath. Reactions at 0 °C were performed using and ice/water bath, reactions at -5 °C were performed using an ice/brine mixture,

reactions at -78 °C were performed using dry ice/acetone baths, reactions at -84 °C were performed using liquid nitrogen/ethyl acetate baths.

¹H, ¹³C, and ¹⁹F (with ¹H decoupling) NMR spectra recorded at 400, 101, and 376 MHz, respectively, were recorded on a Bruker AVII 400 (BBFO probe). ¹H, ¹³C, and ¹⁹F (with ¹H decoupling) NMR spectra recorded at 500, 126, and 377 MHz, respectively, were recorded on either a Bruker AVIII-HD 500 (BBFO probe) or a Bruker AVIII 500 (BBFO+ probe). ¹H, and ¹³C NMR spectra recorded at 600 and 151 MHz, respectively, were recorded on a Bruker AVIII 600 (TXI probe). ¹H, and ¹³C NMR spectra recorded at 700 and 176 MHz, respectively, were recorded on a Bruker AVIII-HD 700 (Prodigy TCI probe). All spectra were recorded at room temperature with the deuterated solvents used as a lock for spectra and internal reference (CDCl₃: ¹H, 7.26 ppm; ¹³C, 77.16 ppm; (CD₃)₂CO: ¹H, 2.05 ppm, ¹³C, 29.8 ppm; (CD₃)₂SO: ¹H 2.50 ppm, ¹³C 39.5 ppm; CD₃OD: ¹H 3.31 ppm, ¹³C 49.0 ppm). NMR spectra are reported as follows: chemical shift/ppm (multiplicity, coupling constant(s), number of nuclei). Multiplicity given as bs (broad singlet), s (singlet), d (doublet), t (triplet), q (quartet), p (pentet), h (hextet), m (multiplet), and combinations thereof. Signals which overlap with one another are described as multiplets. Note that rotameric behavior was observed in some ¹H and ¹³C NMR spectra.

IR spectra were recorded using a Shimadzu IT Affinity-1 Fourier transform IR spectrophotometer with a Specac Quest ATR (diamond puck). The spectra were recorded as specified in the procedure as films, solids, or as neat liquids. Transmittance was recorded with maximal absorption wavenumbers given as cm⁻¹.

High resolution mass spectrometry (HRMS) spectra were recorded on a Bruker micrOTOF benchtop ESI with either positive or negative electrospray ionization or EI using a Thermo Mat 900XP, Double Focusing Hi-resolution mass spectrometer at the University of Edinburgh mass spectrometry facility (SIRCAMS).

TLC was carried out using Merck aluminum-backed silica plates coated with F254 fluorescent indicator, analyzed under UV light, and developed using aqueous KMnO₄, ethanolic vanillin, or *n*-butanol ninhydrin solutions where appropriate. Column chromatography was performed using silica gel (40-62 μm, Fluorochem), or in a Biotage SP1 MPLC system using Fisher Chemical silica gel 60 Å. Preparative high-performance liquid chromatography (HPLC) was performed on a Gilson system using Waters C18 OBD 5 μ m column (30 × 75 mm) with water buffer (either 0.1% aq. TFA, or 50 mM aq. NH₄HCO₃) and acetonitrile as mobile phases using a flow rate of 45 mL/min. Compound purity was measured by HPLC analysis performed on the Agilent 1260 Infinity II LC system coupled to single quadrupole MS Agilent LC/MSD XT. The separation was achieved with either an Avantor ACE 3 C8 (3.0 \times 50 mm, 3.0 μ m), an Avantor ACE Phenyl (3.0 \times 50 mm, 3.0 μ m), or a Waters XBridge C18 (3.0 × 50 mm, 3.5 μ m) column with a flow rate of 1 mL/min with a linear gradient of MeCN in either 0.1% aqueous TFA or 10 mM NH₄CO₃. All compounds used in biological assays had a > 95% purity as determined by HPLC.

General Procedure for the Preparation of Compounds 2–6. A Pyrex reaction vial was charged with tryptamine derivative (1.0 equiv), RuPhos Pd G1 methyl *t*-butyl ether adduct (5.0 mol %), K₂CO₃ (2.0 equiv), 3-

bromopyridine (1.5 equiv) and DMA (400 μ L per 0.10 mmol of tryptamine). The vial was flushed with N₂, sealed, and heated to 120 °C for 24 h. After cooling to RT, the reaction mixture was diluted with EtOAc (5 mL per 0.10 mmol of tryptamine) and filtered through a plug of Celite. The volatiles were removed under reduced pressure, and the residue was purified by preparative HPLC.

2-(5-Methyl-2-(pyridin-3-yl)-1H-indol-3-yl)ethan-1-amine (2). Prepared according to General Procedure A from 5-methyltryptamine hydrochloride (21.1 mg, 1.00 equiv., 0.100 mmol) and K_2CO_3 (41.5 mg, 3.00 equiv., 0.300 mmol). Purified by preparative HPLC (10 to 50% MeCN in 50 mM aq. NH₄CO₃) to afford the product as a colorless solid (5.5 mg, 22%). ¹H NMR (600 MHz, (CD₃)₂SO with H₂SO₄) δ 11.20 (s, 1H), 8.88 (s, 1H), 8.55 (d, J = 5.2 Hz, 1H), 8.12 -7.99 (m, 1H), 7.53 -7.48 (m, 1H), 7.40 (d, J = 5.2 Hz, 1H), 7.27 (d, J = 8.5 Hz, 1H), 6.96 (d, J = 8.7 Hz, 1H), 3.25 -3.18 (m, 1H), 2.96 -2.85 (m, 3H), 2.40 (s, 3H). ¹³C NMR (151 MHz, (CD₃)₂SO with H₂SO₄) δ 144.8, 140.4, 140.3, 135.8, 132.2, 129.0, 128.7, 128.7, 128.2, 125.9, 119.1, 112.4, 111.0, 39.0, 22.8, 21.8. HRMS (ESI) m/z calcd. for [M + H]⁺ (C₁₆H₁₈N₃): 252.1495, found: 252.1495.

2-(5-Methoxy-2-(pyridin-3-yl)-1H-indol-3-yl)ethan-1-amine, TFA Salt (3). Prepared according to General Procedure A from 5-methoxytryptamine (19.0 mg, 1.00 equiv., 0.100 mmol). Purified by preparative HPLC (0 to 50% MeCN in 0.1% aq. TFA) to afford the product as a beige solid (6.4 mg, 13%). ¹H NMR (600 MHz, $(CD_3)_2SO)$ δ 11.36 (s, 1H), 8.87 (s, 1H), 8.63 (d, J = 5.0 Hz, 1H), 8.07 (dt, J = 8.3, 2.0 Hz, 1H), 7.86 (s, 3H), 7.60 (dd, J = 8.2, 5.0 Hz, 1H), 7.31 (d, J = 9.1 Hz, 1H), 7.14 (d, J = 2.5 Hz, 1H), 6.83 (dd, J = 9.1, 2.1 Hz, 1H), 3.81 (s, 3H), 3.14 – 3.04 (m, 4H). ¹³C NMR (151 MHz, $(CD_3)_2SO)$ δ 153.6, 147.6, 135.9, 132.2, 131.5, 128.8, 128.5, 124.1, 112.6, 112.3, 107.9, 100.3, 55.5, 40.0, 22.7. HRMS (ESI) m/z calcd. for $[M + H]^+$ $(C_{16}H_{18}N_3O_1)$: 268.1444, found: 268.1460.

2-(5-Chloro-2-(pyridin-3-yl)-1H-indol-3-yl)ethan-1-amine (4). Prepared according to General Procedure A from 5-chlorotryptamine hydrochloride (57.8 mg, 1.00 equiv., 0.250 mmol). Purified by preparative HPLC (0 to 50% MeCN in 50 mM aq. NH₄CO₃) to afford the product as a beige solid (1.7 mg, 2.5%). H NMR (600 MHz, (CD₃)₂SO) δ 11.56 (s, 1H), 8.89 (d, J = 2.4 Hz, 1H), 8.59 (d, J = 4.5 Hz, 1H), 8.08 (d, J = 8.7 Hz, 1H), 7.67 (d, J = 2.1 Hz, 1H), 7.54 (dd, J = 8.2, 5.0 Hz, 1H), 7.39 (d, J = 8.7 Hz, 1H), 7.13 (dd, J = 8.7, 2.1 Hz, 1H), 2.97 – 2.78 (m, 4H). ¹³C NMR (151 MHz, (CD₃)₂SO) δ 148.4 (2C), 135.2, 134.7, 133.0, 129.8, 128.5, 123.8, 123.5, 121.9, 118.2, 112.8, 111.1, 42.7, 28.4. HRMS (ESI) m/z calcd. for [M + H]⁺ (C₁₅H₁₅ ³⁵Cl₁N₃): 272.0949, found: 272.0939.

2-(7-Methyl-2-(pyridin-3-yl)-1H-indol-3-yl)ethan-1-amine, TFA salt (5). Prepared according to General Procedure A from 7-methyltryptamine (17.4 mg, 1.00 equiv., 0.100 mmol). Purified by preparative HPLC (10 to 50% MeCN in 0.1% aq. TFA) to afford the product as an off-white solid (11.4 mg, 22%). 1 H NMR (600 MHz, (CD₃)₂SO) δ 11.26 (s, 1H), 8.92 (s, 1H), 8.68 (d, J = 5.2 Hz, 1H), 8.16 (dt, J = 8.2, 2.0 Hz, 1H), 7.89 (s, 3H), 7.66 (dd, J = 8.2, 5.2 Hz, 1H), 7.49 (d, J = 8.2 Hz, 1H), 7.06 – 6.91 (m, 2H), 3.16 – 3.00 (m, 4H), 2.51 (s, 3H). 13 C NMR (151 MHz, (CD₃)₂SO) δ 147.7, 147.2, 137.3, 136.0, 131.6, 128.9, 127.7, 124.2, 122.9, 121.1, 119.6, 116.1, 108.7, 22.7, 16.9. Note: overlap of CH₂NH₂ signal with residual solvent signal at 39.5 ppm. HRMS (ESI) m/z calcd. for $[M + H]^+$ (C₁₆H₁₈N₃): 252.1495, found: 252.1503.

2-Amino-3-(2-(pyridin-3-yl)-1H-indol-3-yl)propanoic Acid, TFA Salt (6). Prepared according to General Procedure A from DL-tryptophan (20.4 mg, 1.00 equiv., 0.100 mmol). Purified by preparative HPLC (0 to 40% MeCN in 0.1% aq. TFA) to afford the product as a beige solid (1.0 mg, 2%). ¹H NMR (600 MHz, (CD₃)₂SO with H₂SO₄) δ 9.06 (s, 1H), 8.90 (d, J = 6.2 Hz, 1H), 8.74 (d, J = 8.6 Hz, 1H), 8.19 (dd, J = 8.4, 6.2 Hz, 1H), 8.13 (d, J = 5.5 Hz, 3H), 7.66 (d, J = 8.3 Hz, 1H), 7.46 (d, J = 8.3 Hz, 1H), 7.19 (t, J = 7.5 Hz, 1H), 7.07 (t, J = 7.6 Hz, 1H), 3.99 – 3.93 (m, 1H), 3.45 (dd, J = 14.9, 7.5 Hz, 1H), 3.38 (dd, J = 15.1, 7.4 Hz, 1H). ¹³C NMR (151 MHz, (CD₃)₂SO with H₂SO₄) δ 171.0, 145.9, 141.2, 140.8, 137.3, 132.3, 130.3, 128.2, 128.1, 123.8, 120.4, 119.7, 112.6, 108.6, 53.1, 25.9. HRMS (ESI) m/z calcd. for [M + H]⁺ (C₁₆H₁₆N₃O₂): 282.1237, found: 282.1254.

General Procedure B for the Preparation of Compounds 7–9. A Pyrex reaction vial was charged with tryptamine derivative (1.0 equiv), $Pd(OAc)_2$ (15 mol %), $Pd(OAc)_2$ (16 mol %), $Pd(OAc)_2$ (17 mol %), $Pd(OAc)_2$ (17 mol %), $Pd(OAc)_2$ (18 m

2-Phenyltryptamine (7). Prepared according to General Procedure B from tryptamine (34 mg, 1.0 equiv., 0.21 mmol). Product was purified by column chromatography (0 to 15% MeOH in CH₂Cl₂ + 1% NH₄OH 37% aq. solution) to afford the product as a brown solid (2.9 mg, 6%). H NMR (500 MHz, (CD₃)₂SO) δ 11.17 (s, 1H), 7.67 (d, J = 6.9 Hz, 2H), 7.59 (d, J = 7.7 Hz, 1H), 7.51 (t, J = 7.7 Hz, 2H), 7.40 – 7.33 (m, 2H), 7.10 (t, J = 7.5 Hz, 1H), 7.01 (t, J = 7.3 Hz, 1H), 2.99 – 2.93 (m, 2H), 2.92 – 2.81 (m, 2H). 13 C NMR (126 MHz, (CD₃)₂SO) δ 136.0, 134.5, 132.9, 128.8, 128.7, 127.8, 127.3, 121.5, 118.7, 118.7, 111.2, 109.4, 42.4, 28.1. Spectral data were consistent with those reported in the literature.

5-Hydroxy-2-phenyltryptamine (8). Prepared according to General Procedure B from 5-hydroxytryptamine (17.6 mg, 1.00 equiv., 0.100 mmol). Product was purified by preparative HPLC (30 to 80% MeCN in 50 mM aq. NH₄CO₃) to afford the product as a dark brown solid (2.8 mg, 11%). ¹H NMR (500 MHz, CD₃OD) δ 7.63 – 7.57 (m, 2H), 7.47 (t, J = 7.8 Hz, 2H), 7.38 – 7.31 (m, 1H), 7.21 (d, J = 8.7 Hz, 1H), 6.97 (d, J = 2.3 Hz, 1H), 6.71 (dd, J = 8.6, 2.3 Hz, 1H), 3.11 – 3.05 (m, 2H), 3.02 – 2.96 (m, 2H). ¹³C NMR (126 MHz, CD₃OD) δ 151.6, 137.5, 134.8, 132.7, 130.9, 129.8, 129.1, 128.5, 112.9, 112.7, 108.4, 103.5, 42.4, 27.2. HRMS (ESI) m/z calcd. for [M + H]⁺ (C₁₆H₁₇N₂O₁): 253.1335, found: 253.1348.

6-Fluoro-2-phenyltryptamine TFA Salt (9). Prepared according to General Procedure B from 6-fluorotryptamine hydrochloride (21.5 mg, 1.00 equiv., 0.100 mmol). Product was purified by preparative HPLC (30 to 70% MeCN in 0.1% aq. TFA) to afford the product as a brown solid (13.9 mg, 39%). ¹H NMR (600 MHz, (CD₃)₂SO) δ 11.48 (s, 1H), 8.00 (s, 3H), 7.64 – 7.61 (m, 3H), 7.52 (t, J = 7.5 Hz, 2H), 7.42 (t, J = 7.4 Hz, 1H), 7.14 (dd, J = 9.9, 2.4 Hz, 1H), 6.93 (td, J = 9.4, 2.4 Hz, 1H), 3.17 – 3.11 (m, 2H), 3.09 – 3.03 (m, 2H). ¹³C NMR (151 MHz, (CD₃)₂SO) δ, 159.2 (d, ${}^{1}J_{CF}$ = 235.5 Hz), 135.9 (d, ${}^{3}J_{CF}$ = 12.8 Hz),135.7, 132.2, 128.9, 127.8, 127.7, 125.2, 119.4 (d, ${}^{3}J_{CF}$ = 10.2 Hz), 107.5 (d, ${}^{2}J_{CF}$ = 24.2

Hz), 106.8, 97.3 (d, ${}^2J_{CF}$ = 25.6 Hz), 39.3, 22.8. HRMS (ESI) m/z calcd. for [M + H]⁺ (C₁₆H₁₆F₁N₂): 255.1292, found: 255.1304.

General Procedure C for the Preparation of Compounds 10-13, 24. A microwave vial under air was charged with substituted phenylhydrazine hydrochloride (1.50 equiv., 0.750 mmol), KOAc (73.6 mg, 1.50 equiv., 0.750 mmol), 3acetylpyridine (67 μ L, 1.0 equiv., 0.50 mmol), and EtOH (0.75 mL). The vial was sealed, and the mixture was stirred at 80 °C in a microwave reactor for 5 min. The mixture was then directly transferred to a Pyrex reaction tube containing preheated polyphosphoric acid (approximately 1 to 1.5 g) at 110 °C. The mixture was stirred at this temperature for 90 min. After cooling to RT, the mixture was partitioned between water (5 mL) and CH₂Cl₂ (5 mL). The aqueous phase was further extracted with CH_2Cl_2 (3 × 15 mL). The combined organic phases were dried over anhydrous MgSO₄, filtered, and volatiles were removed under reduced pressure. The residue was purified by preparative HPLC or column chromatography (silica gel).

2-(Pyridin-3-yl)-1H-indole (10). Prepared according to General Procedure C from 3-acetylpyridine (110 μL, 1.00 equiv., 1.00 mmol) and phenylhydrazine (108 μL, 1.10 equiv., 1.10 mmol). Product was purified by column chromatography (30 to 55% EtOAc in hexane) to afford the product as a beige solid (21.7 mg, 11%). H NMR (500 MHz, CDCl₃) δ 8.98 (d, J = 2.3 Hz, 1H), 8.79 (s, 1H), 8.56 (dd, J = 4.8, 1.6 Hz, 1H), 7.95 (dt, J = 8.1, 2.0 Hz, 1H), 7.66 (d, J = 7.9 Hz, 1H), 7.42 (d, J = 8.1 Hz, 1H), 7.37 (dd, J = 8.0, 4.8 Hz, 1H), 7.23 (t, J = 7.5 Hz, 1H), 7.15 (t, J = 7.4 Hz, 1H), 6.90 (d, J = 2.1 Hz, 1H). NMR (126 MHz, CDCl₃) δ 148.5, 146.5, 137.4, 134.6, 132.6, 129.1, 128.7, 124.0, 123.2, 121.0, 120.7, 111.3, 101.4. Spectral data were consistent with those reported in literature.

5-Methyl-2-(pyridin-3-yl)-1H-indole, TFA Salt (11). Prepared according to General Procedure C from 4-methylphenylhydrazine hydrochloride (119 mg, 1.50 equiv., 0.750 mmol). Product was purified by preparative HPLC (20 to 50% MeCN in 0.1% aq. TFA) to afford the product as a light brown solid (22.4 mg, 14%). H NMR (600 MHz, (CD₃)₂SO) δ 9.25 (s, 1H), 8.67 (d, J = 5.8 Hz, 1H), 8.63 (dt, J = 8.6, 1.6 Hz, 1H), 7.84 (dd, J = 8.6, 5.6 Hz, 1H), 7.36 (s, 1H), 7.35 (d, J = 8.7 Hz, 1H), 7.11 (d, J = 2.2 Hz, 1H), 7.01 (dd, J = 8.5, 1.6 Hz, 1H), 2.37 (s, 3H). The NMR (151 MHz, (CD₃)₂SO) δ 143.0, 141.3, 136.7, 136.1, 132.5, 130.4, 128.6, 128.5, 126.0, 124.7, 120.2, 111.4, 101.3, 21.2. HRMS (ESI) m/z calcd. for $[M + H]^+$ (C₁₄H₁₃N₂): 209.1073, found: 209.1070.

5-Fluoro-2-(pyridin-3-yl)-1H-indole, TFA Salt (12). Prepared according to General Procedure C from 4-fluorophenylhydrazine hydrochloride (122 mg, 1.50 equiv., 0.750 mmol). Product was purified by preparative HPLC (20 to 50% MeCN in 0.1% aq. TFA) to afford the product as a redbrown solid (5.2 mg, 3%). ¹H NMR (600 MHz, (CD₃)₂SO) δ 11.89 (s, 1H), 9.18 (s, 1H), 8.62 (d, J = 5.4 Hz, 1H), 8.43 (d, J = 9.1 Hz, 1H), 7.69 (dd, J = 8.4, 5.3 Hz, 1H), 7.44 (dd, J = 9.2, 4.5 Hz, 1H), 7.35 (dd, J = 9.8, 2.6 Hz, 1H), 7.12 (d, J = 2.3 Hz, 1H), 7.01 (td, J = 9.3, 2.6 Hz, 1H). ¹³C NMR (151 MHz, (CD₃)₂SO) δ 157.3 (d, ${}^{1}J_{CF}$ = 232.9 Hz), 146.0, 144.0, 135.4, 134.6, 134.2, 128.9, 128.5 (d, ${}^{3}J_{CF}$ = 10.6 Hz), 125.0, 112.6 (d, ${}^{3}J_{CF}$ = 9.8 Hz), 110.8 (d, ${}^{2}J_{CF}$ = 26.2 Hz), 104.9 (d, ${}^{2}J_{CF}$ = 23.3 Hz), 100.9. HRMS (ESI) m/z calcd. for [M + H]⁺ (C₁₃H₁₀F₁N₂): 213.0823, found: 213.0820.

5-Bromo-2-(pyridin-3-yl)-1H-indole, TFA Salt (13). Prepared according to General Procedure C from 4-bromophe-

nylhydrazine hydrochloride (168 mg, 1.50 equiv., 0.750 mmol). Product was purified by preparative HPLC (20 to 50% MeCN in 0.1% aq. TFA) to afford the product as a brown solid (2.1 mg, 1%). 1 H NMR (400 MHz, (CD₃)₂SO) δ 11.90 (s, 1H), 9.10 (d, J = 2.5 Hz, 1H), 8.53 (dd, J = 4.7, 1.6 Hz, 1H), 8.22 (ddd, J = 8.0, 2.4, 1.6 Hz, 1H), 7.75 (d, J = 1.9 Hz, 1H), 7.50 (ddd, J = 8.0, 4.8, 0.9 Hz, 1H), 7.39 (d, J = 8.6 Hz, 1H), 7.24 (dd, J = 8.6, 2.0 Hz, 1H), 7.03 (s, 1H). 13 C NMR (151 MHz, (CD₃)₂SO) δ 148.6, 146.4, 136.1, 136.0, 132.3, 130.3, 127.6, 124.5, 124.0, 122.4, 113.4, 112.1, 99.4. HRMS (ESI) m/z calcd. for [M + H]⁺ (C₁₃H₁₀⁷⁹Br₁N₂): 273.0022, found: 273.0044.

(2-Pyridin-4-yl)-1H-indole (24). Prepared according to General Procedure C from 4-acetylpyridine (111 μL, 1.00 equiv., 1.00 mmol) and phenylhydrazine (108 μL, 1.10 equiv., 1.10 mmol). Product was purified by column chromatography (30 to 55% EtOAc in hexane) to afford the product as a beige solid (19.2 mg, 10%). Note: rotary evaporator bath kept at 30 °C to avoid decomposition. ¹H NMR (500 MHz, CD₃OD) δ 8.51 (d, J = 5.9 Hz, 2H), 7.80 - 7.74 (m, 2H), 7.58 (dt, J = 8.0, 1.0 Hz, 1H), 7.43 (dd, J = 8.2, 1.0 Hz, 1H), 7.18 (ddd, J = 8.2, 7.0, 1.1 Hz, 1H), 7.11 (d, J = 0.9 Hz, 1H), 7.05 (ddd, J = 8.0, 7.0, 1.0 Hz, 1H). ¹³C NMR (126 MHz, CD₃OD) δ 150.4, 142.4, 139.6, 135.5, 130.0, 124.4, 122.0, 121.1, 120.6, 112.5, 103.5. Spectral data were consistent with those reported in literature.

5-Methoxy-2-(pyridin-3-yl)-1H-indole, TFA Salt (14). A Pyrex reaction tube was charged with N-Boc-5-methoxy-1Hindole-2-boronic acid (150 mg, 1.00 equiv., 0.51 mmol), 3bromopyridine (50 μ L, 1.0 equiv., 0.52 mmol,), Pd(PPh₃)₄ (27.3 mg, 5.0 mol %, 0.024 mmol), Na₂CO₃ (133 mg, 2.50 equiv., 1.25 mmol), and a 1,4-dioxane/water mixture (2:1, 3.0 mL). The vial was flushed with N2, sealed, and the mixture was stirred at 60 °C for 18 h. After cooling to RT, volatiles were removed under reduced pressure, and CH₂Cl₂ (5.0 mL) was added, followed by TFA (2.0 mL). The mixture was stirred at RT for 2 h, after which sat. NaHCO₃ solution (10 mL) was added. The mixture was extracted with CH_2Cl_2 (2 × 15 mL), the combined organic phases were dried over anhydrous MgSO₄, filtered, and volatiles were removed under reduced pressure. The residue was purified by preparative HPLC (20 to 50% MeCN in 0.1% aq. TFA) to afford the product as an offwhite solid (71 mg, 41%). ¹H NMR (400 MHz, (CD₃)₂SO) δ 11.69 (s, 1H), 9.18 (d, J = 2.3 Hz, 1H), 8.61 (dd, J = 5.1, 1.5 Hz, 1H), 8.50 (dt, J = 8.3, 1.8 Hz, 1H), 7.75 (dd, J = 8.2, 5.1 Hz, 1H), 7.34 (d, J = 8.8 Hz, 1H), 7.10 - 7.05 (m, 2H), 6.82(dd, J = 8.8, 2.4 Hz, 1H), 3.77 (s, 3H). ¹³C NMR (151 MHz, $(CD_3)_2SO)$ δ 153.9, 143.5, 141.8, 136.1, 133.1, 132.9, 130.1, 128.7, 125.7, 113.5, 112.4, 101.7, 101.3, 55.3. HRMS (ESI) *m*/ z calcd. for $[M + H]^+$ $(C_{14}H_{13}N_2O_1)$: 225.1022, found: 225.1033.

2-(Pyridin-3-yl)-1H-indol-5-ol (15). A round-bottom flask under air was charged with 5-methoxy-2-(pyridin-3-yl)-1H-indole (68 mg, 1.0 equiv., 0.20 mmol), and HBr (1.0 mL, 33% in AcOH). The solution was heated 70 °C for 2 min and was then allowed to cool to RT, and was stirred for 18 h. The volatiles were removed under reduced pressure, and the residue was purified by preparative HPLC (10 to 50% MeCN in 50 mM aq. NH₄CO₃) to afford the product as a light brown solid (12 mg, 29%). ¹H NMR (600 MHz, (CD₃)₂SO) δ 11.36 (s, 1H), 9.05 (s, 1H), 8.74 (s, 1H), 8.46 (d, J = 4.9 Hz, 1H), 8.15 (d, J = 8.9 Hz, 1H), 7.45 (dd, J = 8.4, 5.0 Hz, 1H), 7.21 (d, J = 9.1 Hz, 1H), 6.87 – 6.83 (m, 2H), 6.66 (dd, J = 8.9, 2.3

Hz, 1H). ¹³C NMR (151 MHz, (CD₃)₂SO) δ 151.1, 147.9, 146.1, 134.7, 132.0, 131.7, 129.2, 128.3, 123.9, 112.7, 111.8, 103.9, 99.1. HRMS (ESI) m/z calcd. for [M + H]⁺ (C₁₃H₁₁N₂O₁): 211.0866, found: 211.0861.

General Procedure D for the Preparation of Compounds 16–23. A Pyrex reaction tube was charged with N-Boc-1H-indole-2-boronic acid (52 mg, 1.0 equiv., 0.20 mmol), aryl halide (1.0 equiv., 0.20 mmol), Pd(PPh₃)₄ (12 mg, 5.0 mol %, 0.010 mmol,), Na₂CO₃ (55 mg, 2.5 equiv., 0.50 mmol), and a 1,4-dioxane/water mixture (2:1, 1.5 mL). The vial was flushed with N₂, sealed, and the mixture was stirred at 100 °C for 18 h. After cooling to RT, volatiles were removed under reduced pressure, and the residue was purified by MPLC (0 to 30% MeOH in CH₂Cl₂). The Boc-protected indole was dissolved in CH₂Cl₂/TFA (1:1, 2.0 mL), and the mixture was stirred at RT for 2 h. Volatiles were removed under reduced pressure to afford the product as the TFA salt.

2-(6-Fluoropyridin-3-yl)-1H-indole, TFA Salt (17). Prepared according to General Procedure D from 5-bromo-2-fluoropyridine (35.2 mg, 1.00 equiv., 0.200 mmol) to afford the product as a brown solid (26.9 mg, 41%). H NMR (600 MHz, (CD₃)₂SO) δ 11.69 (s, 1H), 8.75 (d, J = 2.7 Hz, 1H), 8.42 (td, J = 8.2, 2.7 Hz, 1H), 7.56 (d, J = 8.2 Hz, 1H), 7.43 (d, J = 8.3 Hz, 1H), 7.30 (dd, J = 8.8, 2.7 Hz, 1H), 7.14 (t, J = 7.7 Hz, 1H), 7.05 – 6.98 (m, 2H). CNMR (151 MHz, (CD₃)₂SO) δ 162.2 (d, $^{1}J_{CF} = 236.2$ Hz), 143.8 (d, $^{3}J_{CF} = 15.3$ Hz), 138.4 (d, $^{3}J_{CF} = 7.8$ Hz), 137.3, 133.5, 128.4, 126.9 (d, $^{4}J_{CF} = 4.4$ Hz), 122.2, 120.3, 119.7, 111.4, 109.90 (d, $^{2}J_{CF} = 38.0$ Hz), 99.9. HRMS (ESI) m/z calcd. for [M + H]⁺ (C₁₃H₁₀F₁N₂): 213.0823, found: 213.0836.

(1H-Indol-2-yl)pyridin-3-amine, TFA Salt (18). Prepared according to General Procedure D from 3-bromo-5-amino-pyridine (34.6 mg, 1.00 equiv., 0.200 mmol) to afford the product as a beige solid (21.9 mg, 34%). ¹H NMR (600 MHz, (CD₃)₂SO) δ 8.47 (s, 1H), 7.97 (s, 1H), 7.89 (s, 1H), 7.60 (d, J = 8.2 Hz, 1H), 7.45 (d, J = 8.3 Hz, 1H), 7.18 (t, J = 7.7 Hz, 1H), 7.08 (d, J = 2.2 Hz, 1H), 7.05 (t, J = 7.7 Hz, 1H). ¹³C NMR (151 MHz, (CD₃)₂SO) δ 147.5, 137.6, 132.3, 131.5, 128.1, 126.0, 125.7, 123.0, 121.2, 120.8, 120.0, 111.8, 101.8. HRMS (ESI) m/z calcd. for [M + H]⁺ (C₁₃H₁₂N₃): 210.1026, found: 210.1027.

5-(1H-Indol-2-yl)pyridin-2-amine, TFA Salt (19). Prepared according to General Procedure D from 5-bromo-2-amino-pyridine (34.7 mg, 1.00 equiv., 0.200 mmol). To afford the product as a light brown solid (11.0 mg, 17%). ¹H NMR (600 MHz, (CD₃)₂SO) δ 11.59 (s, 1H), 8.39 (d, J = 2.3 Hz, 1H), 8.34 (dd, J = 9.4, 2.2 Hz, 1H), 7.53 (d, J = 8.3 Hz, 1H), 7.39 (d, J = 8.3 Hz, 1H), 7.12 (t, J = 7.7 Hz, 1H), 7.05 – 6.99 (m, 2H), 6.89 (d, J = 2.3 Hz, 1H). ¹³C NMR (151 MHz, (CD₃)₂SO) δ 153.6, 140.3, 137.1, 132.9, 132.4, 128.3, 122.0,

120.1, 119.6, 117.7, 113.4, 111.2, 99.1. HRMS (ESI) m/z calcd. for $[M + H]^+$ ($C_{13}H_{11}N_3$): 210.1026, found: 210.1034.

5-(1H-Indol-2-yl)pyridin-3-ol, TFA Salt (20). Prepared according to General Procedure D from 3-bromo-5-hydrox-ypyridine (34.9 mg, 1.00 equiv., 0.200 mmol) to afford the product as a beige solid (18.1 mg, 28%). ¹H NMR (600 MHz, (CD₃)₂SO) δ 11.73 (s, 1H), 8.69 (s, 1H), 8.16 (s, 1H), 7.85 (s, 1H), 7.58 (d, J = 8.3 Hz, 1H), 7.43 (d, J = 8.4 Hz, 1H), 7.16 (t, J = 7.7 Hz, 1H), 7.08 (d, J = 2.2 Hz, 1H), 7.04 (t, J = 7.6 Hz, 1H). ¹³C NMR (151 MHz, (CD₃)₂SO) δ 154.9, 137.5, 134.4, 133.3, 133.2, 130.4, 128.2, 122.6, 121.0, 120.5, 119.8, 111.6, 101.0. HRMS (ESI) m/z calcd. for [M + H]⁺ (C₁₃H₁₀N₂O₁): 211.0866, found: 211.0879.

5-(1H-Indol-2-yl)pyridin-2-ol, TFA Salt (21). Prepared according to General Procedure D from 2-hydroxy-5-iodopyridine (44.3 mg, 1.00 equiv., 0.200 mmol) to afford the product as a dark green solid (21.9 mg, 34%). ¹H NMR (600 MHz, (CD₃)₂SO) δ 11.34 (s, 1H), 7.95 (dd, J = 9.6, 2.6 Hz, 1H), 7.91 (d, J = 2.7 Hz, 1H), 7.46 (d, J = 8.3 Hz, 1H), 7.33 (d, J = 8.4 Hz, 1H), 7.05 (t, J = 7.7 Hz, 1H), 6.96 (t, J = 7.6 Hz, 1H), 6.68 (d, J = 2.2 Hz, 1H), 6.46 (d, J = 9.7 Hz, 1H). ¹³C NMR (151 MHz, (CD₃)₂SO) δ 161.6, 139.0, 136.8, 134.6, 131.1, 128.6, 121.2, 120.4, 119.5, 119.3, 111.2, 110.9, 97.3. HRMS (ESI) m/z calcd. for [M + H]⁺ (C₁₃H₁₀N₂O₁): 211.0866, found: 211.0867.

2-(6-Chloropyridin-3-yl)-1H-indole, TFA Salt (22). Prepared according to General Procedure D from 5-bromo-2-chloropyridine (38.5 mg, 1.00 equiv., 0.200 mmol) to afford the product as a brown solid (8.6 mg, 13%). ¹H NMR (600 MHz, CDCl₃) δ 8.68 (d, J = 2.7 Hz, 1H), 8.54 (s, 1H), 7.89 (dd, J = 8.5, 2.7 Hz, 1H), 7.64 (d, J = 8.5 Hz, 1H), 7.41 (d, J = 8.3 Hz, 1H), 7.38 (d, J = 8.8 Hz, 1H), 7.24 (t, J = 7.7 Hz, 1H), 7.15 (t, J = 7.8 Hz, 1H), 6.87 (d, J = 2.3 Hz, 1H). ¹³C NMR (151 MHz, CDCl₃) δ 150.2, 146.0, 137.4, 135.3, 133.3, 129.0, 127.7, 124.7, 123.5, 121.1, 120.9, 111.3, 102.0. HRMS (ESI) m/z calcd. for $[M + H]^+$ ($C_{13}H_{10}^{35}Cl_1N_2$): 229.0527, found: 229.0541

2-(6-Methylpyridin-3-yl)-1H-indole, TFA Salt (23). Prepared according to General Procedure D from 5-bromo-2-methylpyridine (34.3 mg, 1.00 equiv., 0.200 mmol) to afford the product as a light brown solid (11.2 mg, 19%). H NMR (600 MHz, (CD₃)₂SO) δ 11.80 (s, 1H), 9.09 (d, J = 2.5 Hz, 1H), 8.54 - 8.49 (m, 1H), 7.69 (d, J = 9.0 Hz, 1H), 7.58 (d, J = 8.4 Hz, 1H), 7.44 (d, J = 8.5 Hz, 1H), 7.19 - 7.12 (m, 2H), 7.04 (t, J = 7.6 Hz, 1H), 2.62 (s, 3H). To NMR (151 MHz, (CD₃)₂SO) δ 153.9, 140.9, 137.5, 136.7, 132.9, 128.3, 127.4, 125.7, 122.6, 120.5, 119.9, 111.5, 100.9, 21.3. HRMS (ESI) m/z calcd. for M = M + M + M + M =

General Procedure E for the Preparation of Compounds 25–27. A Pyrex reaction tube was charged with N-Boc-1H-indole-2-boronic acid (26 mg, 1.0 equiv., 0.10 mmol), aryl halide (1.0 equiv., 0.10 mmol), Pd(OAc)₂ (1.1 mg, 5.0 mol %, 5.0 μ mol), XPhos (4.8 mg, 10 mol %, 10 μ mol), K₂CO₃ (28 mg, 2.0 equiv., 0.20 mmol), and a 1,4-dioxane/water mixture (2:1, 0.60 mL). The vial was flushed with N₂, sealed, and the mixture was stirred at 60 °C for 18 h. After cooling to RT, the mixture was diluted with CH₂Cl₂ (5 mL), filtered through a plug of Celite, and volatiles were removed under reduced pressure. The residue was dissolved in CH₂Cl₂ (5 mL) and TFA (2 mL). The mixture was stirred at RT for 2 h, after which sat. aq. NaHCO₃ (10 mL) was added. The mixture was extracted with CH₂Cl₂ (2 × 15 mL), and the combined organic phases were dried over anhydrous MgSO₄,

filtered, and volatiles were removed under reduced pressure. The residue was purified by MPLC (silica gel) or preparative HPLC.

2-(Pyrimidin-5-yl)-1H-indole (25). Prepared according to General Procedure E from 5-bromopyrimidine (15.9 mg, 1.00 equiv., 0.100 mmol). Purified by preparative HPLC (10 to 50% MeCN in 50 mM aq. NH₄CO₃) to afford the product as a tan solid (6.0 mg, 31%). H NMR (600 MHz, (CD₃)₂SO) δ 9.29 (s, 2H), 9.10 (s, 1H), 7.59 (d, J = 8.3 Hz, 1H), 7.46 (d, J = 8.4 Hz, 1H), 7.19 – 7.15 (m, 2H), 7.05 (t, J = 7.6 Hz, 1H). NMR (151 MHz, (CD₃)₂SO) δ 156.7, 152.9, 137.6, 131.2, 128.2, 126.4, 122.7, 120.6, 119.9, 111.6, 101.1. Spectral data were consistent with those reported in literature.

5-(1H-Indol-2-yl)-1H-pyrrolo[2,3-b]pyridine (26). Prepared according to General Procedure E from 5-bromo-1H-pyrrolo-[2,3-b]pyridine (19.7 mg, 1.00 equiv., 0.100 mmol). Purified by MPLC (0 to 35% MeOH in CH_2Cl_2) to afford the product as a light brown solid (4.4 mg, 19%). H NMR (600 MHz, $(CD_3)_2SO)$ δ 11.56 (s, 1H), 8.77 (d, J = 2.2 Hz, 1H), 8.41 (d, J = 2.2 Hz, 1H), 7.54 - 7.51 (m, 2H), 7.41 (d, J = 8.4 Hz, 1H), 7.08 (t, J = 7.7 Hz, 1H), 7.00 (t, J = 7.6 Hz, 1H), 6.89 (d, J = 2.2 Hz, 1H), 6.53 (dd, J = 3.4, 1.8 Hz, 1H). ^{13}C NMR (151 MHz, $(CD_3)_2SO)$ δ 147.7, 140.4, 137.0, 136.9, 128.8, 127.2, 124.4, 121.1, 120.7, 119.7, 119.3, 111.1, 100.2, 97.7. LCMS found m/z 234.

3-(1H-Indol-2-yl)quinoline (27). Prepared according to General Procedure E from 3-bromoquinoline (20.8 mg, 1.00 equiv., 0.100 mmol). Purified by column chromatography (0 to 30% MeOH in CH₂Cl₂) to afford the product as a brown solid (6.7 mg, 27%). ¹H NMR (400 MHz, (CD₃)₂SO) δ 11.85 (s, 1H), 9.48 (d, J = 2.3 Hz, 1H), 8.77 (d, J = 2.3 Hz, 1H), 8.05 (d, J = 8.4 Hz, 1H), 8.01 (dd, J = 8.1, 1.4 Hz, 1H), 7.77 (ddd, J = 8.5, 6.9, 1.5 Hz, 1H), 7.67 (ddd, J = 8.1, 6.7, 1.2 Hz, 1H), 7.61 (d, J = 7.9 Hz, 1H), 7.47 (dd, J = 8.2, 0.7 Hz, 1H), 7.23 (d, J = 2.1 Hz, 1H), 7.21 – 7.10 (m, 1H), 7.09 – 6.99 (m, 1H). ¹³C NMR (151 MHz, (CD₃)₂SO) δ 148.5, 146.6, 137.5, 134.7, 129.8, 129.3, 128.8, 128.5, 128.1, 127.6, 127.3, 125.5, 122.3, 120.4, 119.7, 111.4, 100.5. HRMS (ESI) m/z calcd. for $[M + H]^+$ (C₁₂H₁₃N₂): 245.1073, found: 245.1082.

3-(Benzofuran-2-yl)pyridine (28). A Pyrex reaction tube was charged with benzofuran (54 μ L, 1.0 equiv., 0.50 mmol), 3-iodopyridine (153 mg, 1.50 equiv., 0.750 mmol), transbis(acetato)bis[ortho-(di-ortho-tolylphosphino)benzyldipalladi-um(II) (46 mg, 10 mol %, 0.050 mmol), AgOAc (125 mg, 1.50 equiv., 0.750 mmol,), and TFA (2.5 mL). The vial was sealed and heated to 70 °C for 24 h. After cooling to RT, the reaction mixture was diluted with CH2Cl2 (25 mL). The mixture was further cooled to 0 °C and was quenched by slow addition of aq. NaOH (5 M, 15 mL) with stirring. The phases were separated, and the aqueous phase was extracted with CH_2Cl_2 (2 × 25 mL). The combined organic phases were dried over anhydrous MgSO₄, filtered, and volatiles were removed under reduced pressure. The residue was purified by column chromatography (silica gel, 0 to 10% MeCN in CH₂Cl₂) to afford the product as a white solid (62) mg, 64%). H NMR (500 MHz, CDCl₃) δ 9.09 (s, 1H), 8.56 (d, J = 4.8 Hz, 1H), 8.10 - 8.04 (m, 1H), 7.58 (d, J = 7.1 Hz,1H), 7.52 (d, J = 8.0 Hz, 1H), 7.35 - 7.27 (m, 2H), 7.24 (t, J= 7.1 Hz, 1H), 7.08 - 7.03 (m, 1H). ¹³C NMR (126 MHz, $CDCl_3$) δ 155.1, 152.9, 149.3, 146.4, 131.8, 128.8, 126.6, 125.0, 123.6, 123.3, 121.2, 111.3, 102.8. Spectral data were consistent with those reported in literature.

General Procedure F for the Preparation of Compounds 29a-29v. In an Ar-filled glovebox, a flame-dried Schlenk flask was charged with Pd(PtBu₃)₂ (5.1 mg, 5.0 mol %, 10 μmol). A separate, oven-dried microwave vial was charged with the acetamide (1.33 equiv., 0.266 mmol) and the alkyne (1.00 equiv., 0.200 mmol) after which the vial was sealed, evacuated, and refilled with N₂ three times. Dry DMF (600 μ L) and Cy₂NMe (53.3 μ L, 2.50 equiv., 0.250 mmol, purged with N_2 for 5 min prior to use) were added to the microwave vial, after which the contents were transferred to the Schlenk vial. The mixture was then stirred at 80 °C for 24 h. After cooling to RT, volatiles were removed under reduced pressure to produce a residue which was dissolved in EtOAc (10 mL) and washed with 10% aq. LiCl (2 \times 10 mL). The organic phase was dried over anhydrous Na2SO4, filtered, and volatiles were removed under reduced pressure. The residue was dissolved in THF/H₂O (1.0 mL, 3:1), LiOH (24 mg, 5.0 equiv., 0.50 mmol), was added, and the mixture was stirred at 45 °C for 2.5 h. Volatiles were removed under reduced pressure and the residue was purified by column chromatography (silica gel).

tert-Butyl (2-(5-Methoxy-2-(pyridin-3-yl)-1H-indol-3-yl)ethyl)carbamate (29a). Prepared according to General Procedure F from tert-butyl (4-(pyridin-3-yl)but-3-yn-1-yl)carbamate S2a (36.9 mg, 1.00 equiv., 0.150 mmol) and N-(2iodo-4-methoxyphenyl)acetamide S1a (58.1 mg, 1.33 equiv., 0.200 mmol). Purified by column chromatography (20 to 55% EtOAc in hexane) to afford the product as an orange solid (30.4 mg, 55%). ¹H NMR (500 MHz, CDCl₃) δ 8.77 (s, 1H), 8.75 (s, 1H), 8.54 (d, I = 4.9 Hz, 1H), 7.88 (d, I = 7.9 Hz, 1H), 7.38 - 7.32 (m, 1H), 7.29 (d, J = 8.7 Hz, 1H), 7.09 (s, 1H), 6.89 (dd, J = 8.8, 2.4 Hz, 1H), 4.76 (bs, 1H), 3.88 (s, 3H), 3.44 (q, J = 6.7 Hz, 2H), 3.02 (t, J = 7.0 Hz, 2H), 1.39 (s, 9H). 13 C NMR (126 MHz, CDCl₃) δ 156.0, 154.5, 148.6, 148.4, 135.5, 132.7, 131.7, 129.4, 129.3, 123.9, 113.4, 112.1, 111.4, 101.1, 79.3, 56.1, 41.1, 28.5, 25.5. v_{max} (film) 3277, 2928, 1684, 1456, 1157, 735 cm⁻¹. HRMS (ESI) m/z calcd. for $[M + H]^+$ ($C_{21}H_{26}N_3O_3$): 368.1969, found: 368.1963.

tert-Butyl (2-(6-(Benzyloxy)-2-(pyridin-3-yl)-1H-indol-3yl)ethyl)carbamate (29b). Prepared according to General Procedure F from tert-butyl (4-(pyridin-3-yl)but-3-yn-1-yl)carbamate S2a (36.9 mg, 1.00 equiv., 0.150 mmol) and N-(5-(benzyloxy)-2-iodophenyl)acetamide S1b (73.4 mg, 1.33 equiv., 0.200 mmol). Purified by column chromatography (10 to 50% EtOAc in hexane) then repurified by column chromatography (0 to 1% MeOH in CH₂Cl₂) to afford the product as an orange solid (9.6 mg, 19%). ¹H NMR (500 MHz, CDCl₃) δ 8.78 (s, 1H), 8.55 (s, 1H), 8.38 (s, 1H), 7.87 (d, J = 7.7 Hz, 1H), 7.54 (d, J = 8.6 Hz, 1H), 7.46 (d, J = 7.1)Hz, 2H), 7.41 - 7.30 (m, 4H), 6.94 (d, J = 2.2 Hz, 1H), 6.91(dd, J = 8.6, 2.2 Hz, 1H), 5.12 (s, 2H), 4.72 - 4.65 (m, 1H),3.44 (q, J = 7.0 Hz, 2H), 3.04 (t, J = 7.2 Hz, 2H), 1.40 (s, 9H).¹³C NMR (126 MHz, CDCl₃) δ 156.4, 156.0, 148.5, 148.3, 137.4, 137.2, 135.2, 130.7, 129.4, 128.7, 128.0, 127.6, 123.9, 123.7, 120.3, 111.8, 111.0, 96.0, 79.3, 70.7, 41.3, 28.5, 25.5. v_{max} (film) 2924, 1709, 1593, 1454, 1366, 1163 cm⁻¹. HRMS (ESI) m/z calcd. for $[M + H]^+$ ($C_{27}H_{30}N_3O_3$): 444.2282, found: 444.2278.

tert-Butyl (2-(7-(Benzyloxy)-2-(pyridin-3-yl)-1H-indol-3-yl)ethyl)carbamate (29c). Prepared according to General Procedure F from tert-butyl (4-(pyridin-3-yl)but-3-yn-1-yl)-carbamate S2a (36.9 mg, 1.00 equiv., 0.150 mmol) and N-(2-(benzyloxy)-6-iodophenyl)acetamide S1d (73.4 mg, 1.33

equiv., 0.200 mmol). Purified by column chromatography (20 to 45% EtOAc in hexane) to afford a mixture of C2-pyridyl and C3-pyridyl products (85:15) as a light brown solid (48.2 mg, 72%). $^1\mathrm{H}$ NMR (500 MHz, CDCl3) δ 8.77 (s, 2H), 8.55 (s, 1H), 7.88 (d, J=7.9 Hz, 1H), 7.50 - 7.46 (m, 2H), 7.43 - 7.32 (m, 4H), 7.30 (d, J=8.1 Hz, 1H), 7.07 (t, J=7.9 Hz, 1H), 6.78 (d, J=7.7 Hz, 1H), 5.21 (s, 2H), 4.73 - 4.66 (m, 1H), 3.46 (q, J=6.8 Hz, 2H), 3.05 (t, J=7.1 Hz, 2H), 1.40 (s, 9H). $^{13}\mathrm{C}$ NMR (126 MHz, CDCl3) δ 156.0, 149.0, 148.7, 145.4, 136.9, 135.6, 131.8, 130.4, 128.8, 128.7, 128.4, 128.1, 127.1, 123.7, 120.6, 112.5, 112.0, 104.1, 79.2, 70.5, 41.2, 28.5, 25.6. v_{max} (film) 3262, 2974 1686, 1506, 1161, 777, 731 cm $^{-1}$. HRMS (ESI) m/z calcd. for [M + H] $^+$ (C27H30N3O3): 444.2282, found: 444.2273.

tert-Butyl (2-(4-Methoxy-2-(pyridin-3-yl)-1H-indol-3-yl)ethyl)carbamate (29d). Prepared according to General Procedure F from tert-butyl (4-(pyridine-3-yl)but-3-yn-1yl)carbamate S2a (49.3 mg, 1.00 equiv., 0.200 mmol) and N-(2-iodo-3-methoxyphenyl)acetamide S1e (77.4 mg, 1.33 equiv., 0.266 mmol). Purified by column chromatography (40 to 60% EtOAc in hexane) to afford the product as a gray solid (9.9 mg, 13%). ¹H NMR (500 MHz, CDCl₃) δ 8.81 (bs, 1H), 8.60 (bs, 1H), 8.23 (s, 1H), 7.93 (d, I = 6.1 Hz, 1H), 7.40 (bs, 1H), 7.15 (t, I = 8.0 Hz, 1H), 7.02 (d, I = 8.1 Hz, 1H), 6.55 (d, J = 7.8 Hz, 1H), 4.89 (bs, 1H), 3.97 (s, 3H), 3.54 - 3.47 (m, 2H), 3.11 (t, J = 6.8 Hz, 2H), 1.35 (s, 9H). ¹³C NMR (126 MHz, CDCl₃) δ 156.1, 154.8, 149.0, 148.6, 138.0, 136.0, 130.9, 123.9 (2C), 118.7, 112.3, 104.5, 100.2, 78.9, 55.3, 42.4, 28.5, 26.2. v_{max} (film) 3285, 2926, 1688, 1248, 1167, 1107, 735 cm⁻¹. HRMS (ESI) m/z calcd. for $[M + H]^+$ ($C_{21}H_{26}N_3O_3$): 368.1969, found: 368.1974.

tert-Butyl (2-(5-Fluoro-2-(pyridin-3-yl)-1H-indol-3-yl)ethyl)carbamate (29e). Prepared according to General Procedure F from tert-butyl (4-(pyridin-3-yl)but-3-yn-1-yl)carbamate **S2a** (49.3 mg, 1.00 equiv., 0.200 mmol) and N-(4fluoro-2-iodophenyl)acetamide S 1f (74.2 mg, 1.33 equiv., 0.266 mmol). Purified by column chromatography (0 to 1.5% MeOH in CH₂Cl₂), then repurified by column chromatography (50 to 65% EtOAc in hexane) to afford the product as an off-white solid (11.4 mg, 16%). ¹H NMR (500 MHz, CDCl₃) δ 8.80 (s, 1H), 8.63 – 8.58 (m, 2H), 7.90 (d, I = 7.9Hz, 1H), 7.39 (dd, J = 7.9, 4.9 Hz, 1H), 7.34 - 7.28 (m, 2H), 6.99 (td, J = 9.0, 2.5 Hz, 1H), 4.67 (s, 1H), 3.41 (q, J = 6.9 Hz, 1Hz)2H), 3.01 (t, J = 7.1 Hz, 2H), 1.40 (s, 9H). ¹³C NMR (126 MHz, CDCl₃) δ 158.2 (d, ${}^{1}J_{CF}$ = 235.9 Hz), 156.0, 148.9, 148.8, 135.6, 133.7, 132.9, 129.5 (d, ${}^{3}J_{CF} = 7.9$ Hz), 129.0, 123.9, 112.0, 111.9, 111.6 (d, J = 26.2 Hz), 104.4 (d, ${}^2J_{CF} =$ 23.4 Hz), 79.4, 41.2, 28.5, 25.4. ¹⁹F NMR (377 MHz, CDCl₃) δ – 123.50. v_{max} (film) 3350, 2926, 1680, 1171, 1153, 793 cm⁻¹. HRMS (ESI) m/z calcd. for $[M + H]^+$ ($C_{20}H_{23}F_1N_3O_2$): 356.1769, found: 356.1759.

tert-Butyl (2-(6-Fluoro-2-(pyridin-3-yl)-1H-indol-3-yl)-ethyl)carbamate (29f). Prepared according to General Procedure F from tert-butyl (4-(pyridin-3-yl)but-3-yn-1-yl)-carbamate S2a (49.3 mg, 1.00 equiv., 0.200 mmol) and N-(5-fluoro-2-iodophenyl)acetamide S1g (74.2 mg, 1.33 equiv., 0.266 mmol). Purified by column chromatography (0 to 1.5% MeOH in CH₂Cl₂) to afford the product as a light yellow solid (13.8 mg, 19%). ¹H NMR (500 MHz, CDCl₃) δ 8.81 (s, 1H), 8.71 (s, 1H), 8.58 (s, 1H), 7.91 (d, J = 7.9 Hz, 1H), 7.58 (dd, J = 8.8, 5.4 Hz, 1H), 7.43 – 7.37 (m, 1H), 7.09 (dd, J = 9.4, 2.3 Hz, 1H), 6.92 (td, J = 9.2, 2.3 Hz, 1H), 4.70 (t, J = 6.4 Hz, 1H), 3.43 (q, J = 6.9 Hz, 2H), 3.04 (t, J = 7.2 Hz, 2H), 1.40 (s,

9H). ¹³C NMR (126 MHz, CDCl₃) δ 160.6 (d, ¹ J_{CF} = 239.5 Hz), 156.0, 148.6, 136.5 (d, ³ J_{CF} = 12.6 Hz), 135.5, 132.1, 129.1, 125.6, 124.0, 120.4 (d, ³ J_{CF} = 10.2 Hz), 111.8, 109.0 (d, ² J_{CF} = 24.6 Hz), 97.6 (d, ² J_{CF} = 26.0 Hz), 79.4, 41.3, 28.5, 25.5. ¹⁹F NMR (470 MHz, CDCl₃) δ – 119.40. v_{max} (film) 3260, 2976, 1686, 1364, 1248, 1165 cm⁻¹. HRMS (ESI) m/z calcd. for [M + Na]⁺ (C₂₀H₂₂F₁N₃O₂Na₁): 378.1588, found: 378.1588.

tert-Butyl (2-(5-((tert-Butoxycarbonyl)amino)-2-(pyridin-3-yl)-1H-indol-3-yl)ethyl)carbamate (29g). Prepared according to General Procedure F from tert-butyl (4-(pyridine-3yl)but-3-yn-1-yl)carbamate S2a (36.9 mg, 1.00 equiv., 0.150 mmol) and tert-butyl (4-acetamido-3-iodophenyl)carbamate S1h (75.0 mg, 1.33 equiv., 0.200 mmol). Purified by column chromatography (0 to 5% MeOH in CH2Cl2) to afford the product as a light brown powder (19.4 mg, 29%). ¹H NMR (700 MHz, CDCl₃) δ 8.83 (s, 1H), 8.77 (s, 1H), 8.58 – 8.45 (m, 1H), 7.88 (d, J = 7.8 Hz, 1H), 7.61 (s, 1H), 7.34 (t, J = 6.4Hz, 1H), 7.25 (d, J = 8.7 Hz, 1H), 7.16 (s, 1H), 6.64 (s, 1H), 4.75 (s, 1H), 3.43 - 3.36 (m, 2H), 2.98 (t, J = 7.2 Hz, 2H), 1.53 (s, 9H), 1.38 (s, 9H). 13 C NMR (176 MHz, CDCl₃) δ 156.0, 153.7, 148.6, 148.5, 135.6, 133.4, 132.8, 131.2, 129.3, 129.1, 123.8, 116.8, 111.4, 111.4, 109.8, 80.2, 79.2, 41.1, 28.6, 28.5, 25.4. v_{max} (film) 3308, 2976, 1686, 1244, 1159 cm⁻¹. HRMS (ESI) m/z calcd. for $[M + H]^+$ ($C_{25}H_{33}N_4O_4$): 453.2496, found: 453.2497.

Methyl 3-(2-((tert-Butoxycarbonyl)amino)ethyl)-2-(pyridin-3-yl)-1H-indole-5-carboxylate (29h). Prepared according to General Procedure F from tert-butyl (4-(pyridin-3-yl)but-3yn-1-yl)carbamate S2a (49.3 mg, 1.00 equiv., 0.200 mmol) and methyl 4-acetamido-3-iodobenzoate S1i (84.9 mg, 1.33 equiv., 0.266 mmol). Purified by column chromatography (0 to 2% MeOH in CH₂Cl₂) to afford the product as a light brown solid (8.9 mg, 11%). 1 H NMR (500 MHz, (CD₃)₂CO) δ 10.89 (s, 1H), 8.96 (s, 1H), 8.61 (s, 1H), 8.44 (d, J = 1.7 Hz, 1H), 8.16 (d, J = 8.0 Hz, 1H), 7.87 (dd, J = 8.5, 1.6 Hz, 1H), 7.53 - 7.48(m, 2H), 6.25 - 6.17 (m, 1H), 3.89 (s, 3H), 3.44 (q, J = 6.8)Hz, 2H), 3.18 - 3.12 (m, 2H), 1.39 (s, 9H). ¹³C NMR (126 MHz, $(CD_3)_2CO)$ δ 168.2, 156.7, 149.7 (2C), 140.2, 136.1, 134.4, 129.6, 129.5, 124.5, 124.3, 122.6, 122.4, 113.2, 111.9, 78.6, 51.9, 42.1, 28.6, 26.2. v_{max} (film) 2926, 1699, 1250, 1169, 1105, 772 cm⁻¹. HRMS (ESI) m/z calcd. for $[M + Na]^+$ $(C_{22}H_{25}N_3O_4Na_1)$: 418.1737, found: 418.1738.

tert-Butyl (2-(6-Fluoro-5-methoxy-2-(pyridin-3-yl)-1Hindol-3-yl)ethyl)carbamate (29i). Prepared according to General Procedure F from tert-butyl (4-(pyridin-3-yl)but-3yn-1-yl)carbamate S2a (49.3 mg, 1.00 equiv., 0.200 mmol) and N-(5-fluoro-2-iodo-4-methoxyphenyl)acetamide S1j (82.2 mg, 1.33 equiv., 0.266 mmol). Purified by column chromatography (0 to 1.5% MeOH in CH₂Cl₂) to afford the product as a light yellow solid (25.5 mg, 33%). 1 H NMR (500 MHz, CDCl₃) δ 8.78 (bs, 1H), 8.64 (s, 1H), 8.57 (bs, 1H), 7.88 (d, J = 5.8 Hz, 1H), 7.38 (bs, 1H), 7.17 (d, J = 8.1 Hz, 1H), 7.13 (d, J = 11.1Hz, 1H), 4.72 (s, 1H), 3.95 (s, 3H), 3.42 (q, J = 5.2 Hz, 2H), 3.02 (t, J = 7.1 Hz, 2H), 1.40 (s, 9H). ¹³C NMR (126 MHz, CDCl₃) δ 156.0, 151.4 (d, ${}^{1}J_{CF}$ = 241.8 Hz), 148.6 (2C), 143.6 (d, ${}^{3}J_{CF}$ = 12.8 Hz), 135.3, 132.2, 130.0 (d, ${}^{3}J_{CF}$ = 11.3 Hz), 129.2, 124.6, 123.9, 111.6, 102.8, 98.9 (d, ${}^{2}J_{CF}$ = 23.4 Hz), 79.4, 57.1, 41.2, 28.5, 25.6. ${}^{19}F$ NMR (377 MHz, CDCl₃) δ – 138.32. v_{max} (film) 3379, 2934, 1686, 1520, 1215, 1169, 1142 cm⁻¹. HRMS (ESI) m/z calcd. for $[M + H]^+$ ($C_{21}H_{25}F_1NO_3$): 386.1875, found: 386.1880.

tert-Butyl (2-(6-Fluoro-5-methoxy-3-(pyridin-3-yl)-1Hindol-2-yl)ethyl)carbamate (29j). Prepared according to General Procedure F from tert-butyl (4-(pyridin-3-yl)but-3yn-1-yl)carbamate S2a (49.3 mg, 1.00 equiv., 0.200 mmol) and N-(5-fluoro-2-iodo-4-methoxyphenyl)acetamide S1j (82.2 mg, 1.33 equiv., 0.266 mmol). Purified by column chromatography (0 to 2% MeOH in CH₂Cl₂), then repurified by column chromatography (45 to 60% EtOAc in hexane) to afford the product as a white solid (6.5 mg, 8%). ¹H NMR (500 MHz, CDCl₃) δ 9.21 (s, 1H), 8.74 (s, 1H), 8.58 (s, 1H), 7.79 (d, J =7.8 Hz, 1H), 7.43 (bs, 1H), 7.12 (d, J = 11.1 Hz, 1H), 7.05 (d, J = 8.1 Hz, 1H), 4.82 (s, 1H), 3.87 (s, 3H), 3.49 (q, J = 6.5 Hz, 2H), 3.04 (t, J = 6.6 Hz, 2H), 1.41 (s, 9H). 13 C NMR (126 MHz, CDCl₃) δ 156.7, 150.8 (d, ${}^{1}J_{CF} = 240.5$ Hz), 150.1, 147.1, 143.8 (d, ${}^{2}J_{CF}$ = 12.8 Hz), 136.9, 134.0, 134.0, 129.1 (d, ${}^{3}J_{CF}$ = 11.2 Hz), 124.0, 123.1, 111.4, 102.0, 98.8 (d, ${}^{2}J_{CF}$ = 23.4 Hz), 80.3, 57.1, 39.8, 28.5, 28.0. ¹⁹F NMR (377 MHz, CDCl₃) δ – 140.0. v_{max} (film) 2922, 1682, 1481, 1157, 1128 cm⁻¹. HRMS (ESI) m/z calcd. for $[M + H]^+$ ($C_{21}H_{25}F_1N_3O_3$): 386.1875, found: 386.1878.

tert-Butyl ((5-Methoxy-2-(pyridin-3-yl)-1H-indol-3-yl)methyl)carbamate (29k). Prepared according to General Procedure F from tert-butyl (3-(pyridin-3-yl)prop-2-yn-1yl)carbamate S2c (46.5 mg, 1.00 equiv., 0.200 mmol) and N-(2-iodo-4-methoxyphenyl)acetamide S1a (77.4 mg, 1.33 equiv., 0.266 mmol). Purified by column chromatography (0 to 2% MeOH in CH₂Cl₂) to afford the product as a light pink solid (26.9 mg, 38%). Note: unstable, rotary evaporator bath kept at 30 °C. ¹H NMR (500 MHz, CDCl₃) δ 8.79 (s, 1H), 8.63 (d, J = 4.8 Hz, 1H), 8.22 (s, 1H), 7.86 (dt, J = 7.9, 1.9 Hz, 1H), 7.42 (dd, J = 7.9, 4.8 Hz, 1H), 7.31 (d, J = 8.8 Hz, 1H), 7.18 (s, 1H), 6.93 (dd, J = 8.8, 2.4 Hz, 1H), 4.69 (bs, 1H), 4.56 (d, J = 5.1 Hz, 2H), 3.88 (s, 3H), 1.47 (s, 9H). 13 C NMR (126 MHz, CDCl₃) δ 155.9, 154.9, 149.2, 148.8, 135.6, 133.4, 131.4, 128.9, 128.5, 123.9, 114.0, 112.1, 111.1, 100.9, 79.5, 56.0, 35.4, 28.6. $v_{\rm max}$ (film) 2922, 1699, 1506, 1497, 1223, 1163 cm⁻¹. HRMS (ESI) m/z calcd. for $[M + H]^+$ (C₂₀H₂₄N₃O₃): 354.1812, found: 354.1813.

tert-Butyl (3-(5-Methoxy-2-(pyridin-3-yl)-1H-indol-3-yl)propyl)carbamate (291). Prepared according to General Procedure F from tert-butyl (5-(pyridin-3-yl)pent-4-yn-1yl)carbamate S 2d (46.6 mg, 1.00 equiv., 0.179 mmol) and N-(2-iodo-4-methoxyphenyl)acetamide S1a (69.3 mg, 1.33 equiv., 0.238 mmol). Purified by column chromatography (0 to 2% MeOH in CH₂Cl₂) to afford the product as a white solid (31.0 mg, 45%). 1 H NMR (500 MHz, CDCl₃) δ 8.78 (s, 1H), 8.72 (s, 1H), 8.55 (d, J = 4.8 Hz, 1H), 7.81 (dt, J = 8.0, 2.0 Hz, 1H), 7.34 (dd, J = 8.0, 4.9 Hz, 1H), 7.28 (d, J = 8.7 Hz, 1H), 7.03 (d, J = 2.4 Hz, 1H), 6.88 (dd, J = 8.8, 2.4 Hz, 1H), 4.57 (bs, 1H), 3.87 (s, 3H), 3.13 (q, I = 6.7 Hz, 2H), 2.88 - 2.83(m, 2H), 1.86 (p, J = 7.0 Hz, 2H), 1.41 (s, 9H). ¹³C NMR (126 MHz, CDCl₃) δ 156.1, 154.3, 148.8, 148.4, 135.2, 131.8, 131.8, 129.6, 129.3, 123.8, 113.9, 113.1, 112.1, 101.0, 79.2, 56.1, 40.6, 31.0, 28.5, 21.9. $v_{\rm max}$ (film) 3302, 2932, 1684, 1474, 1163, 1024 cm⁻¹. HRMS (ESI) m/z calcd. for $[M + H]^+$ $(C_{22}H_{28}N_3O_3)$: 382.2125, found: 382.2116.

tert-Butyl (2-(2-(5-Fluoropyridin-3-yl)-5-methoxy-1H-indol-3-yl)ethyl)carbamate (29m). Prepared according to General Procedure F from tert-butyl (4-(5-fluoropyridin-3-yl)but-3-yn-1-yl)carbamate S 2f (52.9 mg, 1.00 equiv., 0.200 mmol) and N-(2-iodo-4-methoxyphenyl)acetamide S1a (77.4 mg, 1.33 equiv., 0.266 mmol). Purified by column chromatography (0 to 1.5% MeOH in CH₂Cl₂) to afford the product as

an orange solid (35.0 mg, 45%). ¹H NMR (500 MHz, CDCl₃) δ 8.63 (s, 1H), 8.45 (s, 1H), 8.27 (s, 1H), 7.63 (d, J = 9.3 Hz, 1H), 7.30 (d, J = 8.8 Hz, 1H), 7.10 (s, 1H), 6.92 (dd, J = 8.8, 2.4 Hz, 1H), 4.67 (s, 1H), 3.88 (s, 3H), 3.50 – 3.44 (m, 2H), 3.04 (t, J = 6.9 Hz, 2H), 1.40 (s, 9H). ¹³C NMR (126 MHz, CDCl₃) δ 159.6 (${}^{1}J_{CF}$ = 259.4 Hz), 156.0, 154.7, 144.5, 137.0 (d, ${}^{2}J_{CF}$ = 23.2 Hz), 131.7, 131.1, 130.7, 129.3, 121.9 (d, ${}^{2}J_{CF}$ = 18.8 Hz), 114.0, 112.5, 112.2, 101.2, 79.5, 56.1, 41.0, 28.5, 25.5. ¹⁹F NMR (376 MHz, CDCl₃) δ – 125.76. v_{max} (film) 3275, 2928, 1684, 1215, 1165 cm⁻¹. HRMS (ESI) m/z calcd. for [M + H]⁺ ($C_{21}H_{25}F_1N_3O_3$): 386.18745, found: 386.1880. tert-Butyl (2-(5-Methoxy-2-(pyridin-2-yl)-1H-indol-3-yl)-ethyl)carbamate (29n). Prepared according to General Procedure F from tert-butyl (4-(pyridin-2-yl)but-3-yn-1-yl)-carbamate S2h (36.9 mg, 1.00 equiv., 0.150 mmol) and N-(2-

Procedure F from tert-butyl (4-(pyridin-2-yl)but-3-yn-1-yl)carbamate **S2h** (36.9 mg, 1.00 equiv., 0.150 mmol) and N-(2iodo-4-methoxyphenyl)acetamide S1a (58.1 mg, 1.33 equiv., 0.200 mmol). Purified by column chromatography (20 to 40% EtOAc in hexane) to afford the product as a yellow solid (30.9 mg, 56%). 1 H NMR (500 MHz, CDCl₃) δ 9.48 (s, 1H), 8.62 (d, J = 4.3 Hz, 1H), 7.85 (d, J = 8.2 Hz, 1H), 7.76 (t, J = 7.8)Hz, 1H), 7.28 (d, J = 8.8 Hz, 1H), 7.19 (t, J = 6.0 Hz, 1H), 7.07 (d, J = 2.4 Hz, 1H), 6.92 (dd, J = 8.8, 2.4 Hz, 1H), 5.26 (bs, 1H), 3.90 (s, 3H), 3.54 (q, J = 6.2 Hz, 2H), 3.28 (t, J = 6.8Hz, 2H), 1.44 (s, 9H). 13 C NMR (126 MHz, CDCl₃) δ 156.3, 154.3, 150.8, 149.4, 137.1, 133.9, 131.0, 130.0, 121.8, 121.1, 114.1, 112.2, 111.9, 100.7, 79.1, 56.0, 41.0, 28.6, 25.6. $v_{\rm max}$ (film) 3348, 2974, 1684, 1215, 1163, 787 cm⁻¹. HRMS (ESI) m/z calcd. for $[M + H]^+$ $(C_{21}H_{26}N_3O_3)$: 368.1969, found:368.1977.

tert-Butyl (2-(5-Methoxy-2-(pyridin-4-yl)-1H-indol-3-yl)ethyl)carbamate (290). Prepared according to General Procedure F from tert-butyl (4-(pyridin-4-yl)but-3-yn-1-yl)carbamate S2i (52.1 mg, 1.00 equiv., 0.212 mmol) and N-(2iodo-4-methoxyphenyl)acetamide S1a (77.5 mg, 1.26 equiv., 0.266 mmol). Purified by column chromatography (0 to 1.5% MeOH in CH₂Cl₂) to afford the product as a yellow solid (38.0 mg, 49%). ¹H NMR (400 MHz, CDCl₃) δ 9.22 (s, 1H), 8.55 (bs, 2H), 7.52 (bs, 2H), 7.30 (d, J = 8.7 Hz, 1H), 7.05 (s, 1H), 6.91 – 6.87 (m, 1H), 4.83 (s, 1H), 3.85 (s, 3H), 3.47 – 3.38 (m, 2H), 3.09 (t, J = 7.1 Hz, 2H), 1.39 (s, 9H). ¹³C NMR (101 MHz, CDCl₃) δ 156.1, 154.5, 149.6, 141.3, 132.4, 132.1, 129.5, 122.0, 114.4, 113.2, 112.5, 100.9, 79.4, 56.0, 41.0, 28.5, 25.7. v_{max} (film) 3308, 2932, 1684, 1217, 1163 cm⁻¹. HRMS (ESI) m/z calcd. for $[M + H]^+$ $(C_{21}H_{26}N_3O_3)$: 368.1969, found: 368.1969.

tert-Butyl (2-(5-Methoxy-2-(pyrimidin-5-yl)-1H-indol-3yl)ethyl)carbamate (29p). Prepared according to General Procedure F from tert-butyl (4-(pyrimidin-5-yl)but-3-yn-1yl)carbamate **S2g** (37.1 mg, 1.00 equiv., 0.150 mmol) and N-(2-iodo-4-methoxyphenyl)acetamide S1a (58.1 mg, 1.33 equiv., 0.200 mmol). Purified by column chromatography (0 to 2% MeOH in CH₂Cl₂), then repurified by column chromatography (50 to 55% EtOAc in hexane) to afford the product as a brown solid (25.9 mg, 47%). ¹H NMR (500 MHz, CDCl₃) δ 9.21 (s, 1H), 8.96 (s, 2H), 8.13 (s, 1H), 7.32 (d, J =8.8 Hz, 1H), 7.12 (s, 1H), 6.95 (dd, J = 8.8, 2.4 Hz, 1H), 4.65 (bs, 1H), 3.90 (s, 3H), 3.52 - 3.42 (m, 2H), 3.05 (t, J = 7.0Hz, 2H), 1.40 (s, 9H). 13 C NMR (126 MHz, CDCl₃) δ 157.3, 156.2, 156.0, 155.4, 154.8, 132.1, 129.3, 128.9, 127.7, 114.2, 113.0, 112.3, 101.2, 79.5, 56.1, 41.1, 28.5, 25.6. v_{max} (film) 3298, 2924, 1699, 1456, 1167 cm⁻¹. HRMS (ESI) m/z calcd. for $[M + Na]^+$ ($C_{20}H_{24}N_4O_3Na_1$): 391.1741, found: 391.1740.

tert-Butyl (2-(5-Methoxy-3-(pyrimidin-5-yl)-1H-indol-2yl)ethyl)carbamate (29q). Prepared according to General Procedure F from tert-butyl (4-(pyrimidin-5-yl)but-3-yn-1yl)carbamate S2g (37.1 mg, 1.00 equiv., 0.150 mmol) and N-(2-iodo-4-methoxyphenyl)acetamide S1a (58.1 mg, 1.33 equiv., 0.200 mmol). Purified by column chromatography (0 to 2% MeOH in CH₂Cl₂) to afford the product as a brown solid (13.3 mg, 24%). ¹H NMR (500 MHz, CDCl₃) δ 9.34 (s, 1H), 9.17 (s, 1H), 8.88 (s, 2H), 7.30 (d, J = 8.8 Hz, 1H), 7.00(d, J = 2.4 Hz, 1H), 6.88 (dd, J = 8.8, 2.4 Hz, 1H), 4.84 (s, 1)1H), 3.81 (s, 3H), 3.52 (q, J = 6.6 Hz, 2H), 3.06 (t, J = 6.5 Hz, 2H), 1.42 (s, 9H). 13 C NMR (126 MHz, CDCl₃) δ 156.8, 156.2, 155.2, 135.1, 130.8, 130.1, 127.6, 112.7, 112.2, 107.7, 99.8, 80.4, 56.0, 39.7, 28.4, 28.1. v_{max} (film) 3264, 2928, 1686, 1489, 1474, 1159 cm⁻¹. HRMS (ESI) m/z calcd. for [M + H]⁺ (C₂₀H₂₅N₄O₃): 369.1921, found: 369.1924.

tert-Butyl (2-(5-Methoxy-2-(thiazol-5-yl)-1H-indol-3-yl)ethyl)carbamate (29r). Prepared according to General Procedure F from tert-butyl (4-(thiazol-5-yl)but-3-yn-1-yl)carbamate S2j (50.5 mg, 1.00 equiv., 0.200 mmol) and N-(2iodo-4-methoxyphenyl)acetamide S1a (77.5 mg, 1.26 equiv., 0.266 mmol). Purified by column chromatography (0 to 1.5% MeOH in CH₂Cl₂), then repurified by column chromatography (40 to 55% EtOAc in hexane) to afford the product as a brown solid (18.0 mg, 24%). ¹H NMR (500 MHz, CDCl₃) δ 8.79 (s, 1H), 8.44 (s, 1H), 8.03 (s, 1H), 7.28 - 7.22 (m, 1H), 7.05 (s, 1H), 6.90 (dd, J = 8.8, 2.4 Hz, 1H), 4.70 (s, 1H), 3.87(s, 3H), 3.44 (q, J = 6.7 Hz, 2H), 3.07 (t, J = 6.8 Hz, 2H), 1.41(s, 9H). 13 C NMR (126 MHz, CDCl₃) δ 156.0, 154.7, 152.5, 140.3, 131.6, 129.9, 129.4, 126.2, 113.9, 112.7, 111.9, 101.0, 79.4, 56.1, 40.9, 28.5, 25.8. v_{max} (film) 3277, 2974, 1684, 1215, 1165, 1111 cm⁻¹. HRMS (ESI) m/z calcd. for [M + H]⁺ $(C_{19}H_{24}N_3O_3S_1)$: 374.1533, found: 374.1522.

tert-Butyl (2-(5-(Methoxymethoxy)-2-(pyridin-3-yl)-1Hindol-3-yl)ethyl)(methyl)carbamate (29s). Prepared according to General Procedure F from tert-butyl methyl (4-(pyridin-3-yl)but-3-yn-1-yl)carbamate S2b (52.1 mg, 1.00 equiv., 0.200 mmol) and N-(2-iodo-4-(methoxymethoxy)phenyl)acetamide S1k (85.4 mg, 1.33 equiv., 0.266 mmol). Purified by column chromatography (0 to 2% MeOH in CH₂Cl₂), then repurified by column chromatography (50 to 60% EtOAc in hexane) to afford the product as a yellow solid (26.3 mg, 32%). ¹H NMR (500 MHz, CDCl₃, mixture of rotamers) δ 8.80 (s, 1H), 8.59 (s, 1H), 8.46 (m, 1H), 8.00 - 7.94 (m, 1H)*, 7.84 - 7.80 (m, 1H)*1H)*, 7.41 - 7.35 (m, 1H), 7.32 - 7.27 (m, 2H), 7.00 (dd, J =8.7, 2.3 Hz, 1H), 5.22 (s, 2H), 3.53 (s, 3H), 3.51 - 3.46 (m, 2H), 3.07 - 3.00 (m, 2H), 2.73 (s, 3H), 1.27 (s, 9H). *rotamer signal splitting. ¹³C NMR (126 MHz, CDCl₃, mixture of rotamers) δ 155.6, 152.0, 149.0, 148.8, 135.6, 132.8, 132.6, 129.6, 129.4, 123.9, 114.5, 111.8, 111.8, 105.7, 96.0, 79.4, 56.0, 49.5, 34.3, 28.3, 23.4. v_{max} (film) 3248, 2920, 1657, 1150, 1011, 810 cm⁻¹. HRMS (ESI) m/z calcd. for M + 1 $H]^+$ ($C_{23}H_{30}N_3O_4$): 412.2231, found: 412.2231.

3-(2-((tert-Butyldimethylsilyl)oxy)ethyl)-5-(methoxymethoxy)-2-(pyridin-3-yl)-1H-indole (29t). Prepared according to General Procedure F from 3-(4-((tert-butyldimethylsilyl)oxy)but-1-yn-1-yl)pyridine S2e (52.3 mg, 1.00 equiv., 0.200 mmol) and N-(2-iodo-4-(methoxymethoxy)phenyl)acetamide S1k (85.4 mg, 1.33 equiv., 0.266 mmol). Purified by column chromatography (0 to 1.5% MeOH in CH₂Cl₂) to afford the product as a yellow solid (34.0 mg, 41%). 1 H NMR (400 MHz, CDCl₃) δ 8.85 (s, 1H), 8.72 (s, 1H), 8.59 – 8.52 (m, 1H), 8.03 (d, I = 7.9 Hz, 1H), 7.40 – 7.32 (m, 1H), 7.31 – 7.27 (m,

2H), 6.97 (d, J = 8.9 Hz, 1H), 5.22 (s, 2H), 3.92 (t, J = 7.2 Hz, 2H), 3.53 (t, J = 1.7 Hz, 3H), 3.07 (t, J = 7.2 Hz, 2H), 0.83 (s, 9H), -0.05 (s, 6H). 13 C NMR (176 MHz, CDCl₃) δ 151.8, 148.7, 148.5, 135.7, 133.0, 132.5, 129.8, 129.4, 123.7, 114.6, 111.8, 111.6, 105.8, 96.0, 63.5, 56.0, 28.4, 26.1, 18.5, -5.3. v_{max} (film) 2926, 1464, 1152, 1080, 1005, 833 cm $^{-1}$. HRMS (ESI) m/z calcd. for [M + Na] $^+$ (C₂₃H₃₂N₂O₃Si₁Na₁) 435.2074, found: 435.2073.

tert-Butyl (2-(2-(pyridin-3-yl)-1H-indol-3-yl)ethyl)carbamate (29u). Prepared according to General Procedure F from tert-butyl (4-(pyridin-3-yl)but-3-yn-1-yl)carbamate S2a (49.3 mg, 1.00 equiv., 0.200 mmol) and N-(2-iodophenyl)acetamide (69.4 mg, 1.33 equiv., 0.266 mmol). Purified by column chromatography (0 to 1.5% MeOH in CH₂Cl₂), then repurified by column chromatography (40 to 55% EtOAc in hexane) to afford the product as a yellow solid (18.7 mg, 28%). ¹H NMR (500 MHz, CDCl₃) δ 8.82 (s, 1H), 8.77 (s, 1H), 8.59 - 8.55 (m, 1H), 7.92 (d, J = 7.9 Hz, 1H), 7.67 (d, J = 7.9Hz, 1H), 7.41 (d, J = 8.1 Hz, 1H), 7.41 - 7.34 (m, 1H), 7.26 -7.22 (m, 1H), 7.16 (ddd, J = 8.0, 7.0, 1.0 Hz, 1H), 4.72 (s, 1H), 3.45 (t, J = 7.0 Hz, 2H), 3.07 (t, J = 7.1 Hz, 2H), 1.40 (s, 9H). ¹³C NMR (126 MHz, CDCl₃) δ 156.0, 148.7, 148.5, 136.5, 135.7, 131.8, 129.4, 128.9, 123.9, 123.1, 120.2, 119.5, 111.7, 111.3, 79.3, 41.2, 28.5, 25.5. $v_{\rm max}$ (film) 3292, 2976, 1686, 1364, 1161 cm⁻¹. HRMS (ESI) m/z calcd. for [M + H]⁺ $(C_{20}H_{24}N_3O_2)$: 338.1863, found: 338.1852.

tert-Butyl (2-(3-(pyridin-3-yl)-1H-indol-2-yl)ethyl)carbamate (29v). Prepared according to General Procedure F from tert-butyl (4-(pyridin-3-yl)but-3-yn-1-yl)carbamate S2a (49.3 mg, 1.00 equiv., 0.200 mmol) and N-(2-iodophenyl)acetamide (69.4 mg, 1.33 equiv., 0.266 mmol). Purified by column chromatography (0 to 1.5% MeOH in CH2Cl2) to afford the product as a light-brown solid (27.8 mg, 41%). ¹H NMR (500 MHz, CDCl₃) δ 9.49 (s, 1H), 8.74 (s, 1H), 8.55 (d, I = 4.9 Hz, 1H), 7.82 (dt, I = 7.9, 1.8 Hz, 1H), 7.58 (d, I =7.9 Hz, 1H), 7.43 - 7.32 (m, 2H), 7.20 (ddd, I = 8.2, 7.0, 1.2 Hz, 1H), 7.13 (td, J = 7.5, 1.1 Hz, 1H), 4.91 (s, 1H), 3.48 (t, J= 6.8 Hz, 2H), 3.07 (t, J = 6.9 Hz, 2H), 1.41 (s, 9H). ¹³C NMR (126 MHz, CDCl₃) δ 156.5, 150.3, 147.1, 136.9, 135.8, 133.7, 131.6, 127.6, 123.7, 122.2, 120.4, 118.4, 111.5, 111.1, 80.1, 40.0, 28.4, 27.7. v_{max} (film) 3300, 2976, 1703, 1364, 1250, 1165 cm⁻¹. HRMS (ESI) m/z calcd. for [M + H]⁺ $(C_{20}H_{24}N_3O_2)$ 338.18630, found: 338.1858.

General Procedure G for the Preparation of Compounds 30–33, 38–45, 48–49, 52–53. A flame-dried round-bottom flask was charged with protected indole (1.00 equiv), 1,2,4,5-tetramethylbenzene (8.00 equiv), and anhydrous CH₂Cl₂ (2.5 mL per 0.1 mmol indole). The mixture was cooled to – 84 C, and BBr₃ (0.75 M in CH₂Cl₂, 8.00 equiv) was added portion-wise over 5 min via syringe. The mixture was allowed to gradually warm to RT and stirred for 16 h. The mixture was diluted with water (~5 mL per 0.1 mmol of indole, added cautiously) and MeOH (~5 mL per 0.1 mmol indole). The pH of the aqueous phase was adjusted to >10 by addition of aq. NaOH (2 M). Volatiles were removed under reduced pressure and the residue was purified by column chromatography (silica gel).

3-(2-Aminoethyl)-2-(pyridin-3-yl)-1H-indol-5-ol (**30**). Prepared according to General Procedure G from *tert*-butyl (2-(5-methoxy-2-(pyridin-3-yl)-1H-indol-3-yl)ethyl)carbamate **29a** (20.3 mg, 1.00 equiv., 55.2 μ mol). Purified by column chromatography (0 to 12% MeOH in CH₂Cl₂ + 1% NH₄OH 37% aq. solution) to afford the product as a dark

green solid (9.6 mg, 69%). 1 H NMR (400 MHz, CD₃OD) δ 8.78 (s, 1H), 8.53 (d, J = 4.8 Hz, 1H), 8.06 (dt, J = 8.0, 2.0 Hz, 1H), 7.56 (dd, J = 7.9, 4.9 Hz, 1H), 7.25 (d, J = 8.7 Hz, 1H), 7.00 (d, J = 2.3 Hz, 1H), 6.77 (dd, J = 8.7, 2.3 Hz, 1H), 3.20 - 3.05 (m, 4H). 13 C NMR (101 MHz, CD₃OD) δ 152.1, 149.1, 148.8, 137.4, 133.6, 133.2, 131.3, 130.4, 125.5, 114.0, 113.1, 108.9, 103.5, 41.5, 25.2. $v_{\rm max}$ (film) 2922, 2855, 1738, 1711, 1462 cm $^{-1}$. HRMS (ESI) m/z calcd. for [M + H] $^{+}$ (C₁₅H₁₆N₃O₁): 254.1288, found: 254.1291.

3-(2-Aminoethyl)-2-(pyridin-3-yl)-1H-indol-6-ol (31). Prepared according to General Procedure G from tert-butyl (2-(6-(benzyloxy)-2-(pyridin-3-yl)-1H-indol-3-yl)ethyl) carbamate 29b (10.2 mg, 1.00 equiv., 23.0 μmol). Purified by column chromatography (8 to 12% MeOH in $CH_2Cl_2 + 1\%$ NH₄OH 37% aq. solution) to afford the product as a yellow solid (2.4 mg, 41%). ¹H NMR (700 MHz, CD₃OD) δ 8.76 (s, 1H), 8.53 (s, 1H), 8.05 (dt, J = 8.0, 1.9 Hz, 1H), 7.57 (dd, J = 7.9, 4.9 Hz, 1H), 7.45 (d, J = 8.5 Hz, 1H), 6.83 (d, J = 2.1 Hz, 1H), 6.69 (dd, J = 8.6, 2.1 Hz, 1H), 3.25 – 3.21 (m, 2H), 3.21 – 3.17 (m, 2H). ¹³C NMR (176 MHz, CD₃OD) δ 155.5, 148.9, 148.5, 139.6, 137.2, 131.5 (2C), 125.6, 123.5, 120.0, 111.3, 108.9, 97.7, 41.1, 24.0. v_{max} (film) 3229, 2924, 1558, 1541, 1506, 1456 cm⁻¹. HRMS (ESI) m/z calcd. for [M + H]⁺ ($C_{15}H_{16}N_3O_1$): 254.1288, found: 254.1294.

3-(2-Aminoethyl)-2-(pyridin-3-yl)-1H-indol-7-ol (32). Prepared according to General Procedure G from a mixture of tert-butyl (2-(7-(benzyloxy)-2-(pyridin-3-yl)-1H-indol-3-yl)ethyl)carbamate and tert-butyl (2-(7-methoxy-3-(pyridin-3yl)-1*H*-indol-2-yl)ethyl)carbamate (85:15) **29c** (30.6 mg, 1.00 equiv., 69.0 μ mol). Purified by column chromatography (8 to 15% MeOH in $CH_2Cl_2 + 1\% NH_4OH 37\%$ aq. solution) to afford the product as a red-brown solid (10.8 mg, 62%). ¹H NMR (700 MHz, CD₃OD) δ 8.80 (d, J = 2.3 Hz, 1H), 8.51 (dd, J = 5.0, 1.6 Hz, 1H), 8.08 (dt, J = 7.8, 2.0 Hz, 1H), 7.55(dd, J = 7.9, 4.8 Hz, 1H), 7.12 (d, J = 8.0 Hz, 1H), 6.89 (t, J = 8.0 Hz, 1H)7.8 Hz, 1H), 6.59 (d, I = 7.5 Hz, 1H), 3.07 (t, I = 7.6 Hz, 2H), 2.98 (dd, J = 8.9, 6.3 Hz, 2H). ¹³C NMR (176 MHz, CD₃OD) δ 149.4, 148.5, 145.1, 137.7, 132.2, 131.9, 131.6, 128.5, 125.4, 121.3, 112.1, 111.1, 107.8, 43.0, 28.2. $v_{\rm max}$ (film) 3329, 2974, 1653, 1456, 1045, 878 cm⁻¹. HRMS (ESI) m/z calcd. for [M + H^{+} (C₁₅ $H_{16}N_3O_1$): 254.1288, found: 254.1283.

3-(2-Aminoethyl)-2-(pyridin-3-yl)-1H-indol-4-ol (33). Prepared according to General Procedure G from tert-butyl (2-(4methoxy-2-(pyridin-3-yl)-1*H*-indol-3-yl)ethyl)carbamate **29d** (8.7 mg, 1.0 equiv., 24 μ mol). Purified by column chromatography (4 to 8% MeOH in CH₂Cl₂ + 1% NH₄OH 37% aq. solution) to afford the product as a yellow solid (1.8 mg, 30%). ¹H NMR (500 MHz, CD₃OD) δ 8.74 (d, J = 2.4Hz, 1H), 8.54 (dd, J = 4.9, 1.6 Hz, 1H), 8.03 (dt, J = 7.9, 2.1 Hz, 1H), 7.57 (dd, J = 8.0, 5.0 Hz, 1H), 6.97 (t, J = 7.8 Hz, 1H), 6.90 (d, I = 8.1 Hz, 1H), 6.43 (d, I = 7.5 Hz, 1H), 3.28 (s, 4H). 13 C NMR (126 MHz, CD₃OD) δ 153.1, 149.4, 148.7, 140.5, 137.8, 131.5, 125.4, 124.8, 110.1, 105.1, 104.2, 43.0, 30.8 note: additional signals observed by (1 H, 13 C) HMBC at \sim 131.7 ppm and \sim 119.5 ppm. $v_{\rm max}$ (film) 3335, 2924, 2855, 1593, 1456, 1254 cm⁻¹. HRMS (ESI) m/z calcd. for [M + H]⁺ $(C_{15}H_{16}N_3O_1)$: 254.1288, found: 254.1282.

3-(2-Aminoethyl)-6-fluoro-2-(pyridin-3-yl)-1H-indol-5-ol (38). Prepared according to General Procedure G from tertbutyl (2-(6-fluoro-5-methoxy-2-(pyridin-3-yl)-1H-indol-3-yl)-ethyl)carbamate 29i (13.9 mg, 1.00 equiv., 36.1 μ mol). Purified by column chromatography (8 to 12% MeOH in $CH_2Cl_2 + 1\%$ NH_4OH 37% aq. solution). Further purified by

dissolving in minimum volume of DMSO followed by addition of toluene (10 mL). The solution was cooled to $-94\,^{\circ}\mathrm{C}$ in a liquid nitrogen/acetone bath and the precipitate was collected and dried to afford the product as a yellow solid (5.4 mg, 55%). $^{1}\mathrm{H}$ NMR (500 MHz, CD3OD) δ 8.81 (bs, 1H), 8.60 (bs, 1H), 8.12 (d, J=7.9 Hz, 1H), 7.69 -7.59 (m, 1H), 7.15 (d, J=8.4 Hz, 1H), 7.14 (d, J=11.0 Hz, 1H), 3.26 -3.20 (m, 2H), 3.20 -3.14 (m, 2H). $^{13}\mathrm{C}$ NMR (126 MHz, CD3OD) δ 152.2 (d, $^{1}J_{CF}=236.8$ Hz), 148.5, 148.4, 141.0 (d, $^{2}J_{CF}=15.7$ Hz), 138.1, 133.4, 133.3, 131.8 (d, $^{3}J_{CF}=11.1$ Hz), 125.9, 125.7, 108.5, 106.0 (d, $^{3}J_{CF}=2.5$ Hz), 99.3 (d, $^{2}J_{CF}=23.6$ Hz), 40.9, 23.9. $^{19}\mathrm{F}$ NMR (377 MHz, CD3OD) δ - 142.16. $v_{\rm max}$ (solid) 3119, 2924, 1466, 1402, 1275, 1028, 806 cm $^{-1}$. HRMS (ESI) m/z calcd. for [M + H] $^{+}$ (C15 H15 F1N3O1): 272.1194, found: 272.1197.

2-(2-Aminoethyl)-6-fluoro-3-(pyridin-3-yl)-1H-indol-5-ol (52). Prepared according to General Procedure G from tertbutyl (2-(6-fluoro-5-methoxy-3-(pyridin-3-yl)-1*H*-indol-2-yl)ethyl)carbamate 29j (6.3 mg, 1.0 equiv., 16 μ mol). Purified by column chromatography (8 to 10% MeOH in CH₂Cl₂ + 1% NH₄OH 37% ag. solution) to afford the product as a yellow solid (3.0 mg, 68%). ¹H NMR (500 MHz, CD₃OD) δ 8.61 (d, J = 2.2 Hz, 1H), 8.47 (dd, J = 5.0, 1.6 Hz, 1H), 7.93 (dt, J =7.9, 2.0 Hz, 1H), 7.54 (dd, J = 7.9, 4.9 Hz, 1H), 7.09 (d, J =11.2 Hz, 1H), 6.98 (d, J = 8.4 Hz, 1H), 3.10 - 2.98 (m, 4H). ¹³C NMR (126 MHz, CD₃OD) δ 151.4 (d, ${}^{1}J_{CF}$ = 235.9 Hz), 150.5, 147.3, 141.2 (d, ${}^{2}J = 15.0 \text{ Hz}$), 138.9, 134.6, 133.7, 130.8 (d, ${}^{3}J_{CF}$ = 10.9 Hz), 125.5, 124.6, 111.4, 105.5 (d, ${}^{3}J_{CF}$ = 2.2 Hz), 99.0 (d, ${}^{2}J_{CF}$ = 23.2 Hz), 41.5, 28.6. ${}^{19}F$ NMR (376 MHz, CD₃OD) δ – 143.46. v_{max} (solid) 2920, 2851, 1472, 1098, 1026, 804 cm⁻¹. HRMS (ESI) m/z calcd. for [M + H]⁺ $(C_{15}H_{15}F_1N_3O_1)$: 272.1194, found: 272.1195.

3-(Aminomethyl)-2-(pyridin-3-yl)-1H-indol-5-ol (39). Prepared according to General Procedure G from tert-butyl ((5-methoxy-2-(pyridin-3-yl)-1H-indol-3-yl)methyl) carbamate 29k (10.0 mg, 1.00 equiv., 28.3 μmol). Purified by column chromatography (0 to 14% MeOH in $\mathrm{CH_2Cl_2}+1\%$ NH₄OH 37% aq. solution) to afford the product as a yellow solid (2.7 mg, 40%). ¹H NMR (700 MHz, $\mathrm{CD_3OD}$) δ 9.28 – 8.50 (m, 2H), 8.12 (d, J=7.7 Hz, 1H), 7.82 – 7.62 (m, 1H), 7.31 (d, J=8.6 Hz, 1H), 7.11 (d, J=2.2 Hz, 1H), 6.84 (dd, J=8.7, 2.2 Hz, 1H), 4.36 (s, 2H). ¹³C NMR (176 MHz, $\mathrm{CD_3OD}$) δ 152.8, 149.6, 137.8, 136.3, 132.9, 129.7, 127.2, 123.5, 114.6, 113.3, 105.4, 103.4, 35.1. v_{max} (film) 3211, 2922, 2856, 1628, 1456, 1217 cm⁻¹. HRMS (ESI): [M + H]+ m/z calcd. for ($\mathrm{C_{14}H_{14}N_3O_1}$): 240.1131, found: 240.1132.

3-(3-Aminopropyl)-2-(pyridin-3-yl)-1H-indol-5-ol (40). Prepared according to General Procedure G from tert-butyl (3-(5-methoxy-2-(pyridin-3-yl)-1H-indol-3-yl)propyl)carbamate 291 (15.0 mg, 1.00 equiv., 39.3 μ mol). Purified by column chromatography (8 to 15% MeOH in CH₂Cl₂ + 1% NH₄OH 37% aq. solution) to afford the product as a yellow solid (3.6 mg, 34%). ¹H NMR (500 MHz, CD₃OD) δ 8.77 (s, 1H), 8.53 (s, 1H), 8.06 (dt, I = 8.0, 1.8 Hz, 1H), 7.57 (dd, I =8.0, 4.8 Hz, 1H), 7.24 (d, I = 8.7 Hz, 1H), 6.97 (d, I = 2.2 Hz, 1H), 6.76 (dd, J = 8.6, 2.3 Hz, 1H), 2.97 (t, J = 7.7 Hz, 2H), 2.95 - 2.91 (m, 2H), 2.01 (p, J = 7.8 Hz, 2H). ¹³C NMR (126 MHz, CD₃OD) δ 151.8, 148.9, 148.5, 137.2, 133.2, 132.6, 130.9, 130.6, 125.4, 113.9, 112.9, 112.5, 103.7, 40.7, 29.9, 22.5. $v_{\rm max}$ (film) 3215, 2924, 2853, 1456, 1206, 802 cm⁻¹. HRMS (ESI) m/z calcd. for $[M + H]^+$ $(C_{16}H_{18}N_3O_1):268.1444$, found: 268.1453.

3-(2-Aminoethyl)-2-(5-fluoropyridin-3-yl)-1H-indol-5-ol (41). Prepared according to General Procedure G from tertbutyl (2-(2-(5-fluoropyridin-3-yl)-5-methoxy-1*H*-indol-3-yl)ethyl)carbamate 29m (9.5 mg, 1.0 equiv., 25 μ mol). Purified by column chromatography (0 to 12% MeOH in $CH_2Cl_2 + 1\%$ NH₄OH 37% aq. solution) to afford the product as a dark green solid (5.3 mg, 55%). ¹H NMR (700 MHz, CD₃OD) δ 8.66 (s, 1H), 8.45 (d, J = 2.6 Hz, 1H), 7.85 (dt, J = 9.8, 2.4 Hz, 1H), 7.25 (d, J = 8.6 Hz, 1H), 7.00 (d, J = 2.3 Hz, 1H), 6.78(dd, J = 8.7, 2.3 Hz, 1H), 3.13 - 3.09 (m, 2H), 3.03 (t, J = 7.7)Hz, 2H).¹³C NMR (176 MHz, CD₃OD) δ 161.2 (d, ${}^{1}J_{CF}$ = 254.9 Hz), 152.1, 145.4, 136.8 (d, ${}^{2}J_{CF} = 23.7$ Hz), 133.3, 132.9, 131.9, 130.6, 123.3 (d, ${}^{2}J_{CF} = 18.8 \text{ Hz}$), 114.4, 113.1, 111.0, 103.7, 42.2, 27.0. ¹⁹F NMR (470 MHz, CD₃OD) δ – 127.95. v_{max} (film) 3219, 2924, 1558, 1541, 1506, 1456 cm⁻¹. HRMS (ESI) m/z calcd. for $[M + Na]^+$ ($C_{15}H_{14}F_1N_3O_1Na_1$): 294.1013, found: 294.1010.

3-(2-Aminoethyl)-2-(pyridin-2-yl)-1H-indol-5-ol (42). Prepared according to General Procedure G from tert-butyl (2-(5methoxy-2-(pyridin-2-yl)-1*H*-indol-3-yl)ethyl)carbamate **29n** (20.0 mg, 1.00 equiv., 54.4 μ mol). Purified by column chromatography (8 to 12% MeOH in CH₂Cl₂ + 1% NH₄OH 37% aq. solution) to afford the product as a dark yellow solid (8.7 mg, 63%). ¹H NMR (500 MHz, CD₃OD) δ 8.62 (ddd, J = 5.0, 1.9, 0.9 Hz, 1H), 7.88 (td, J = 7.8, 1.9 Hz, 1H), 7.77 (dt, *J* = 8.1, 1.1 Hz, 1H), 7.29 (ddd, *J* = 7.5, 4.9, 1.1 Hz, 1H); H, 7.26 (d, J = 8.7 Hz, 1H), 6.99 (d, J = 2.3 Hz, 1H), 6.77 (dd, J = 8.7, 2.3 Hz, 1H), 3.26 (t, J = 7.0 Hz, 2H), 3.09 (t, $J = 7.0 \text{ Hz}, 2\text{H}).^{13}\text{C NMR}$ (126 MHz, CD₃OD) δ 153.0, 151.9, 150.2, 138.5, 135.2, 133.0, 131.0, 123.0, 122.7, 114.6, 113.1, 111.9, 103.6, 42.5, 27.1. v_{max} (film) 3242, 2922, 1589, 1456, 1207, 1020, 787 cm⁻¹. HRMS (ESI) m/z calcd. for $[M + H]^+$ $(C_{15}H_{16}N_3O_1)$: 254.1288, found: 254.1284.

3-(2-Aminoethyl)-2-(pyridin-4-yl)-1H-indol-5-ol (43). Prepared according to General Procedure G from tert-butyl (2-(5methoxy-2-(pyridin-4-yl)-1*H*-indol-3-yl)ethyl)carbamate **290** (16.9 mg, 1.00 equiv., 46.0 μ mol). Purified by column chromatography (5 to 10% MeOH in CH₂Cl₂ + 1% NH₄OH 37% aq. solution) to afford a residue which was further purified by dissolving in the minimum volume of MeOH (approximately 0.2 mL) followed by addition of Et₂O (2 mL). The precipitate was collected and dried under vacuum to afford the product as a yellow-green solid (5.9 mg, 50%). ¹H NMR (400 MHz, CD₃OD) δ 8.59 (d, I = 5.0 Hz, 2H), 7.71 -7.60 (m, 2H), 7.26 (d, J = 8.7 Hz, 1H), 7.00 (d, J = 2.2 Hz, 1H), 6.79 (dd, J = 8.7, 2.1 Hz, 1H), 3.18 (t, J = 7.6 Hz, 2H), 3.10 - 3.01 (m, 2H). ¹³C NMR (126 MHz, CD₃OD) δ 152.1, 150.5, 143.2, 133.4, 133.2, 130.9, 123.3, 115.0, 113.2, 112.0, 103.7, 42.1, 27.0. v_{max} (film) 3244, 2924, 2855, 1503, 1558, 1456, 1211 cm⁻¹. HRMS (ESI) m/z calcd. for $[M + H]^+$ $(C_{15}H_{16}N_3O_1)$: 254.1288, found: 254.1277.

3-(2-Aminoethyl)-2-(pyrimidin-5-yl)-1H-indol-5-ol (44). Prepared according to General Procedure G from tert-butyl (2-(5-methoxy-2-(pyrimidin-5-yl)-1H-indol-3-yl)ethyl)-carbamate 29p (15.4 mg, 1.00 equiv., 41.8 μmol). Purified by column chromatography (5 to 10% MeOH in $\mathrm{CH_2Cl_2} + 1\%$ NH₄OH 37% aq. solution) to afford the product as a dark green solid (6.1 mg, 57%). ¹H NMR (500 MHz, CD₃OD) δ 9.13 (s, 1H), 9.02 (s, 2H), 7.27 (d, J = 8.7 Hz, 1H), 7.01 (d, J = 2.3 Hz, 1H), 6.79 (dd, J = 8.7, 2.3 Hz, 1H), 3.19 – 3.07 (m, 4H). ¹³C NMR (126 MHz, CD₃OD) δ 157.5, 156.6, 152.2, 133.6, 130.4, 130.0, 129.4, 114.7, 113.2, 110.7, 103.7, 41.9, 25.8. v_{max} (film) 3244, 2922, 2853, 1624, 1458, 1412, 1015

cm⁻¹. HRMS (ESI): m/z calcd. for $[M + H]^+$ ($C_{14}H_{15}N_4O_1$): 255.1240, found: 255.1236.

2-(2-Aminoethyl)-3-(pyrimidin-5-yl)-1H-indol-5-ol (53). Prepared according to General Procedure G from tert-butyl (2-(5-methoxy-3-(pyrimidin-5-yl)-1H-indol-2-yl)ethyl)-carbamate 29q (9.2 mg, 1.00 equiv., 25 μmol). Purified by column chromatography (5 to 10% MeOH in CH₂Cl₂ + 1% NH₄OH 37% aq. solution) to afford the product as a dark green solid (5.8 mg, 91%). ¹H NMR (500 MHz, CD₃OD) δ 9.06 (s, 1H), 8.90 (s, 2H), 7.23 (d, J = 8.7 Hz, 1H), 6.91 (d, J = 2.3 Hz, 1H), 6.73 (dd, J = 8.7, 2.3 Hz, 1H), 3.04 (s, 4H). ¹³C NMR (126 MHz, CD₃OD) δ 157.8, 156.1, 152.8, 136.6, 132.3, 132.3, 128.9, 113.1, 112.8, 107.4, 102.6, 42.0, 29.7. $v_{\rm max}$ (film) 3217, 2924, 1558, 1412, 1163, 802 cm⁻¹. HRMS (ESI) m/z calcd. for [M + H]⁺ (C₁₄H₁₅N₄O₁): 255.1240, found: 255.1246.

3-(2-Aminoethyl)-2-(thiazol-5-yl)-1H-indol-5-ol (45). Prepared according to General Procedure G from tert-butyl (2-(5-methoxy-2-(thiazol-5-yl)-1H-indol-3-yl)ethyl)carbamate 29r (8.6 mg, 1.0 equiv., 23 μmol). Purified by column chromatography (8 to 12% MeOH in CH₂Cl₂ + 1% NH₄OH 37% aq. solution) to afford the product as a yellow solid (4.1 mg, 69%). ¹H NMR (500 MHz, CD₃OD) δ 9.03 (s, 1H;), 8.13 (s, 1H), 7.21 (d, J = 8.7 Hz, 1H), 6.96 (d, J = 2.3 Hz, 1H), 6.76 (dd, J = 8.7, 2.3 Hz, 1H), 3.15 – 3.10 (m, 2H), 3.03 – 2.99 (m, 2H). ¹³C NMR (126 MHz, CD₃OD) δ 154.4, 152.1, 140.6, 133.2, 131.7, 130.6, 127.2, 114.4, 112.9, 111.2, 103.5, 42.1, 27.2. $v_{\rm max}$ (film) 3210, 2920, 1456, 1217, 837, 802 cm⁻¹. HRMS (ESI): [M + H]⁺ (C₁₃H₁₄N₃O₁S₁): 260.0852, found: 260.0854.

3-(2-Aminoethyl)-1-methyl-2-(pyridin-3-yl)-1H-indol-5-ol (48). Prepared according to General Procedure G from 2-(5-(benzyloxy)-1-methyl-2-(pyridin-3-yl)-1H-indol-3-yl)ethan-1amine S19 (6.5 mg, 1.0 equiv., 18 μ mol). Purified by column chromatography (5 to 10% MeOH in CH₂Cl₂ + 1% NH₄OH 37% ag. solution) to afford the product as a brown solid (2.4) mg, 50%). ¹H NMR (500 MHz, CD₃OD) δ 8.67 – 8.63 (m, 1H), 8.62 (d, J = 1.8 Hz, 1H), 7.94 (dt, J = 7.9, 1.9 Hz, 1H), 7.62 (ddd, J = 7.8, 4.9, 0.9 Hz, 1H), 7.28 (d, J = 8.8 Hz, 1H), 7.01 (d, J = 2.3 Hz, 1H), 6.89 - 6.78 (m, 1H), 3.56 (s, 3H), 2.98 - 2.94 (m, 2H), 2.93 - 2.89 (m, 2H). ¹³C NMR (126 MHz, CD₃OD) δ 152.3, 151.4, 149.8, 140.3, 136.4, 134.3, 130.0, 129.2, 125.3, 113.7, 111.5, 110.2, 103.8, 42.1, 31.2, 26.2. $v_{\rm max}$ (solid) 3354, 2922, 2490, 1456, 1020, 797 cm $^{-1}$. HRMS (ESI) m/z calcd. for $[M + H]^+$ ($C_{16}H_{18}N_3O_1$): 268.1444, found: 268.1449.

2-(5-(2-Aminoethyl)pyridin-3-yl)-1H-indol-5-ol (49). Prepared according to General Procedure G from tert-butyl (2-(5-(5-methoxy-1H-indol-2-yl)pyridin-3-yl)ethyl)carbamate S25 (12.2 mg, 1.00 equiv., 33.2 μmol). Purified by column chromatography (8 to 12% MeOH in $CH_2Cl_2 + 1\%$ NH₄OH 37% aq. solution) to afford the product as a brown solid (7.7 mg, 92%). ¹H NMR (500 MHz, CD₃OD) δ 8.82 (d, J=2.2 Hz, 1H), 8.31 (d, J=2.0 Hz, 1H), 8.08 (t, J=2.1 Hz, 1H), 7.24 (d, J=8.7 Hz, 1H), 6.94 (dd, J=2.4, 0.6 Hz, 1H), 6.81 (d, J=0.9 Hz, 1H), 6.72 (dd, J=8.7, 2.4 Hz, 1H), 3.06 (t, J=7.4 Hz, 2H), 2.91 (t, J=7.4 Hz, 2H). ¹³C NMR (126 MHz, CD₃OD) δ 152.1, 148.4, 144.8, 136.7, 135.8, 134.3, 134.2, 131.1, 131.0, 113.9, 112.8, 105.4, 100.9, 43.1, 35.6. v_{max} (solid) 2918, 2851, 1458, 1192, 785 cm⁻¹. HRMS (ESI) m/z calcd. for $[M+H]^+$ ($C_{15}H_{16}N_3O_1$): 254.1288, found: 254.1293.

General Procedure H for the Preparation of Compounds 1, 34–36, 50. A round-bottom flask under air was

charged with N-Boc-amide (1.00 equiv) and $\mathrm{CH_2Cl_2}$ (1.20 mL per 0.10 mmol amide). The mixture was cooled to 0 °C, and TFA (300 $\mu\mathrm{L}$ per 0.10 mmol amide) was added. The mixture was stirred at 0 °C for 40 min, after which it was allowed to warm to RT and was stirred for a further 80 min. Volatiles were removed under reduced pressure to afford the product. Where purification was necessary, this was achieved by column chromatography (silica gel).

2-(2-(Pyridin-3-yl)-1H-indol-3-yl)ethan-1-amine, TFA salt (1). Prepared according to General Procedure H from tertbutyl (2-(2-(pyridin-3-yl)-1H-indol-3-yl)ethyl)carbamate 29u (11.5 mg, 1.00 equiv., 34.1 μmol) to afford the product as a yellow solid (16.3 mg, quant.). ¹H NMR (500 MHz, CD₃OD) δ 8.99 (s, 1H), 8.73 (s, 1H), 8.45 (d, J = 8.3 Hz), 7.93 – 7.86 (m, 1H), 7.69 (dt, J = 8.1, 1.0 Hz, 1H), 7.46 (d, J = 8.2 Hz, 1H), 7.25 (ddd, J = 8.2, 7.0, 1.1 Hz, 1H), 7.15 (ddd, J = 8.0, 7.1, 1.0 Hz, 1H), 3.34 – 3.31 (m, 2H), 3.27 – 3.21 (m, 2H). ¹³C NMR (126 MHz, CD₃OD) δ 145.5, 145.1, 141.6, 138.6, 132.7, 131.3, 129.4, 127.2, 124.6, 121.2, 119.7, 112.8, 110.3, 40.9, 23.8. v_{max} (film) 2922, 1682, 1566, 1188, 1134, 835, 802 cm⁻¹. HRMS (ESI) m/z calcd. for [M + H]⁺ (C₁₅H₁₆N₃): 238.1339, found: 238.1342.

2-(5-Fluoro-2-(pyridin-3-yl)-1H-indol-3-yl)ethan-1-amine (34). Prepared according to General Procedure H from tertbutyl (2-(5-fluoro-2-(pyridin-3-yl)-1*H*-indol-3-yl)ethyl)carbamate 29e (10.6 mg, 1.00 equiv., 29.8 μ mol). Purified by column chromatography (4 to 8% MeOH in CH₂Cl₂ + 1% NH₄OH 37% aq. solution) to afford the product as a light brown solid (5.2 mg, 68%). ¹H NMR (500 MHz, (CD₃)₂O) δ 9.03 (d, J = 0.9 Hz, 1H), 8.57 (dd, J = 4.8, 1.7 Hz, 1H), 8.27 (ddd, J = 7.9, 2.3, 1.6 Hz, 1H), 7.48 (ddd, J = 7.9, 4.7, 0.9 Hz, 1H), 7.43 - 7.37 (m, 2H), 6.95 (ddd, J = 9.5, 8.8, 2.5 Hz, 1H), 3.60 (t, J = 7.0 Hz, 2H), 3.15 (t, J = 7.0 Hz, 2H).¹³C NMR (126 MHz, (CD₃)₂O) δ 158.5 (d, ${}^{1}J_{CF}$ = 232.1 Hz), 149.9, 149.4, 136.2, 134.7, 134.1, 130.3 (d, ${}^{3}J = 9.7 \text{ Hz}$), 129.9, 124.3, 113.3 (d, ${}^{4}J_{CF} = 5.0 \text{ Hz}$), 112.9 (d, ${}^{3}J_{CF} = 9.7 \text{ Hz}$), 111.02 (d, $^{2}J_{CF} = 26.5 \text{ Hz}$), 104.7 (d, $^{2}J_{CF} = 23.5 \text{ Hz}$), 52.5, 26.7. ¹⁹F NMR (377 MHz, $(CD_3)_2O$) δ – 126.16. v_{max} (film) 3167, 2922, 1447, 1177, 797 cm⁻¹. HRMS (ESI) m/z calcd. for [M + H]⁺ $(C_{15}H_{15}F_1N_3)$: 256.1245, found: 256.1252.

2-(6-Fluoro-2-(pyridin-3-yl)-1H-indol-3-yl)ethan-1-amine, TFA Salt (35). Prepared according to General Procedure H from tert-butyl (2-(6-fluoro-2-(pyridin-3-yl)-1H-indol-3-yl)ethyl)carbamate 29f (8.2 mg, 1.00 equiv., 23 μ mol) to afford the product as a yellow solid (11.3 mg, quant.). ¹H NMR (500 MHz, CD₃OD) δ 8.93 (s, 1H), 8.70 (s, 1H), 8.34 (dt, J = 8.1, 1.6 Hz, 1H, 7.86 - 7.79 (m, 1H), 7.65 (dd, J = 8.8, 5.1 Hz, 1H), 7.15 (dd, J = 9.7, 2.3 Hz, 1H), 6.94 (ddd, J = 9.6, 8.7, 2.3 Hz, 1H), 3.29 - 3.26 (m, 2H), 3.24 - 3.19 (m, 2H). 13 C NMR (126 MHz, CD₃OD) δ 162.1 (d, ${}^{1}J_{CF}$ = 238.4 Hz), 146.5, 146.3, 140.5, 138.6 (d, ${}^{3}J_{CF} = 12.7 \text{ Hz}$), 132.5, 132.0, 126.8, 126.2, 120.8 (d, ${}^{3}J_{CF} = 10.2 \text{ Hz}$), 110.2, 109.8 (d, ${}^{2}J_{CF} =$ 25.1 Hz), 98.6 (d, ${}^{2}J_{CF}$ = 26.3 Hz), 40.9, 23.8. ${}^{19}F$ NMR (377 MHz, CD₃OD) δ – 77.15 (TFA), – 121.28. v_{max} (solid) 2924, 1668, 1188, 1140, 1126, 839, 804 cm⁻¹. HRMS (ESI) m/zcalcd. for $[M + H]^+$ (C₁₅H₁₅F₁N₃): 256.1245, found: 256.1250.

3-(2-Aminoethyl)-2-(pyridin-3-yl)-1H-indol-5-amine TFA Salt (**36**). Prepared according to General Procedure H from tert-butyl (2-(5-((tert-butoxycarbonyl)amino)-2-(pyridin-3-yl)-1H-indol-3-yl)ethyl)carbamate **29g** (10.0 mg, 1.00 equiv., 22.1 μ mol) to afford the product as a brown solid (11.0 mg, quant.). ¹H NMR (700 MHz, CD₃OD) δ 9.05 – 8.76 (m,

2H), 8.42 (d, J = 7.9 Hz, 1H), 7.91 (s, 1H), 7.78 (d, J = 2.1 Hz, 1H), 7.60 (d, J = 8.6 Hz, 1H), 7.24 (dd, J = 8.6, 2.1 Hz, 1H), 3.33 - 3.31 (m, 2H), 3.25 - 3.21 (m, 2H). ¹³C NMR (176 MHz, CD₃OD) δ 146.6, 146.6, 143.2, 141.0, 137.8, 134.6, 131.7, 129.7, 124.4, 118.6, 114.3, 114.2, 110.5, 40.8, 23.6. v_{max} (film) 2926, 1667, 1431, 1180, 1125, 837, 799, 721 cm⁻¹. HRMS (ESI) m/z calcd. for [M + Na]⁺ (C₁₅H₁₆N₄Na₁): 275.1267, found: 275.1271.

2-(3-(Pyridin-3-yl)-1H-indol-2-yl)ethan-1-amine, TFA Salt (**50**). Prepared according to General Procedure H from tertbutyl (2-(3-(pyridin-3-yl)-1H-indol-2-yl)ethyl)carbamate **29v** (11.3 mg, 1.00 equiv., 33.5 μmol) to afford the product as an orange solid (15.8 mg, quant.). ¹H NMR (500 MHz, CD₃OD) δ 8.92 (s, 1H), 8.73 (s, 1H), 8.56 (d, J = 7.9 Hz, 1H), 8.03 (bs, 1H), 7.59 (dt, J = 8.0, 1.0 Hz, 1H), 7.46 (dt, J = 8.2, 0.9 Hz, 1H), 7.23 (ddd, J = 8.2, 7.1, 1.1 Hz, 1H), 7.14 (ddd, J = 8.1, 7.1, 1.0 Hz, 1H), 3.36 – 3.32 (m, 2H), 3.30 – 3.27 (m, 2H). ¹³C NMR (126 MHz, CD₃OD) δ 145.5, 144.2, 141.6, 137.8, 136.3, 133.8, 128.0, 127.8, 124.0, 122.0, 118.6, 112.6, 110.3, 40.0, 25.4. v_{max} (film) 2924, 1668, 1568, 1177, 1126, 835, 799 cm⁻¹. HRMS (ESI) m/z calcd. for [M + H]⁺ (C₁₅H₁₆N₃): 238.1339, found: 238.1339.

3-(2-Aminoethyl)-2-(pyridin-3-yl)-1H-indole-5-carboxylic Acid Hydrochloride (37). An oven-dried microwave vial was charged with methyl 3-(2-((tert-butoxycarbonyl)amino)ethyl)-2-(pyridin-3-yl)-1H-indole-5-carboxylate 29h (8.4 mg, 1.0 equiv., 21 μ mol), AcOH (0.40 mL) and conc. HCl (0.10 mL). The vial was sealed, and the mixture was stirred at 100 °C for 18 h. After cooling to RT, volatiles were removed under reduced pressure to afford a solid which was dissolved in the minimum volume of MeOH (approximately 0.2 mL) followed by addition of Et₂O (2 mL). The precipitate was collected and dried under vacuum to afford the product as a brown solid (6.0 mg, 80%). 1 H NMR (400 MHz, CD₃OD) δ 9.18 – 9.02 (m, 1H), 8.93 - 8.78 (m, 1H), 8.65 (d, I = 8.1 Hz, 1H), 8.49 (dd, I= 1.6, 0.7 Hz, 1H, 8.12 - 8.07 (m, 1H), 7.97 (dd, I = 8.6, 1.6)Hz, 1H), 7.54 (dd, J = 8.6, 0.7 Hz, 1H), 3.40 - 3.34 (m, 2H), 3.29 - 3.23 (m, 2H). ¹³C NMR (126 MHz, CD₃OD) δ 170.9, 145.6, 142.0, 141.8, 141.1, 131.4, 130.6, 129.3, 129.0, 125.9, 123.6, 123.0, 112.6, 111.7, 41.0, 23.6. v_{max} (solid) 2920, 2853, 1665, 1560, 1221, 814 cm⁻¹. HRMS (ESI) m/z calcd. for [M + Na⁺ ($C_{16}H_{15}N_3O_2Na_1$): 304.1057, found: 304.1055.

3-(2-(Methylamino)ethyl)-2-(pyridin-3-yl)-1H-indol-5-ol Hydrochloride (46). A round-bottom flask fitted with a reflux condenser was charged with tert-butyl (2-(5-(methoxymethoxy)-2-(pyridin-3-yl)-1H-indol-3-yl)ethyl)(methyl)carbamate **29s** (12.4 mg, 1.00 equiv., 30.1 μ mol), MeOH (1.20 mL), and 3 M HCl (0.400 mL). The mixture was heated to reflux for 2 h, after which volatiles were removed under reduced pressure to afford the product as a yellow solid (10.3 mg, quant.). ¹H NMR (500 MHz, CD₃OD) δ 9.13 (s, 1H), 8.87 - 8.73 (m, 2H), 8.22 (s, 1H), 7.32 (d, J = 8.7 Hz, 1H), 7.07 (d, J = 2.2 Hz, 1H), 6.85 (d, J = 8.7 Hz, 1H), 3.35 - 3.32(m, 2H), 3.30 - 3.27 (m, 2H), 2.72 (s, 3H). ¹³C NMR (126) MHz, CD₃OD) δ 152.7, 145.9, 141.3, 140.7, 133.8, 130.1, 130.1, 129.8, 129.0, 115.9, 113.6, 110.7, 103.7, 50.2, 33.8, 22.7. $v_{\rm max}$ (film) 3201, 2920, 2851, 1560, 1464, 797 cm⁻¹. HRMS (ESI) m/z calcd. for $[M + H]^+$ $(C_{16}H_{18}N_3O_1)$: 268.1444, found: 268.1436.

3-(2-Hydroxyethyl)-2-(pyridin-3-yl)-1H-indol-5-ol (47). A round-bottom flask fitted with a reflux condenser was charged with 3-(2-((tert-butyldimethylsilyl)oxy)ethyl)-5-(methoxymethoxy)-2-(pyridin-3-yl)-1H-indole 29t (11.1 mg, 1.00 equiv.,

26.9 μmol), MeOH (1.20 mL), and 3 M HCl (400 μL). The mixture was heated to 80 °C for 2 h, after which volatiles were removed under reduced pressure. The residue was purified by column chromatography (silica gel, 0 to 6% MeOH in CH₂Cl₂) to afford the product as a yellow solid (2.5 mg, 32%). ¹H NMR (500 MHz, CD₃OD) δ 8.85 (s, 1H), 8.50 (d, J = 4.9 Hz, 1H), 8.14 (dt, J = 8.0, 2.0 Hz, 1H), 7.54 (dd, J = 8.0, 4.9 Hz, 1H), 7.22 (d, J = 8.6 Hz, 1H), 6.97 (d, J = 2.2 Hz, 1H), 6.73 (dd, J = 8.5, 1.7 Hz, 1H), 3.84 (t, J = 7.3 Hz, 2H), 3.06 (t, J = 7.3 Hz, 2H). ¹³C NMR (126 MHz, CD₃OD) δ 151.7, 149.0, 148.3, 137.3, 133.3, 133.3, 131.8, 131.0, 125.3, 113.7, 112.8, 110.8, 103.9, 63.2, 29.3. $v_{\rm max}$ (solid) 3215, 2920, 1454, 1204, 1042 cm⁻¹. HRMS (ESI) m/z calcd. for [M + H]⁺ (C₁₅H₁₅N₂O₂): 255.1128, found: 255.1120.

2-(2-Aminoethyl)-3-(pyridin-3-yl)-1H-indol-5-ol (**51**). A round-bottom flask was charged with Pd/C (8.6 mg, 20 mol %, 10 wt % on carbon). The flask was sealed, evacuated, and refilled with N₂ three times. N,N-Dibenzyl-2-(5-(benzyloxy)-3-(pyridin-3-yl)-1*H*-indol-2-yl)ethan-1-amine **S28** (21.3 mg, 1.00 equiv., 40.7 μ mol) in MeOH (1.0 mL) was added, followed by AcOH (47 μ L, 20 equiv., 0.81 mmol). H₂ gas was bubbled through the mixture for 5 min, after which the reaction was heated to 60 °C under H₂ atmosphere (1 atm) for 24 h. After cooling to RT, the mixture was filtered through Celite, volatiles were removed under reduced pressure, and the residue was purified by column chromatography (silica gel, 10 to 12% MeOH in CH₂Cl₂ + 1% NH₄OH 37% aq. solution) to obtain the product as a green-brown solid (6.8 mg, 66%). ¹H NMR (400 MHz, CD₃OD) δ 8.63 (s, 1H), 8.46 (d, I = 3.8 Hz, 1H), 7.97 - 7.90 (m, 1H), 7.54 (dd, J = 8.0, 5.0 Hz, 1H), 7.21(d, J = 8.6 Hz, 1H), 6.89 (d, J = 2.4 Hz, 1H), 6.71 (dd, J = 8.6,2.3 Hz, 1H), 3.08 (m, 4H). 13 C NMR (126 MHz, CD₃OD) δ 152.5, 150.3, 147.0, 138.9, 135.0, 134.0, 132.3, 129.3, 125.4, 112.9, 112.6, 111.2, 103.1, 41.6, 28.8. v_{max} (film) 3210, 2968, 2922, 1458, 1406, 1051 cm⁻¹. HRMS (ESI) m/z calcd. for [M + H]⁺ (C₁₅H₁₆N₃O₁): 254.1288, found: 254.1285.

Biochemical Fluorescence Assay. Enzymes were purified as below and the biochemical assay including materials used was based on the publication by Visnes et al.⁵¹ and "EUbOPEN" protocols (https://www.eubopen.org/protocolsreagents) and adapted where mentioned. OGG1 activation was monitored in a kinetic mode and a time-resolved curve was obtained for each compound concentration in triplicates except where stated otherwise. Initial slopes were taken of the linear part of these curves to determine rates and kinetics. Fluorescence values of each compound concentration were normalized by the DMSO control values and calculated as % activation of the full turnover fluorescence of the APE1 (2 nM) control. The median activation concentration (AC₅₀) for each compound was calculated from the % activation of all tested concentrations and refers to the compound concentration which activates the reaction to 50% of the substrate turnover reached in the assay control coupled to APE1 (2 nM) as described before.⁶⁷ In the screening, primary hits were defined as compounds with an AC₅₀ of below 100 μ M.

Proteins and Reagents. Enzymes (APE1, UDG, TDG, SMUG1, MPG, NEIL1, NTHL1, NUDT15, NUDT22, NUDT5) and mutants were produced as reported previously. 51,67,96,97 8-oxoG-containing oligonucleotide (see sequence below) was radiolabeled at the 5' end with $[\gamma^{32}P]$ -ATP (PerkinElmer Life Sciences) and T4 polynucleotide kinase (T4PNK) from New England Biolabs.

Oligonucleotides. For PAGE Analysis. Oligonucleotide 5GTACCCGGGGATCCGTAA8GCGCATCAGCTGCAG (Integrated DNA Technologies), where 8 stands for 80xodG, was 5'-labeled and further hybridized to the complementary oligonucleotide 5'-CAGCAGCTGATGCGCCTTACGGATCCCCGGGTAC in the presence of 60 mM Tris-HCl (pH 7.5) and 0.2 M NaCl by heating to 80 °C for 5 min before slowly cooling to room temperature overnight. For standard biochemical assay: Complementary strands containing FAM and DAB were ordered from ATD BIO. Sequences were 5'-FAM-TCTGCCA8CACTGCGTCGACCTG-3' and 5'-CAGGTCGACGCAGTGYTGGCAGT-Dab-3' where 8 is a uracil or 8-0xoA, and Y is the corresponding required complementary base.

hOGG1 Activity Assay on Radiolabeled 8-OxoG-Containing Oligonucleotide. To analyze the activity of hOGG1 on 8-oxoG containing substrates, 2 nM of the indicated 34mer [32 P]5'-labeled 8oxoG-containing substrate was incubated with 10 nM wildtype hOGG1 and either 10% DMSO, 6.25 μ M TH10785, 6.25 μ M 30, 10 μ M 38, or 50 μ M TH5487 in the presence of 30 mM Hepes, pH 7.5, 4% glycerol, 20 mM EDTA, 16 mM NaCl, and 0.01% Tween-20 in a final volume of 12.5 μ L. Samples were incubated at 37 °C for the indicated times. The reactions were stopped by addition of 12.5 μ L of formamide buffer (20 mM EDTA, 95% formamide, 0.05% bromophenol blue and 0.05% xylencyanol blue) and further heating at 90 °C for 2 min. DNA products were analyzed by 7 M urea-20% PAGE and visualized with an Amersham Typhoon scanner.

NaBH₄ Trapping Assay. The reactions were carried out in a final volume of 12.5 μ L in the presence of either 10% DMSO or 6.25 μ M compound 30 or 10 μ M compound 38, in the presence of 30 mM HEPES, pH 7.5, 4% glycerol, 20 mM EDTA, 16 mM NaCl and 0.01% Tween-20. In the trapping assay on an AP-containing DNA, 1 nM of the 34mer [32P]5'labeled uridine-containing substrate was treated with 0.2 U E. coli UDG (NEB) for 15 min at 37 °C to leave an intact AP site. 78 pM hOGG1 was added and after 30 s, the Schiff base intermediate was trapped by adding 100 mM NaBH₄ or 100 mM NaCl, as indicated. After incubation for 20 min on ice, samples were analyzed by 12% SDS-PAGE and the reaction products visualized with an Amersham Typhoon scanner. In the trapping assay on an 80xoG-containing DNA, 2 nM of the indicated 34 mer [32P]5'-labeled 80xoG-containing substrate was used. 625 pM hOGG1 was added and after 1 min, the Schiff base intermediate was trapped by adding 100 mM NaBH₄ or 100 mM NaCl, as indicated, and products were processed as indicated above.

Kinetic Solubility Assay. Performed according to Enamine's aqueous solubility standard operating procedure. Briefly, using a 17.5 mM stock solution of **30** in 100% DMSO dilutions were prepared to a theoretical concentration of 350 μM in duplicates in phosphate-buffered saline pH 7.4 (138 mM NaCl, 2.7 mM KCl, 10 mM K-phosphate) with 2% final DMSO. The experimental compound dilutions in PBS were further allowed to equilibrate at 25 °C on a Thermomixer R Block, 1.5 mL (Eppendorf, Germany; Cat # 5355) for 2 h and then filtered through HTS filter plates using a vacuum manifold. The filtrates of test compounds were diluted 2-fold with acetonitrile with 2% DMSO before measuring.

In parallel, using a 17.5 mM stock solution of **30** in 100% DMSO dilutions were prepared to theoretical concentrations of 0 μ M (blank), 8.75 μ M, 21.875 μ M, 43.75 μ M, 87.5 μ M,

and 175 μ M in 50% acetonitrile/PBS with 2% final DMSO to generate calibration curves. Ondansetron was used as a reference compound to control proper assay performance. 200 μ L of each sample was transferred to a 96-well plate and measured in the 230–550 nm range with a 5 nm step on a SpectraMax Paradigm Reader (Multi-Mode Detection Platform, Product # 33270–1279) using SoftMax Pro v.5.4 (Molecular Devices) software.

The concentrations of compounds in PBS filtrate were calculated using a dedicated Microsoft Excel calculation script. Proper absorbance wavelengths for calculations are selected for each compound manually based on absorbance maximums (absolute absorbance unit values for the minimum and maximum concentration points within the 0–3 OD range). Each final data set is visually evaluated by the operator, and goodness-of-fit (R²) is calculated for each calibration curve. The effective range of this assay is approximately 2–350 $\mu\rm M$ and the compounds returning values close to the upper limit of the range may have higher actual solubility (e.g., 5′-deoxy-5-fluorouridine).

Microsomal Stability Assay. Microsomal incubations were carried out in 96-well plates in 5 aliquots of 30 μ L each (one for each time point). Liver microsomal incubation medium comprised of phosphate buffer (100 mM, pH 7.4), MgCl₂ (3.3 mM), NADPH (3 mM), glucose-6-phosphate (5.3 mM), glucose-6-phosphate dehydrogenase (0.67 units/mL) with 0.42 mg of liver microsomal protein per mL. In the control reactions, the NADPH-cofactor system was substituted with phosphate buffer. Test compounds (2 μ M, final acetonitrile concentration 1.6%) were incubated with microsomes at 37 °C, shaking at 100 rpm in a Shaker Innova 4330 (New Brunswick Scientific). Five time points over 40 min were analyzed. The reactions were stopped by adding 5 volumes of acetonitrile with internal standard to incubation aliquots, followed by protein sedimentation by centrifuging at 5500 rpm for 5 min. Each reaction was performed in duplicates. Supernatants were analyzed using a gradient HPLC system (Agilent Technologies) coupled to a triple quadrupole massdetector API 3000 with TurboIonSpray Ion Source (AB Sciex, Canada). The elimination rate constant ($\underline{\mathbf{k}}_{\mathrm{el}}$), half-life ($t_{1/2}$), and intrinsic clearance (Clint) were determined in a plot of ln(AUC) versus time, using linear regression analysis.

Caco-2 Permeability Assay. Caco-2 cells were cultured in 75 mL flasks to 80-90% confluence according to the ATCC and Millipore recommendations⁹⁸ in a humidified atmosphere at 37 °C and 5% CO₂. Cells were detached with Trypsin/ EDTA solution and resuspended in the complete medium containing DMEM high glucose (4500 mg/L) with Lglutamine (4 mM) supplemented with 10% heat-inactivated Fetal Bovine Serum, 1% nonessential amino acids, and 730 nM puromycin and seeded at a density 5 × 105 cells in 75 mL flask. 49 After 5 days, cells were trypsinized and resuspended in the complete medium to a final concentration of 600×103 cells/mL; 400 μ L of the cell suspension was added to each well of the HTS 24-Multiwell Insert System, and 25 mL of prewarmed complete medium was added to the feeder tray. Caco-2 cells were incubated in Multiwell Insert System for 6-10 days before the transport experiments. The medium in the filter plate and feeder tray was refreshed every other day. Prior to the transport experiment, the integrity of the monolayer was verified by measuring the transepithelial electrical resistance (TEER) for every well using the Millicell-ERS system ohm meter. The final TEER values were within the range of 150 $600~\Omega \times \text{cm}^2$ as required for the assay conditions. The 24-well insert plate was removed from its feeder plate and placed in a new sterile 24-well transport analysis plate. The inserts were washed with PBS after medium aspiration. Ketoprofen, Atenolol, and Digoxin were used as reference compounds.

To determine the rate of compound transport in apical (A)-to-basolateral (B) direction, 300 μ L of the test compound dissolved in transport buffer (Hanks' BSS (9.5 g/L) and NaHCO₃ (0.35 g/L) with MgSO₄ to final concentration 0.81 mM, CaCl₂ to final concentration 1.26 mM, HEPES to final concentration 25 mM. pH adjusted to 7.4) was added into the filter wells; 1000 μ L of transport buffer was added to transport analysis plate wells.

To determine transport rates in the basolateral (B)-to-apical (A) direction, 1000 μ L of the test compound solutions was added into the wells of the transport analysis plate, the wells in the filter plate were filled with 300 μ L of buffer (apical compartment).

The effect of the inhibitor on the P-gp-mediated transport of the tested compounds was assessed by determining the bidirectional transport in the presence or absence of verapamil. The Caco-2 cells were preincubated for 30 min at 37 °C with 100 μ M of verapamil in both apical and basolateral compartments. After removal of the preincubation medium, the test compounds with verapamil (100 μ M) in transport buffer were added to donor wells, while the receiver wells were filled with the appropriate volume of transport buffer with 100 μ M of verapamil. The final amount of test and reference compounds was 10 μ M.

The plates were incubated for 90 min at 37 $^{\circ}$ C under continuous shaking at 100 rpm. 75 μ L aliquots were taken from the donor and receiver compartments for LC-MS/MS analysis. All samples were mixed with 2 volumes of acetonitrile followed by protein sedimentation by centrifuging at 10000 rpm for 10 min. Supernatants were analyzed using the HPLC system coupled with a tandem mass spectrometer.

All solutions of test and reference compounds were prepared manually, and further manipulations with the solutions were performed with automation using Opentrons. The apparent permeability $(P_{\rm app})$ was calculated for the Caco-2 permeability assay using the following equation:

$$P_{\text{app}} = \frac{V_A}{\text{Area} \times \text{Time}} \times \frac{[\text{drug}]_{\text{acc}}}{[\text{drug}]_{\text{initial d}}}$$

Where V_A is the volume of transport buffer in acceptor well, Area is the surface area of the inset (equals to the effective growth area of the inset $-0.7 \, \mathrm{cm}^2$), Time is the time of the assay, $[drug]_{\mathrm{acc}}$ is the amount of test compound in acceptor well, $[drug]_{\mathrm{initial, d}}$ is the initial amount of test compound in a donor well.

Efflux ratio $(P_{\rm app}({\rm BA})/P_{\rm app}({\rm AB}))$ reveals the difference in $P_{\rm app}$ as a result of active transport. If the efflux ratio is greater than 2, this indicates the occurred active efflux. To identify P-gp substrates, the P-gp inhibitor verapamil was added to the incubation medium. A decrease of the efflux ratio in the presence of verapamil indicates that the compound is a P-gp substrate.

Virtual Screening of the NCI DTP Collection. Ligand Preparation. the PubChem version of the NCI Developmental Therapeutics Program (DTP) database, 101 amounting to \sim 277 K structures in January 2017, was imported into InstantJChem version 18.22.5 for structure database manage-

ment. 102 Compounds overlapping with our in-house collection and those previously indicated to be unavailable from NCI were annotated as such. A workflow was built in KNIME version 4.0.1 103 to clean the database from unwanted structures before initiating virtual screening. Briefly, SMILES strings were desalted using the Speedy SMILES Desalt node, keeping only the first unique component and the longest SMILES string, canonicalized using the RDKit Canon SMILES node, and then grouped on identical structures to remove duplicates. RDKit Functional Group Filter nodes were applied to remove structures matching REOS¹⁰⁴ and PAINS.¹⁰⁵ The RDKit Descriptor Calculation node was used to calculate molecular weight and logP, and numeric outliers for both descriptors were removed. After applying these filters ~ 99K structures remained and were prepared for docking using LigPrep (Schrödinger Suite 2019–3). Epik was used to assign possible protonation states at pH 7.4 ± 2.0, possible tautomers were enumerated and a maximum of 4 stereoisomers was allowed for unassigned stereocenters. Using these settings, LigPrep generated ~ 200 K structural species for docking.

Protein Preparation. The crystal structure of human OGG1 in complex with the activator TH10785 (7AYY.pdb)⁶⁷ was used for docking and prepared using the Protein Preparation workflow (Schrödinger Suite 2019–3). 106 Chain A was chosen for preparation, and two versions of the protein were prepared: one with Asp268 in neutral form, donating a H-bond to the quinazoline N1 nitrogen of TH10785, and one with Asp268 deprotonated, accepting an H-bond from the protonated quinazoline N1 of TH10785. Ligands other than TH10785 were deleted, as well as any crystal waters. Structural defects such as bond orders were automatically fixed and protonation states at pH 7.4 assigned using Epik. Hydroxyl group, Asn, Gln and His states were automatically optimized using ProtAssign. Finally, an OPLS4-based all-atom restrained minimization to 0.30 Å RMSD was performed to remove any clashes and/or strain. Glide docking grids were centered on TH10785, setting the enclosing box size to be comparable to the size of the bound ligand.

Virtual Screening. The Virtual Screening Workflow as implemented in Schrödinger Suite 2019–3 was used, providing a 3-stage screening funnel employing the Glide docking module with 3 different levels of speed vs. accuracy, namely Glide HTVS, SP, and XP, where the top 10% scoring poses were passed on to the next stage. The prepared ligands were docked to both prepared protein structures without any constraints. Epik state penalties were added to the docking scores and enhanced planarity of conjugated pi groups was enforced. After Glide XP docking 803 unique ligands remained which were further manually triaged to 669 structures. Further triaging was done based on ligand efficiency (LE), calculated as - (docking score)/# heavy atoms, and applying a threshold of 0.40, which left 406 compounds. From these, 40 structures were selected and acquired from NCI, in part based on structural appeal and in part by their availability. These 40 structures covered a Glide XP Gscore range of - 11.14 to -9.12 kcal/mol (LE: 0.40-0.78). Compound 1 had a Gscore of - 9.91 kcal/mol and LE of 0.55, and TH12166 had a Gscore of - 9.86 kcal/mol and LE of 0.52.

Docking Analysis of Tryptamine Library. *Ligand Preparation.* Structures were exported as sdf from ChemDraw, InstantJChem or other sources and imported into the Maestro Suite. Using the OPLS3e force field, possible protonation

states at pH 7.0 \pm 2.0 were generated using Epik. Specific chiralities were retained and a maximum of 32 species per ligand were kept.

Protein Preparation. PDB files were imported to Maestro Suite (Schrödinger 2020–1/2024–1) and prepared using the Protein Preparation Wizard/Workflow. In brief, bond orders were assigned, hydrogens were added, disulfide bonds were generated, missing side chains and loops were filled using Prime and het states were generated using Epik for pH 7.0 \pm 2.0. Afterward, the structure was manually fixed upon problem identification. H-bond assignments were performed, waters removed beyond a 3.0 Å radius of het groups and a restrained minimization was performed using the OPLS3e force field, converging the heavy atoms to an RMSD of 0.30 Å.

Ligand Docking. The docking grid was generated using the prepared structure of mOGG1-1 (TH12163). The ligand was chosen as the center of a 10 Å \times 10 Å \times 10 Å box for ligand docking. No other restrictions were made. The compound was docked using the standard docking protocol (Glide SP) without restrictions. Individual poses were inspected and compound prioritized upon selection.

Molecular Dynamics. Molecular dynamics simulations were performed on OGG1-DNA-30 and OGG1-DNA-38 models, starting from crystallographic structure of hOGG1 complexed with excised DNA, covalently bound to Lys249 Schiff's base, and 8-oxoG (PDB code 1HU0).61 In the investigated systems, 8-oxoG was replaced by 30 or 38 via docking calculations performed with AutoDock vina 1.1.2 suite,10 in agreement with protocol adopted in previous investigations. The grid box's center was positioned at coordinates x = 18.483 Å, y = 19.538 Å, z = 34.466 Å, with dimension box of $20 \times 20 \times 20 \text{ Å}^3$. The lowest energy docked pose was used for subsequent MD simulations. Full geometry optimization of species 30 and 38 was carried out at HF/6-31G* level of theory, to generate parameters. General amber force field (GAFF) and restrained electrostatic potential (RESP)¹¹² methods were adopted to obtain nonbonding parameters and charges. The same protocol was used to extrapolate parameters for the excised DNA-Lys249 system, in proximity to the covalent bond between the excised base and the Schiff base. A list of parameters is provided in Supporting Information. OGG1:DNA-30 and OGG1-DNA-38 were placed in an orthorhombic box (10 Å from the protein), adding TIP3P water molecules and 29 Na+. Overall, the models consisted of 54647 atoms. Protein and DNA were treated with ff14SB¹¹³ and OL15¹¹⁴ force fields, respectively. After an initial minimization, each system was progressively heated from 0 to 298 K over 5 ns and then equilibrated for further 5 ns, using Langevin thermostat in NVT ensemble (T =298 K). The production phase consisted of 2 × 200 ns of molecular dynamics simulations for OGG1-DNA-30 and OGG1-DNA-38 systems, selecting 2 fs integration steps, using the SHAKE algorithm, Berendsen barostat in NPT ensemble (p = 1 bar) and a time constant $\tau p = 2.0$ ps. In all simulations, electrostatic potential calculations were managed under Particle Mesh Ewald summation method, with longrange electrostatic interactions computed using a 12 Å cutoff distance. Amber 2020 software package was adopted to perform all the simulations. 90 To identify 10 representative conformations during the molecular dynamics simulations, RMSD-based clustering of entire trajectories was performed, by RMS-fitting of the positions of the $C\alpha$ atoms and adopting

average linkage clustering algorithm as implemented in $\it cpptraj$ module. 115

ASSOCIATED CONTENT

Data Availability Statement

The research data supporting this publication can be accessed at 10.17630/6bca1a78-19d6-4567-a7ee-c99900865cfb. The atomic coordinates and structure factors (codes 9FNV, 9FNU) have been deposited in the Protein Data Bank (www.wwpdb.org/).

Solution Supporting Information

The Supporting Information is available free of charge at https://pubs.acs.org/doi/10.1021/acs.jmedchem.5c01454.

Supplementary figures and tables with associated biochemistry, computational, and crystallographic methods, chemistry experimental for starting material synthesis, LCMS traces for compounds used in biological assays, and NMR spectra for all compounds (PDF)

Molecular formular strings and activities (CSV)

Parameters in AMBER format for OGG1-DNA-30 and OGG1-DNA-38 (PDF)

Ligand-bound molecular docking structures of OGG1-32 and OGG1-35 (PDB)

Ligand-bound clustered molecular dynamics structures of OGG1-30 and OGG1-38 (PDB)

Crystal structure of an HOGG1-DNA borohydride trapped intermediate complex (PDB)

Ligand-bound molecular docking structures (PDB)

AUTHOR INFORMATION

Corresponding Authors

Marek Varga — EaStCHEM, School of Chemistry, University of St Andrews, St Andrews KY16 9ST, United Kingdom; orcid.org/0000-0002-9685-8145; Email: mv61@st-andrews.ac.uk

Allan J. B. Watson — EaStCHEM, School of Chemistry, University of St Andrews, St Andrews KY16 9ST, United Kingdom; orcid.org/0000-0002-1582-4286; Email: aw260@st-andrews.ac.uk

Maurice Michel – Karolinska Institute, Oncology and Pathology Science for Life Laboratory, Stockholm 171 65, Sweden; Karolinska Institute, Oncology and Pathology, Center for Molecular Medicine, Karolinska Institute and Karolinska Hospital, Stockholm 171 76, Sweden; Email: maurice.michel@ki.se

Authors

Florian Ortis — Karolinska Institute, Oncology and Pathology Science for Life Laboratory, Stockholm 171 65, Sweden Alicia Del Prado — Centro de Biología Molecular Severo Ochoa, CSIC-UAM, Madrid 28049, Spain; orcid.org/

0000-0002-5480-0367

Alice Eddershaw — Karolinska Institute, Oncology and Pathology, Center for Molecular Medicine, Karolinska Institute and Karolinska Hospital, Stockholm 171 76, Sweden; orcid.org/0000-0002-8381-4135

Emma Scaletti Hutchinson — Stockholm University, Biochemistry and Biophysics, Stockholm 106 91, Sweden; orcid.org/0000-0002-8741-8981

Emily C. Hank – Karolinska Institute, Oncology and Pathology Science for Life Laboratory, Stockholm 171 65, Sweden; Occid.org/0000-0002-3777-4697

Kaixin Zhou – Karolinska Institute, Oncology and Pathology Science for Life Laboratory, Stockholm 171 65, Sweden

Natálie Rudolfová – Karolinska Institute, Oncology and Pathology, Center for Molecular Medicine, Karolinska Institute and Karolinska Hospital, Stockholm 171 76, Sweden

Alessia Dodaro – Dipartimento di Chimica E Tecnologie Chimiche, Università Degli Studi della, Rende, Calabria 87036, Italy

Elisée Wiita – Karolinska Institute, Oncology and Pathology Science for Life Laboratory, Stockholm 171 65, Sweden

Ingrid Almlöf – Karolinska Institute, Oncology and Pathology Science for Life Laboratory, Stockholm 171 65, Sweden

Stella Karsten – Karolinska Institute, Oncology and Pathology Science for Life Laboratory, Stockholm 171 65, Sweden

Kirill Mamonov – Karolinska Institute, Oncology and Pathology Science for Life Laboratory, Stockholm 171 65, Sweden

Sara H. Ahmed — EaStCHEM, School of Chemistry, University of St Andrews, St Andrews KY16 9ST, United Kingdom

Kirsty Bentley – Karolinska Institute, Oncology and Pathology Science for Life Laboratory, Stockholm 171 65, Sweden

Olov Wallner – Karolinska Institute, Oncology and Pathology Science for Life Laboratory, Stockholm 171 65, Sweden

Evert J. Homan – Karolinska Institute, Oncology and Pathology Science for Life Laboratory, Stockholm 171 65, Sweden

Martin Scobie – Karolinska Institute, Oncology and Pathology Science for Life Laboratory, Stockholm 171 65, Sweden

Thomas Helleday — Karolinska Institute, Oncology and Pathology Science for Life Laboratory, Stockholm 171 65, Sweden; orcid.org/0000-0002-7384-092X

Mario Prejanò – Dipartimento di Chimica E Tecnologie Chimiche, Università Degli Studi della, Rende, Calabria 87036, Italy; o orcid.org/0000-0002-9140-6246

Pål Stenmark – Stockholm University, Biochemistry and Biophysics, Stockholm 106 91, Sweden; orcid.org/0000-0003-4777-3417

Miguel de Vega — Centro de Biología Molecular Severo Ochoa, CSIC-UAM, Madrid 28049, Spain; o orcid.org/0000-0003-1285-7549

Complete contact information is available at: https://pubs.acs.org/10.1021/acs.jmedchem.5c01454

Notes

The authors declare the following competing financial interest(s): OW and TH are listed as inventors on a U.S. patent no. WO2019166639 A1, covering OGG1 inhibitors. The patent is fully owned by a non-profit public foundation, the Helleday Foundation, and TH is a member of the foundation board. MS is an employee of Oxcia, a company developing OGG1 inhibitors. EW, OW, EJH, IA, MS, PS and TH are shareholders of Oxcia. The remaining authors declare no competing financial interests.

ACKNOWLEDGMENTS

We are thankful to Athina Pliakou, Mari Kullman Magnusson, Kristina Edfeldt, Ivan Vilotijević and Michael Sundström for administrative support. We thank MAXIV Laboratory (Sweden, proposal 20200204) and their beamline scientists from the BioMAX beamline for their support in data

collection. Part of the computer simulations were carried out using resources of Leonardo supercomputer from ISCRA (ID: HP10CI0 × 87). MV thanks Prof Sir David W. C. MacMillan, Princeton University, and the EaSI-CAT Centre for Doctoral Training for financial PhD support. AJBW thanks the Leverhulme Trust for a Research Fellowship (RF-2022-014). AD and MP thank Dipartimento di Chimica e Tecnologie Chimiche-Università della Calabria- for financial support. This work was funded by the Åke-Olsson foundation for haematological research (2020-00306, MM), the Helleday Foundation (FO), a Novo Nordisk Pioneer Innovator Grant (NNF23OC0085944, MM), the Åke Wiberg Foundation (M23-0043, MM), the Maximon Longevity Foundation (MM), EU ERC PoC OGG (202011-202110 OW), European Research Council (EJH, IA, MS), Karolinska Institute KID (SK), Swedish Research Council (2015-00162 2016-2025 to TH; 2022-03681 to PS), Swedish Cancer Society (CF 2019-2021 to OW; 24 3848 Pj to PS), grant PID2023-148757NB-I00 funded by MCIU/AEI/10.13039/501100011033 (MdV), and Karolinska Institute Research Foundation Grant (2022-01776, MM). This project has received funding from the Innovative Medicines Initiative 2 Joint Undertaking (JU) under grant agreement No 875510 (MM, EJH, EW, IA, AE, NR). The JU receives support from the European Union's Horizon 2020 research and innovation programme and EFPIA and Ontario Institute for Cancer Research, Royal Institution for the Advancement of Learning McGill University, Kungliga Tekniska Högskolan, Diamond Light Source Limited. This communication reflects the views of the authors and the JU is not liable for any use that may be made of the information contained herein.

ABBREVIATIONS

ΕI

ESI

FAM

EMSA

Α adenine AB apical-basolateral acetyl Ac AC_{50} half-maximal activation concentration AP apurinic/apyrimidinic APE1 apurinic/apyrimidinic endonuclease 1 aqueous aq Ar aryl ATR attenuated total reflectance **AUC** area under curve BA basolateral-apical Bn benzyl Boc tert-butoxycarbonyl C cytosine CI confidence interval Cl_{int} intrinsic clearance calculated logarithm of partition coefficient clogP Cy cyclohexyl DAB dabcyl quencher-3' Dulbecco's Modified Eagle Medium **DMEM DMF** dimethylformamide **DMSO** dimethyl sulfoxide DNA DNA DTP Developmental Therapeutics Program elimination unimolecular E1 **EDTA** ethylenediaminetetraacetic acid

electrophoretic mobility shift assay

electron impact

electrospray ionization

6-carboxyfluorescein

G guanine **GAFF** general amber force field h **HMBC** heteronuclear multiple bond correlation HPLC high-performance liquid chromatography HRMS high resolution mass spectrometry IC_{50} half-maximal inhibitory concentration IR infrared $K_{\rm a}$ acid dissociation constant $k_{
m el}$ elimination rate constant **LCMS** liquid chromatography mass spectrometry LE ligand efficiency LLE ligand-lipophilicity efficiency molar M murine MASH metabolic dysfunction-associate steatohepatitis MD molecular dynamics Me **MPLC** medium pressure liquid chromatography NADPH nicotinamide adenine dinucleotide phosphate National Cancer Institute NCI NIH National Institutes of Health **NMR** nuclear magnetic resonance NPT isothermal-isobaric ensemble Nth endonuclease III **NVT** canonical ensemble OGG1 8-oxoguanine DNA glycosylase 1 **ORCA** organocatalytic switch P-gp P-glycoprotein PAGE polyacrylamide gel electrophoresis **PAINS** pan-assay interference compounds $\begin{array}{c} P_{app} \\ PBS \end{array}$ apparent permeability phosphate-buffered saline PDB Protein Data Bank phenyl Ph pivalic acid PivOH **PBMC** peripheral blood mononuclear cell PNKP1 polynucleotide kinase-phosphatase 1 parts per million ppm **PTFE** polytetrafluoroethylene **PUA** phospho- α , β -unsaturated aldehyde **REOS** rapid elimination of swill RESP restrained electrostatic potential RDF radial distribution function **RMSD** root-mean-square deviation **RMSF** root-mean-square fluctuation RPM revolutions per minute RT room temperature SAR structure-activity relationship SEM standard error of the mean **SMILES** Simplified Molecular Input Line Entry System T4 PNK T4 polynucleotide kinase Т thymine t 1/2 half-life t-Bu tert-butyl **TEER** transepithelial electrical resistance **TFA** trifluoroacetic acid THF tetrahydrofuran TLC thin-layer chromatography U **UDG** uracil DNA glycosylase UV ultraviolet wildtype. wt

REFERENCES

- (1) Mullard, A. 2023 FDA Approvals. Nat. Rev. Drug Discovery 2024, 23 (2), 88-95.
- (2) Teng, M.; Young, D. W.; Tan, Z. The Pursuit of Enzyme Activation: A Snapshot of the Gold Rush. J. Med. Chem. 2022, 65 (21), 14289–14304.
- (3) Dow, L. F.; Case, A. M.; Paustian, M. P.; Pinkerton, B. R.; Simeon, P.; Trippier, P. C. The Evolution of Small Molecule Enzyme Activators. *RSC Med. Chem.* **2023**, *14* (11), 2206–2230.
- (4) Mullard, A. 2022 FDA Approvals. *Nat. Rev. Drug Discovery* **2023**, 22 (2), 83–88.
- (5) Kung, C.; Hixon, J.; Kosinski, P. A.; Cianchetta, G.; Histen, G.; Chen, Y.; Hill, C.; Gross, S.; Si, Y.; Johnson, K.; DeLabarre, B.; Luo, Z.; Gu, Z.; Yao, G.; Tang, H.; Fang, C.; Xu, Y.; Lv, X.; Biller, S.; Su, S.-S. M.; Yang, H.; Popovici-Muller, J.; Salituro, F.; Silverman, L.; Dang, L. AG-348 Enhances Pyruvate Kinase Activity in Red Blood Cells from Patients with Pyruvate Kinase Deficiency. *Blood* **2017**, *130* (11), 1347–1356.
- (6) Mullard, A. 2021 FDA Approvals. *Nat. Rev. Drug Discovery* **2022**, 21 (2), 83–88.
- (7) Mullard, A. 2020 FDA Drug Approvals. *Nat. Rev. Drug Discovery* **2021**, 20 (2), 85–90.
- (8) Mullard, A. 2019 FDA Drug Approvals. *Nat. Rev. Drug Discovery* **2020**, 19 (2), 79–84.
- (9) Mullard, A. 2018 FDA Drug Approvals. *Nat. Rev. Drug Discovery* **2019**, 18 (2), 85–89.
- (10) Mullard, A. 2017 FDA Drug Approvals. *Nat. Rev. Drug Discovery* **2018**, *17* (2), 81–85.
- (11) Mullard, A. 2016 FDA Drug Approvals. *Nat. Rev. Drug Discovery* **2017**, 16 (2), 73–76.
- (12) Mullard, A. 2015 FDA Drug Approvals. *Nat. Rev. Drug Discovery* **2016**, 15 (2), 73–76.
- (13) Mullard, A. 2014 FDA Drug Approvals. *Nat. Rev. Drug Discovery* **2015**, 14 (2), 77–81.
- (14) Kraft, A. S.; Smith, J. B.; Berkow, R. L. Bryostatin, an Activator of the Calcium Phospholipid-Dependent Protein Kinase, Blocks Phorbol Ester-Induced Differentiation of Human Promyelocytic Leukemia Cells HL-60. *Proc. Natl. Acad. Sci. U. S. A.* **1986**, 83 (5), 1334–1338.
- (15) Gómez-Galeno, J. E.; Dang, Q.; Nguyen, T. H.; Boyer, S. H.; Grote, M. P.; Sun, Z.; Chen, M.; Craigo, W. A.; van Poelje, P. D.; MacKenna, D. A.; Cable, E. E.; Rolzin, P. A.; Finn, P. D.; Chi, B.; Linemeyer, D. L.; Hecker, S. J.; Erion, M. D. A Potent and Selective AMPK Activator That Inhibits de Novo Lipogenesis. *ACS Med. Chem. Lett.* **2010**, *1* (9), 478–482.
- (16) Yang, J.; Campobasso, N.; Biju, M. P.; Fisher, K.; Pan, X.-Q.; Cottom, J.; Galbraith, S.; Ho, T.; Zhang, H.; Hong, X.; Ward, P.; Hofmann, G.; Siegfried, B.; Zappacosta, F.; Washio, Y.; Cao, P.; Qu, J.; Bertrand, S.; Wang, D.-Y.; Head, M. S.; Li, H.; Moores, S.; Lai, Z.; Johanson, K.; Burton, G.; Erickson-Miller, C.; Simpson, G.; Tummino, P.; Copeland, R. A.; Oliff, A. Discovery and Characterization of a Cell-Permeable, Small-Molecule c-Abl Kinase Activator That Binds to the Myristoyl Binding Site. *Chem. Biol.* **2011**, *18* (2), 177–186.
- (17) Hawley, S. A.; Fullerton, M. D.; Ross, F. A.; Schertzer, J. D.; Chevtzoff, C.; Walker, K. J.; Peggie, M. W.; Zibrova, D.; Green, K. A.; Mustard, K. J.; Kemp, B. E.; Sakamoto, K.; Steinberg, G. R.; Hardie, D. G. The Ancient Drug Salicylate Directly Activates AMP-Activated Protein Kinase. *Science* **2012**, *336* (6083), 918–922.
- (18) Yee Ng, P.; Bemis, J. E.; Disch, J. S.; Vu, C. L.; Oalmann, C.; Lynch, A.; Carney, D. P.; Riera, T. V.; Song, J.; Smith, J. J.; et al. The Identification of the SIRT1 Activator SRT2104 as a Clinical Candidate. *Lett. Drug Des. Discovery* **2013**, *10* (9), 793–797.
- (19) Rumpf, T.; Schiedel, M.; Karaman, B.; Roessler, C.; North, B. J.; Lehotzky, A.; Oláh, J.; Ladwein, K. I.; Schmidtkunz, K.; Gajer, M.; Pannek, M.; Steegborn, C.; Sinclair, D. A.; Gerhardt, S.; Ovádi, J.; Schutkowski, M.; Sippl, W.; Einsle, O.; Jung, M. Selective Sirt2 Inhibition by Ligand-Induced Rearrangement of the Active Site. *Nat. Commun.* **2015**, *6* (1), 6263.

- (20) Cabrol, C.; Huzarska, M. A.; Dinolfo, C.; Rodriguez, M. C.; Reinstatler, L.; Ni, J.; Yeh, L.-A.; Cuny, G. D.; Stein, R. L.; Selkoe, D. J.; Leissring, M. A. Small-Molecule Activators of Insulin-Degrading Enzyme Discovered through High-Throughput Compound Screening. *PLoS One* **2009**, *4* (4), No. e5274.
- (21) Wong, K. S.; Mabanglo, M. F.; Seraphim, T. V.; Mollica, A.; Mao, Y.-Q.; Rizzolo, K.; Leung, E.; Moutaoufik, M. T.; Hoell, L.; Phanse, S.; et al. Acyldepsipeptide Analogs Dysregulate Human Mitochondrial ClpP Protease Activity and Cause Apoptotic Cell Death. *Cell Chem. Biol.* **2018**, 25 (8), 1017–1030.e9.
- (22) Graves, P. R.; Aponte-Collazo, L. J.; Fennell, E. M. J.; Graves, A. C.; Hale, A. E.; Dicheva, N.; Herring, L. E.; Gilbert, T. S. K.; East, M. P.; McDonald, I. M.; Lockett, M. R.; Ashamalla, H.; Moorman, N. J.; Karanewsky, D. S.; Iwanowicz, E. J.; Holmuhamedov, E.; Graves, L. M. Mitochondrial Protease ClpP Is a Target for the Anticancer Compounds ONC201 and Related Analogues. *ACS Chem. Biol.* 2019, 14 (5), 1020–1029.
- (23) Hwang, S.; Mruk, K.; Rahighi, S.; Raub, A. G.; Chen, C.-H.; Dorn, L. E.; Horikoshi, N.; Wakatsuki, S.; Chen, J. K.; Mochly-Rosen, D. Correcting Glucose-6-Phosphate Dehydrogenase Deficiency with a Small-Molecule Activator. *Nat. Commun.* **2018**, *9* (1), 4045.
- (24) Li, P.; Zhu, D. Clinical Investigation of Glucokinase Activators for the Restoration of Glucose Homeostasis in Diabetes. *J. Diabetes* **2024**, *16* (5), No. e13544.
- (25) Chang, N.; Li, J.; Lin, S.; Zhang, J.; Zeng, W.; Ma, G.; Wang, Y. Emerging Roles of SIRT1 Activator, SRT2104, in Disease Treatment. Sci. Rep. 2024, 14 (1), 5521.
- (26) den Heijer, J. M.; Kruithof, A. C.; Moerland, M.; Walker, M.; Dudgeon, L.; Justman, C.; Solomini, I.; Splitalny, L.; Leymarie, N.; Khatri, K.; Cullen, V. C.; Hilt, D. C.; Groeneveld, G. J.; Lansbury, P. A Phase 1B Trial in -Associated Parkinson's Disease of BIA-28–6156, a Glucocerebrosidase Activator. *Mov. Disord.* 2023, 38 (7), 1197–1208.
- (27) Chatterjee, N.; Walker, G. C. Mechanisms of DNA Damage, Repair, and Mutagenesis. *Environ. Mol. Mutagen.* **2017**, 58 (5), 235–263
- (28) Nishimura, S. 8-Hydroxyguanine: A Base for Discovery. *DNA Repair* **2011**, *10* (11), 1078–1083.
- (29) Sliwinska, A.; Kwiatkowski, D.; Czarny, P.; Toma, M.; Wigner, P.; Drzewoski, J.; Fabianowska-Majewska, K.; Szemraj, J.; Maes, M.; Galecki, P.; Sliwinski, T. The Levels of 7,8-Dihydrodeoxyguanosine (8-oxoG) and 8-Oxoguanine DNA Glycosylase 1 (OGG1) A Potential Diagnostic Biomarkers of Alzheimer's Disease. *J. Neurol. Sci.* **2016**, 368, 155–159.
- (30) Zhang, X.; Li, L. The Significance of 8-oxoGsn in Aging-Related Diseases. Aging Dis. 2020, 11 (5), 1329–1338.
- (31) Liguori, I.; Russo, G.; Curcio, F.; Bulli, G.; Aran, L.; Della-Morte, D.; Gargiulo, G.; Testa, G.; Cacciatore, F.; Bonaduce, D.; Abete, P. Oxidative Stress, Aging, and Diseases. *Clin. Interventions Aging* **2018**, *13*, 757–772.
- (32) Cadet, J.; Douki, T.; Gasparutto, D.; Ravanat, J.-L. Oxidative Damage to DNA: Formation, Measurement and Biochemical Features. *Mutat. Res., Fundam. Mol. Mech. Mutagen.* **2003**, 531 (1), 5–23
- (33) Minowa, O.; Arai, T.; Hirano, M.; Monden, Y.; Nakai, S.; Fukuda, M.; Itoh, M.; Takano, H.; Hippou, Y.; Aburatani, H.; Masumura, K.; Nohmi, T.; Nishimura, S.; Noda, T. Mmh/Ogg1 Gene Inactivation Results in Accumulation of 8-Hydroxyguanine in Mice. *Proc. Natl. Acad. Sci. U. S. A.* **2000**, *97* (8), 4156–4161.
- (34) Nakabeppu, Y.; Sakumi, K.; Sakamoto, K.; Tsuchimoto, D.; Tsuzuki, T.; Nakatsu, Y. Mutagenesis and Carcinogenesis Caused by the Oxidation of Nucleic Acids. *Biol. Chem.* **2006**, *387* (4), *373*–379.
- (35) Paz-Elizur, T.; Krupsky, M.; Blumenstein, S.; Elinger, D.; Schechtman, E.; Livneh, Z. DNA Repair Activity for Oxidative Damage and Risk of Lung Cancer. *JNCI J. Natl. Cancer Inst.* **2003**, 95 (17), 1312–1319.
- (36) Yuzefovych, L. V.; Kahn, A. G.; Schuler, M. A.; Eide, L.; Arora, R.; Wilson, G. L.; Tan, M.; Rachek, L. I. Mitochondrial DNA Repair

- through OGG1 Activity Attenuates Breast Cancer Progression and Metastasis. Cancer Res. 2016, 76 (1), 30–34.
- (37) Kang, S. W.; Kim, S. K.; Park, H. J.; Chung, J.-H.; Ban, J. Y. Human 8-Oxoguanine DNA Glycosylase Gene Polymorphism (Ser326Cys) and Cancer Risk: Updated Meta-Analysis. *Oncotarget* **2017**, 8 (27), 44761–44775.
- (38) Oka, S.; Leon, J.; Sakumi, K.; Abolhassani, N.; Sheng, Z.; Tsuchimoto, D.; LaFerla, F. M.; Nakabeppu, Y. MTH1 and OGG1Maintain a Low Level of 8-Oxoguanine in Alzheimer's Brain, and Prevent the Progression of Alzheimer's Pathogenesis. *Sci. Rep.* **2021**, *11* (1), 5819.
- (39) Tumurkhuu, G.; Shimada, K.; Dagvadori, J.; Crother, T. R.; Zhang, W.; Luthringer, D.; Gottlieb, R. A.; Chen, S.; Arditi, M. Ogg1-Dependent DNA Repair Regulates NLRP3 Inflammasome and Prevents Atherosclerosis. *Circ. Res.* **2016**, *119* (6), No. e76—e90.
- (40) Karl, F.; Liang, C.; Böttcher-Loschinski, R.; Stoll, A.; Flamann, C.; Richter, S.; Lischer, C.; Völkl, S.; Jacobs, B.; Böttcher, M.; Jitschin, R.; Bruns, H.; Fischer, T.; Holler, E.; Rösler, W.; Dandekar, T.; Mackensen, A.; Mougiakakos, D. Oxidative DNA Damage in Reconstituting T Cells Is Associated with Relapse and Inferior Survival after Allo-SCT. *Blood* 2023, 141 (13), 1626–1639.
- (41) Sampath, H.; Lloyd, R. S. Roles of OGG1 in Transcriptional Regulation and Maintenance of Metabolic Homeostasis. *DNA Repair* **2019**, *81*, 102667.
- (42) Yuzefovych, L.; Pastukh, V. M.; Rachek, L. Elucidating Protective Mechanisms of Targeting of hOGG1 to Mitochondria on the HFD-Induced Insulin Resistance in Mice Lacking OGG1. *Diabetes* **2021**, *70* (Supplement_1), 1152.
- (43) Hussain, M.; Chu, X.; Duan Sahbaz, B.; Gray, S.; Pekhale, K.; Park, J.-H.; Croteau, D. L.; Bohr, V. A. Mitochondrial OGG1 Expression Reduces Age-Associated Neuroinflammation by Regulating Cytosolic Mitochondrial DNA. *Free Radical Biol. Med.* **2023**, 203, 34–44.
- (44) Li, X.-M.; Wu, Z.-J.; Fan, J.-Y.; Liu, M.-Q.; Song, C.-G.; Chen, H.-Q.; Yin, Y.; Li, A.; Wang, Y.-H.; Gao, S.-L.; Xu, Z.-L.; Liu, G.; Wu, K. Role of 8-Hydroxyguanine DNA Glycosidase 1 Deficiency in Exacerbating Diabetic Cardiomyopathy through the Regulation of Insulin Resistance. *J. Mol. Cell. Cardiol.* **2024**, *194*, 3–15.
- (45) Boldogh, I.; Hajas, G.; Aguilera-Aguirre, L.; Hegde, M. L.; Radak, Z.; Bacsi, A.; Sur, S.; Hazra, T. K.; Mitra, S. Activation of Ras Signaling Pathway by 8-Oxoguanine DNA Glycosylase Bound to Its Excision Product, 8-Oxoguanine*. *J. Biol. Chem.* **2012**, 287 (25), 20769–20773.
- (46) Li, G.; Yuan, K.; Yan, C.; Fox, J.; Gaid, M.; Breitwieser, W.; Bansal, A. K.; Zeng, H.; Gao, H.; Wu, M. 8-Oxoguanine-DNA Glycosylase 1 Deficiency Modifies Allergic Airway Inflammation by Regulating STAT6 and IL-4 in Cells and in Mice. *Free Radical Biol. Med.* 2012, 52 (2), 392–401.
- (47) Bacsi, A.; Aguilera-Aguirre, L.; Szczesny, B.; Radak, Z.; Hazra, T. K.; Sur, S.; Ba, X.; Boldogh, I. Down-Regulation of 8-Oxoguanine DNA Glycosylase 1 Expression in the Airway Epithelium Ameliorates Allergic Lung Inflammation. *DNA Repair* **2013**, *12* (1), 18–26.
- (48) Ba, X.; Bacsi, A.; Luo, J.; Aguilera-Aguirre, L.; Zeng, X.; Radak, Z.; Brasier, A. R.; Boldogh, I. 8-Oxoguanine DNA Glycosylase-1 Augments Proinflammatory Gene Expression by Facilitating the Recruitment of Site-Specific Transcription Factors. *J. Immunol.* **2014**, 192 (5), 2384–2394.
- (49) Pan, L.; Zhu, B.; Hao, W.; Zeng, X.; Vlahopoulos, S. A.; Hazra, T. K.; Hegde, M. L.; Radak, Z.; Bacsi, A.; Brasier, A. R.; Ba, X.; Boldogh, I. Oxidized Guanine Base Lesions Function in 8-Oxoguanine DNA Glycosylase-1-Mediated Epigenetic Regulation of Nuclear Factor κΒ-Driven Gene Expression*. *J. Biol. Chem.* **2016**, 291 (49), 25553–25566.
- (50) Pan, L.; Hao, W.; Zheng, X.; Zeng, X.; Ahmed Abbasi, A.; Boldogh, I.; Ba, X. OGG1-DNA Interactions Facilitate NF-κB Binding to DNA Targets. *Sci. Rep.* **2017**, 7 (1), 43297.
- (51) Visnes, T.; Cázares-Körner, A.; Hao, W.; Wallner, O.; Masuyer, G.; Loseva, O.; Mortusewicz, O.; Wiita, E.; Sarno, A.; Manoilov, A.; Astorga-Wells, J.; Jemth, A.-S.; Pan, L.; Sanjiv, K.; Karsten, S.;

- Gokturk, C.; Grube, M.; Homan, E. J.; Hanna, B. M. F.; Paulin, C. B. J.; Pham, T.; Rasti, A.; Berglund, U. W.; von Nicolai, C.; Benitez-Buelga, C.; Koolmeister, T.; Ivanic, D.; Iliev, P.; Scobie, M.; Krokan, H. E.; Baranczewski, P.; Artursson, P.; Altun, M.; Jensen, A. J.; Kalderén, C.; Ba, X.; Zubarev, R. A.; Stenmark, P.; Boldogh, I.; Helleday, T. Small-Molecule Inhibitor of OGG1 Suppresses Proinflammatory Gene Expression and Inflammation. *Science* 2018, 362 (6416), 834–839.
- (52) Xia, J.; Wu, S.; Wu, G.; Yang, J. Inhibition of 8-Oxoguanine DNA Glycosylase (OGG1) Expression Suppresses Polycystic Ovarian Syndrome via the NF-κB Signaling Pathway. *Reprod. Biol.* **2022**, 22 (3), 100679.
- (53) Perillo, B.; Ombra, M. N.; Bertoni, A.; Cuozzo, C.; Sacchetti, S.; Sasso, A.; Chiariotti, L.; Malorni, A.; Abbondanza, C.; Avvedimento, E. V. DNA Oxidation as Triggered by H3K9me2 Demethylation Drives Estrogen-Induced Gene Expression. *Science* **2008**, *319* (5860), 202–206.
- (54) Aguilera-Aguirre, L.; Bacsi, A.; Radak, Z.; Hazra, T. K.; Mitra, S.; Sur, S.; Brasier, A. R.; Ba, X.; Boldogh, I. Innate Inflammation Induced by the 8-Oxoguanine DNA Glycosylase-1–KRAS–NF-κB Pathway. *J. Immunol.* **2014**, *193* (9), 4643–4653.
- (55) Visnes, T.; Benítez-Buelga, C.; Cázares-Körner, A.; Sanjiv, K.; Hanna, B. M. F.; Mortusewicz, O.; Rajagopal, V.; Albers, J. J.; Hagey, D. W.; Bekkhus, T.; Eshtad, S.; Baquero, J. M.; Masuyer, G.; Wallner, O.; Müller, S.; Pham, T.; Göktürk, C.; Rasti, A.; Suman, S.; Torres-Ruiz, R.; Sarno, A.; Wiita, E.; Homan, E. J.; Karsten, S.; Marimuthu, K.; Michel, M.; Koolmeister, T.; Scobie, M.; Loseva, O.; Almlöf, I.; Unterlass, J. E.; Pettke, A.; Boström, J.; Pandey, M.; Gad, H.; Herr, P.; Jemth, A.-S.; El Andaloussi, S.; Kalderén, C.; Rodriguez-Perales, S.; Benítez, J.; Krokan, H. E.; Altun, M.; Stenmark, P.; Berglund, U. W.; Helleday, T. Targeting OGG1 Arrests Cancer Cell Proliferation by Inducing Replication Stress. *Nucleic Acids Res.* **2020**, 48 (21), 12234–12251.
- (56) Bangalore, D. M.; Tessmer, I. Direct hOGG1-Myc Interactions Inhibit hOGG1 Catalytic Activity and Recruit Myc to Its Promoters under Oxidative Stress. *Nucleic Acids Res.* **2022**, *50* (18), 10385–10398.
- (57) Luo, J.; Hosoki, K.; Bacsi, A.; Radak, Z.; Hegde, M. L.; Sur, S.; Hazra, T. K.; Brasier, A. R.; Ba, X.; Boldogh, I. 8-Oxoguanine DNA Glycosylase-1-Mediated DNA Repair Is Associated with Rho GTPase Activation and α -Smooth Muscle Actin Polymerization. *Free Radical Biol. Med.* **2014**, *73*, 430–438.
- (58) Wang, Y.; Chen, T.; Pan, Z.; Lin, Z.; Yang, L.; Zou, B.; Yao, W.; Feng, D.; Huangfu, C.; Lin, C.; Wu, G.; Ling, H.; Liu, G. 8-Oxoguanine DNA Glycosylase Modulates the Cell Transformation Process in Pulmonary Fibrosis by Inhibiting Smad2/3 and Interacting with Smad7. FASEB J. 2020, 34 (10), 13461–13473.
- (59) Tanner, L.; Single, A. B.; Bhongir, R. K. V.; Heusel, M.; Mohanty, T.; Karlsson, C. A. Q.; Pan, L.; Clausson, C.-M.; Bergwik, J.; Wang, K.; Andersson, C. K.; Oommen, R. M.; Erjefält, J. S.; Malmström, J.; Wallner, O.; Boldogh, I.; Helleday, T.; Kalderén, C.; Egesten, A. Small-Molecule-Mediated OGG1 Inhibition Attenuates Pulmonary Inflammation and Lung Fibrosis in a Murine Lung Fibrosis Model. *Nat. Commun.* 2023, 14 (1), 643.
- (60) Pan, L.; Hao, W.; Xue, Y.; Wang, K.; Zheng, X.; Luo, J.; Ba, X.; Xiang, Y.; Qin, X.; Bergwik, J.; Tanner, L.; Egesten, A.; Brasier, A. R.; Boldogh, I. 8-Oxoguanine Targeted by 8-Oxoguanine DNA Glycosylase 1 (OGG1) Is Central to Fibrogenic Gene Activation upon Lung Injury. *Nucleic Acids Res.* **2023**, *51* (3), 1087–1102.
- (61) Fromme, J. C.; Bruner, S. D.; Yang, W.; Karplus, M.; Verdine, G. L. Product-Assisted Catalysis in Base-Excision DNA Repair. *Nat. Struct. Mol. Biol.* **2003**, *10* (3), 204–211.
- (62) Hill, J. W.; Hazra, T. K.; Izumi, T.; Mitra, S. Stimulation of Human 8-Oxoguanine-DNA Glycosylase by AP-Endonuclease: Potential Coordination of the Initial Steps in Base Excision Repair. *Nucleic Acids Res.* **2001**, 29 (2), 430–438.
- (63) Visnes, T.; Grube, M.; Hanna, B. M. F.; Benitez-Buelga, C.; Cázares-Körner, A.; Helleday, T. Targeting BER Enzymes in Cancer Therapy. *DNA Repair* **2018**, *71*, 118–126.

- (64) Kuznetsov, N. A.; Koval, V. V.; Zharkov, D. O.; Nevinsky, G. A.; Douglas, K. T.; Fedorova, O. S. Kinetics of Substrate Recognition and Cleavage by Human 8-Oxoguanine-DNA Glycosylase. *Nucleic Acids Res.* **2005**, *33* (12), 3919–3931.
- (65) Morland, I.; Luna, L.; Gustad, E.; Seeberg, E.; Bjørås, M. Product Inhibition and Magnesium Modulate the Dual Reaction Mode of hOgg1. *DNA Repair* **2005**, *4* (3), 381–387.
- (66) Zharkov, D. O.; Rosenquist, T. A.; Gerchman, S. E.; Grollman, A. P. Substrate Specificity and Reaction Mechanism of Murine 8-Oxoguanine-DNA Glycosylase*. *J. Biol. Chem.* **2000**, 275 (37), 28607–28617.
- (67) Michel, M.; Benítez-Buelga, C.; Calvo, P. A.; Hanna, B. M. F.; Mortusewicz, O.; Masuyer, G.; Davies, J.; Wallner, O.; Sanjiv, K.; Albers, J. J.; Castañeda-Zegarra, S.; Jemth, A.-S.; Visnes, T.; Sastre-Perona, A.; Danda, A. N.; Homan, E. J.; Marimuthu, K.; Zhenjun, Z.; Chi, C. N.; Sarno, A.; Wiita, E.; von Nicolai, C.; Komor, A. J.; Rajagopal, V.; Müller, S.; Hank, E. C.; Varga, M.; Scaletti, E. R.; Pandey, M.; Karsten, S.; Haslene-Hox, H.; Loevenich, S.; Marttila, P.; Rasti, A.; Mamonov, K.; Ortis, F.; Schömberg, F.; Loseva, O.; Stewart, J.; D'Arcy-Evans, N.; Koolmeister, T.; Henriksson, M.; Michel, D.; de Ory, A.; Acero, L.; Calvete, O.; Scobie, M.; Hertweck, C.; Vilotijevic, I.; Kalderén, C.; Osorio, A.; Perona, R.; Stolz, A.; Stenmark, P.; Berglund, U. W.; de Vega, M.; Helleday, T. Small-Molecule Activation of OGG1 Increases Oxidative DNA Damage Repair by Gaining a New Function. *Science* 2022, 376 (6600), 1471–1476.
- (68) Schniertshauer, D.; Gebhard, D.; van Beek, H.; Nöth, V.; Schon, J.; Bergemann, J. The Activity of the DNA Repair Enzyme hOGG1 Can Be Directly Modulated by Ubiquinol. *DNA Repair* **2020**, 87, 102784.
- (69) Baptiste, B. A.; Katchur, S. R.; Fivenson, E. M.; Croteau, D. L.; Rumsey, W. L.; Bohr, V. A. Enhanced Mitochondrial DNA Repair of the Common Disease-Associated Variant, Ser326Cys, of hOGG1 through Small Molecule Intervention. *Free Radical Biol. Med.* **2018**, 124, 149–162.
- (70) Hank, E. C.; D'Arcy-Evans, N.; Wallner, O.; Ortis, F.; Meng, L.; Calvo, P.; Scaletti, E. R.; Kosenina, S.; Dawson, H.; Stewart, J., et al. Nucleobase Catalysts for the Enzymatic Activation of 8-Oxoguanine DNA Glycosylase 1. *ChemRxiv.* 2023.
- (71) Kehler, M.; Zhou, K.; Kemas, A. M.; Del Prado, A.; Hutchinson, E. S.; Nairn, E. H.; Varga, M.; Plattner, Y.; Zhong, Y.; Purewal-Sidhu, O.; et al. Organocatalytic Switches of DNA Glycosylase OGG1 Catalyze a Highly Efficient AP-Lyase Function. *Chem. Eur. J.* 2025, 31 (33), No. e202500382.
- (72) Tian, G.; Katchur, S. R.; Jiang, Y.; Briand, J.; Schaber, M.; Kreatsoulas, C.; Schwartz, B.; Thrall, S.; Davis, A. M.; Duvall, S.; Kaufman, B. A.; Rumsey, W. L. Small Molecule-Mediated Allosteric Activation of the Base Excision Repair Enzyme 8-Oxoguanine DNA Glycosylase and Its Impact on Mitochondrial Function. *Sci. Rep.* 2022, 12 (1), 14685.
- (73) Youhanna, S.; Kemas, A. M.; Wright, S. C.; Zhong, Y.; Klumpp, B.; Klein, K.; Motso, A.; Michel, M.; Ziegler, N.; Shang, M.; Sabatier, P.; Kannt, A.; Sheng, H.; Oliva-Vilarnau, N.; Büttner, F. A.; Seashore-Ludlow, B.; Schreiner, J.; Windbergs, M.; Cornillet, M.; Björkström, N. K.; Hülsmeier, A. J.; Hornemann, T.; Olsen, J. V.; Wang, Y.; Gramignoli, R.; Sundström, M.; Lauschke, V. M. Chemogenomic Screening in a Patient-Derived 3D Fatty Liver Disease Model Reveals the CHRM1-TRPM8 Axis as a Novel Module for Targeted Intervention. *Adv. Sci.* 2025, *12* (3), 2407572.
- (74) Younossi, Z. M.; Koenig, A. B.; Abdelatif, D.; Fazel, Y.; Henry, L.; Wymer, M. Global Epidemiology of Nonalcoholic Fatty Liver Disease—Meta-analytic Assessment of Prevalence, Incidence, and Outcomes. *Hepatology* **2016**, *64* (1), 73.
- (75) Younossi, Z. M.; Golabi, P.; Paik, J. M.; Henry, A.; Van Dongen, C.; Henry, L. The Global Epidemiology of Nonalcoholic Fatty Liver Disease (NAFLD) and Nonalcoholic Steatohepatitis (NASH): A Systematic Review. *Hepatology* **2023**, 77 (4), 1335–1347. (76) Preciado, S.; Mendive-Tapia, L.; Albericio, F.; Lavilla, R. Synthesis of C-2 Arylated Tryptophan Amino Acids and Related

- Compounds through Palladium-Catalyzed C-H Activation. J. Org. Chem. 2013, 78 (16), 8129-8135.
- (77) Larock, R. C.; Yum, E. K. Synthesis of Indoles via Palladium-Catalyzed Heteroannulation of Internal Alkynes. *J. Am. Chem. Soc.* **1991**, *113* (17), 6689–6690.
- (78) Chuang, K. V.; Kieffer, M. E.; Reisman, S. E. A Mild and General Larock Indolization Protocol for the Preparation of Unnatural Tryptophans. *Org. Lett.* **2016**, *18* (18), 4750–4753.
- (79) Gad, H.; Koolmeister, T.; Jemth, A.-S.; Eshtad, S.; Jacques, S. A.; Ström, C. E.; Svensson, L. M.; Schultz, N.; Lundbäck, T.; Einarsdottir, B. O.; Saleh, A.; Göktürk, C.; Baranczewski, P.; Svensson, R.; Berntsson, R. P.-A.; Gustafsson, R.; Strömberg, K.; Sanjiv, K.; Jacques-Cordonnier, M.-C.; Desroses, M.; Gustavsson, A.-L.; Olofsson, R.; Johansson, F.; Homan, E. J.; Loseva, O.; Bräutigam, L.; Johansson, L.; Höglund, A.; Hagenkort, A.; Pham, T.; Altun, M.; Gaugaz, F. Z.; Vikingsson, S.; Evers, B.; Henriksson, M.; Vallin, K. S. A.; Wallner, O. A.; Hammarström, L. G. J.; Wiita, E.; Almlöf, I.; Kalderén, C.; Axelsson, H.; Djureinovic, T.; Puigvert, J. C.; Häggblad, M.; Jeppsson, F.; Martens, U.; Lundin, C.; Lundgren, B.; Granelli, I.; Jensen, A. J.; Artursson, P.; Nilsson, J. A.; Stenmark, P.; Scobie, M.; Berglund, U. W.; Helleday, T. MTH1 Inhibition Eradicates Cancer by Preventing Sanitation of the dNTP Pool. *Nature* 2014, 508 (7495), 215–221.
- (80) Huber, K. V. M.; Salah, E.; Radic, B.; Gridling, M.; Elkins, J. M.; Stukalov, A.; Jemth, A.-S.; Göktürk, C.; Sanjiv, K.; Strömberg, K.; Pham, T.; Berglund, U. W.; Colinge, J.; Bennett, K. L.; Loizou, J. I.; Helleday, T.; Knapp, S.; Superti-Furga, G. Stereospecific Targeting of MTH1 by (S)-Crizotinib as an Anticancer Strategy. *Nature* **2014**, *508* (7495), 222–227.
- (81) Dunker, C.; Schlegel, K.; Junker, A. Phenol (Bio)Isosteres in Drug Design and Development. *Arch. Pharm.* **2025**, 358 (1), No. e2400700.
- (82) Shih, J. C.; Chen, K.; Ridd, M. J. MONOAMINE OXIDASE: From Genes to Behavior. *Annu. Rev. Neurosci.* **1999**, 22, 197–217.
- (83) Prah, A.; Purg, M.; Stare, J.; Vianello, R.; Mavri, J. How Monoamine Oxidase A Decomposes Serotonin: An Empirical Valence Bond Simulation of the Reactive Step. *J. Phys. Chem. B* **2020**, *124* (38), 8259–8265.
- (84) Hopkins, A. L.; Keserü, G. M.; Leeson, P. D.; Rees, D. C.; Reynolds, C. H. The Role of Ligand Efficiency Metrics in Drug Discovery. *Nat. Rev. Drug Discovery* **2014**, *13* (2), 105–121.
- (85) Kuznetsov, N. A.; Koval, V. V.; Nevinsky, G. A.; Douglas, K. T.; Zharkov, D. O.; Fedorova, O. S. Kinetic Conformational Analysis of Human 8-Oxoguanine-DNA Glycosylase. *J. Biol. Chem.* **2007**, 282 (2), 1029–1038.
- (86) Michel, M.; Visnes, T.; Homan, E. J.; Seashore-Ludlow, B.; Hedenström, M.; Wiita, E.; Vallin, K.; Paulin, C. B. J.; Zhang, J.; Wallner, O.; Scobie, M.; Schmidt, A.; Jenmalm-Jensen, A.; Warpman Berglund, U.; Helleday, T. Computational and Experimental Druggability Assessment of Human DNA Glycosylases. *ACS Omega* 2019, 4 (7), 11642–11656.
- (87) Norman, D. P. G.; Chung, S. J.; Verdine, G. L. Structural and Biochemical Exploration of a Critical Amino Acid in Human 8-Oxoguanine Glycosylase. *Biochemistry* **2003**, *42* (6), 1564–1572.
- (88) Fromme, J. C.; Verdine, G. L. Structure of a Trapped Endonuclease III–DNA Covalent Intermediate. *EMBO J* **2003**, 22 (13), 3461–3471.
- (89) Fromme, J. C.; Banerjee, A.; Huang, S. J.; Verdine, G. L. Structural Basis for Removal of Adenine Mispaired with 8-Oxoguanine by MutY Adenine DNA Glycosylase. *Nature* **2004**, 427 (6975), 652–656.
- (90) Case, D. A.; Aktulga, H. M.; Belfon, K.; Cerutti, D. S.; Cisneros, G. S.; Cruzeiro, V. W. D.; Forouzesh, N.; Giese, T. J.; Götz, A. W.; Gohlke, H.; Izadi, S.; et al. AmberTools. *J. Chem. Inf. Model* **2023**, *63* (20), 6183–6191.
- (91) Wang, S.; Yu, B.; Liu, H.-M. Pd(II)-Catalyzed Intramolecular C(Sp2)—H Arylation of Tryptamines Using the Nonsteric NH2 as a Directing Group. *Org. Lett.* **2021**, *23* (1), 42–48.

- (92) Cacchi, S.; Carnicelli, V.; Marinelli, F. Palladium-Catalysed Cyclization of 2-Alkynylanilines to 2-Substituted Indoles under an Acidic Two-Phase System. *J. Organomet. Chem.* **1994**, 475 (1), 289–
- (93) Barolo, S. M.; Lukach, A. E.; Rossi, R. A. Syntheses of 2-Substituted Indoles and Fused Indoles by Photostimulated Reactions of o-Iodoanilines with Carbanions by the SRN1Mechanism. *J. Org. Chem.* **2003**, *68* (7), 2807–2811.
- (94) Fleck, N.; Thomas, R. M.; Müller, M.; Grimme, S.; Lipshutz, B. H. An Environmentally Responsible Route to Tezacaftor, a Drug for Treatment of Cystic Fibrosis Prepared in Water via Ppm Au Catalysis as Entry to 2-Substituted Indoles. *Green Chem.* **2022**, 24 (17), 6517–6523.
- (95) Mandali, P. K.; Chand, D. K. Palladium Nanoparticles Catalyzed Synthesis of Benzofurans by a Domino Approach. *Synthesis* **2015**, *47* (11), 1661–1668.
- (96) Carreras-Puigvert, J.; Zitnik, M.; Jemth, A.-S.; Carter, M.; Unterlass, J. E.; Hallström, B.; Loseva, O.; Karem, Z.; Calderón-Montaño, J. M.; Lindskog, C.; Edqvist, P.-H.; Matuszewski, D. J.; Ait Blal, H.; Berntsson, R. P. A.; Häggblad, M.; Martens, U.; Studham, M.; Lundgren, B.; Wählby, C.; Sonnhammer, E. L. L.; Lundberg, E.; Stenmark, P.; Zupan, B.; Helleday, T. A Comprehensive Structural, Biochemical and Biological Profiling of the Human NUDIX Hydrolase Family. *Nat. Commun.* **2017**, 8 (1), 1541.
- (97) Carroll, B. L.; Zahn, K. E.; Hanley, J. P.; Wallace, S. S.; Dragon, J. A.; Doublié, S. Caught in Motion: Human NTHL1 Undergoes Interdomain Rearrangement Necessary for Catalysis. *Nucleic Acids Res.* **2021**, 49 (22), 13165–13178.
- (98) Jeanne, E. P.; Arena, A. Optimization of Caco-2 Cell Growth and Differentiation for Drug Transport Assay Studies Using a 96 Well MultiScreen Caco-2 Assay System. In *Millipore Corporation, Protocol Note PC1060EN00*; Millipore, 2003.
- (99) Sevin, E.; Dehouck, L.; Fabulas-da Costa, A.; Cecchelli, R.; Dehouck, M. P.; Lundquist, S.; Culot, M. Accelerated Caco-2 Cell Permeability Model for Drug Discovery. *J. Pharmacol. Toxicol. Methods* **2013**, *68* (3), 334–339.
- (100) Srinivasan, B.; Kolli, A. R.; Esch, M. B.; Abaci, H. E.; Shuler, M. L.; Hickman, J. J. TEER Measurement Techniques for In Vitro Barrier Model Systems. *SLAS Technol.* **2015**, *20* (2), 107–126.
- (101) NCI Developmental Therapeutics Program, 2017. https://pubchem.ncbi.nlm.nih.gov/sources/DTP/NCI.
- (102) Instant JChem; Chemaxon: Budapest, Hungary, 2019.
- (103) Berthold, M. R.; Cebron, N.; Dill, F.; Gabriel, T. R.; Kötter, T.; Meinl, T.; Ohl, P.; Sieb, C.; Thiel, K.; Wiswedel, B. KNIME: The Konstanz Information Miner. In *Data Analysis, Machine Learning and Applications*; Preisach, C.; Burkhardt, H.; Schmidt-Thieme, L.; Decker, R., Eds.; Springer: Berlin, Heidelberg, 2008; pp 319–326.
- (104) Walters, W. P.; Stahl, M. T.; Murcko, M. A. Virtual Screening—an Overview. *Drug Discovery Today* **1998**, 3 (4), 160–178.
- (105) Baell, J. B.; Holloway, G. A. New Substructure Filters for Removal of Pan Assay Interference Compounds (PAINS) from Screening Libraries and for Their Exclusion in Bioassays. *J. Med. Chem.* **2010**, 53 (7), 2719–2740.
- (106) Suite, S. Schrödinger; Schrödinger LLC: New York, NY, 2019. (107) Trott, O.; Olson, A. J. A. V. Improving the Speed and Accuracy of Docking with a New Scoring Function, Efficient Optimization, and Multithreading. J. Comput. Chem. 2010, 31 (2), 455–461.
- (108) Prejanò, M.; Romeo, I.; La Serra, M. A.; Russo, N.; Marino, T. Computational Study Reveals the Role of Water Molecules in the Inhibition Mechanism of LAT1 by 1,2,3-Dithiazoles. *J. Chem. Inf. Model.* **2021**, *61* (12), 5883–5892.
- (109) Ciardullo, G.; Parise, A.; Prejanò, M.; Marino, T. Viral RNA Replication Suppression of SARS-CoV-2: Atomistic Insights into Inhibition Mechanisms of RdRp Machinery by ddhCTP. *J. Chem. Inf. Model.* **2024**, *64* (5), 1593–1604.
- (110) Ciardullo, G.; Prejanò, M.; Parise, A.; Russo, N.; Marino, T. The Effect of Chalcogen-Chalcogen Bond Formation in the New

- Delhi Metallo- β -Lactamase 1 Enzyme to Counteract Antibiotic Resistance. *J. Chem. Theory Comput.* **2025**, 21 (3), 1422–1431.
- (111) Wang, J.; Wolf, R. M.; Caldwell, J. W.; Kollman, P. A.; Case, D. A. Development and Testing of a General Amber Force Field. *J. Comput. Chem.* **2004**, 25 (9), 1157–1174.
- (112) Bayly, C. I.; Cieplak, P.; Cornell, W.; Kollman, P. A. A Well-Behaved Electrostatic Potential Based Method Using Charge Restraints for Deriving Atomic Charges: The RESP Model. *J. Phys. Chem.* 1993, 97 (40), 10269–10280.
- (113) Maier, J. A.; Martinez, C.; Kasavajhala, K.; Wickstrom, L.; Hauser, K. E.; Simmerling, C. ff14SB: Improving the Accuracy of Protein Side Chain and Backbone Parameters from ff99SB. *J. Chem. Theory Comput.* **2015**, *11* (8), 3696–3713.
- (114) Zgarbová, M.; Šponer, J.; Otyepka, M.; Cheatham, T. E. I.; Galindo-Murillo, R.; Jurečka, P. Refinement of the Sugar—Phosphate Backbone Torsion Beta for AMBER Force Fields Improves the Description of Z- and B-DNA. J. Chem. Theory Comput. 2015, 11 (12), 5723—5736.
- (115) Roe, D. R.; Cheatham, T. E. I. PTRAJ and CPPTRAJ: Software for Processing and Analysis of Molecular Dynamics Trajectory Data. *J. Chem. Theory Comput.* **2013**, *9* (7), 3084–3095.

